# DUAL-BAND BEAM SCANNING REFLECTARRAYS AND NOVEL WIDEBAND AND POLARIZATION DIVERSIFIED PLANAR ANTENNAS

A Dissertation

by

SHIH-HSUN HSU

Submitted to the Office of Graduate Studies of
Texas A&M University
in partial fulfillment of the requirements for the degree of

DOCTOR OF PHILOSOPHY

August 2008

Major Subject: Electrical Engineering

# DUAL-BAND BEAM SCANNING REFLECTARRAYS

# AND NOVEL WIDEBAND AND POLARIZATION DIVERSIFIED

# PLANAR ANTENNAS

A Dissertation

by

SHIH-HSUN HSU

Submitted to the Office of Graduate Studies of
Texas A&M University
in partial fulfillment of the requirements for the degree of

DOCTOR OF PHILOSOPHY

Approved by:

| | |
|---|---|
| Chair of Committee, | Kai Chang |
| Committee Members, | Robert D. Nevels |
| | Jun Zou |
| | Kenith Meissner |
| Head of Department, | Costas N. Georghiades |

August 2008

Major Subject: Electrical Engineering

# ABSTRACT

Dual-band Beam Scanning Reflectarrays and Novel Wideband and Polarization Diversified Planar Antennas. (August 2008)

Shih-Hsun Hsu, B.S., National Cheng Kung University;

M.S., University of Wisconsin-Madison

Chair of Advisory Committee: Dr. Kai Chang

The reflectarray antenna has been considered as a suitable candidate to replace the traditional parabolic reflectors because of its high-gain and low-profile features. Beam scanning capability and multi-band operation are the current trends of the reflectarray design. It is desired to implement these functionalities with simple and effective techniques. Narrow bandwidth is the main issue which restricts the applications of the microstrip antennas. New microstrip slot antennas and polarization diversified planar antennas are introduced as the solutions to the issue of narrow bandwidth in this dissertation.

A dual-band beam scanning reflectarray has been developed. It is the first offset-fed reflectarray that has been ever practically developed to emulate a cylindrical/parabolic type of reflector. Unlike other beam scanning reflectarrays which integrate phase tuning devices into the reflectarray elements and control the reflection phase, the beam scanning capability of this reflectarray is provided by its feed array. This method significantly reduces the complexity of the design of the beam scanning reflectarray. A

new dual-band reflectarray configuration is also developed to eliminate the possible top layer blocking effects in the dual-layer reflectarray configuration. Perforated patches loaded with slots on the ground plane and rectangular patches loaded with slots on the patches are adopted as the low and high frequency bands, respectively. It is guaranteed that no physical contact between any two elements will occur.

The bandwidth of the conventional microstrip antenna is small. A new wideband circularly polarized microstrip slot antenna is introduced in this dissertation. Very wide 3-dB axial ratio bandwidth is observed for the proposed antenna. The antennas are assembled in triangularly arranged array with sequential rotation feed technique. Polarization polarity is an alternative solution to the narrow bandwidth. A reconfigurable circularly polarized microstrip antenna is proposed. The antenna has both right-hand and left-hand circular polarizations which are controlled by two piezoelectric transducers. In addition, a dual-band dual-linearly-polarized planar array is designed based on the concepts of polarization diversity and multi-band operation.

The research presented in this dissertation suggests useful techniques for reflectarrays and novel antenna designs. The results should have many applications for the modern wireless communication and radar systems.

# DEDICATION

To my grandparents,
my parents,
and
my girlfriend, Hsiao-Wei

# ACKNOWLEDGEMENTS

I would like to express my sincere gratitude to Dr. Kai Chang for his support and guidance with regards to my Ph.D. studies and research at Texas A&M University. I also appreciate Dr. Robert D. Nevels, Dr. Jun Zou, Dr. Kenith Meissner, and Dr. Laszlo Kish for serving as my committee members and for their helpful suggestions and comments. I would also like to thank Mr. Li at Texas A&M University for his technical assistance. I would like to express thanks to Dr. John Huang at the Jet Propulsion Laboratory and Dr. Chulmin Han at Ethertronics for their helpful instructions and comments for the reflectarray design. Thanks also go to Dr. Gregory Huff, Dr. Seung-Pyo Hong, Dr. Wen-Hua Tu, Dr. Yu-Jiun Ren and all other members of the Electromagnetics and Microwave Laboratory at the Texas A&M University for their invaluable discussions.

I would like to give my deepest gratitude to my grandparents and parents for their constant encouragement and financial support. My appreciation also extends to my brother, all other members in my family and my girlfriend's family. This work would not have been possible without their support.

Finally, I wish to express my appreciation and love to my lovely girlfriend, Hsiao-Wei, whose love, patience, and thoughtfulness have been the best comfort and support during the period of my graduate study. I hope to use this dissertation as the first step to requite her immutable love since no words can sufficiently describe my gratitude to her.

# TABLE OF CONTENTS

CHAPTER Page

# LIST OF FIGURES

FIGURE Page

FIGURE Page

# LIST OF TABLES

# CHAPTER I

# INTRODUCTION

## 1. Introduction and research background

Large aperture antennas are attractive to space missions such as satellite communications, radar systems, and radio astronomy observations due to their high-gain feature. Traditionally, large parabolic reflector antennas are selected for the missions mentioned above. However, these antennas are bulky, heavy, and their geometrical shape tends to be distorted during the implementation. To overcome these shortcomings, in 1984, Thomas and Veal proposed the idea of inflatable parabolic reflector antennas with the advantages of lighter payload and lower launching cost [1]. Yet, efforts needed in maintaining the required curved surface accuracy still formed an obstacle to the success of this technology. Microstrip reflectarray technology has become an excellent substitute for the parabolic reflector antennas since first being introduced in the 1980's [2-14]. Reflecting elements of the array are printed on the surface and are illuminated by a feed antenna locating at the focal point of the reflectarray. The special feed illumination eliminate the need of the complicated power dividing and feeding networks, thus the insertion loss is reduced and the efficiency is higher compared to an array with the same aperture size. In view of the good features of the microstrip reflectarray including flat surface, low-profile, easy fabrication and installation during the space missions, the Jet Propulsion Laboratory (JPL) proposed the concept of the inflatable

---

The journal model for this dissertation is *IEEE Transactions on Antennas and Propagation*.

microstrip reflectarray. Several inflatable microstrip reflectarray antennas for different applications have been successfully developed since then [15-17].

In addition, the beam scanning capability is another feature differentiating the traditional parabolic reflector and the microstrip reflectarray. In order to scan the main beam of the parabolic reflector, it is often required to mechanically reposition the feed or move the reflector. Since a parabolic reflector normally has a large size and heavy weight, scanning the main beam of the reflector would be a laborious task. On the other hand, the array elements of a reflectarray can be possibly integrated with the varactor diodes, oscillators and MEMS devices to provide beam scanning capability for the reflectarray [18-20]. However, integrating these elements into the reflectarray elements always increases the manufacturing cost and design complexity. Instead, a phased array can be used as the feed array of the reflectarray. The feeding phased array can provide the beam scanning capability for the reflectarray.

Results of the feed arrays including sidelobe level (SLL), cross-polarization level, and the beam scanning angle determine the performance of the beam scanning reflectarray. A proper element excitation amplitude distribution such as Dolph-Tchebyscheff, Binomial, or Taylor distribution can give the feed array good SLL. It is also important to choose a suitable array configuration so that the SLL and cross-polarization level can be further improved.

Narrow bandwidth is perhaps the most serious concern of the reflectarray. The bandwidth of the microstrip reflectarray is mainly restricted by the microstrip elements, the differential phase delay, the array element spacing, and the feed antenna bandwidth

[21]. Previous studies in increasing the bandwidth of reflectarray include using stacked patches to achieve a 16% bandwidth [22] and using special element configurations to obtain a bandwidth more than 15% [23]. Besides, the multilayer configuration can also support multi-band operation, which is equivalent to bandwidth enhancement. For some spaceborne radar applications, the multi-band operation can help to improve the accuracy and resolution of the acquisition of information including global rainfall, cloud density and surface topography, etc.. In [12-14], dual-band reflectarrays were designed with the dual-layer configuration. Each substrate layer accommodates elements of one frequency band. The reflection phase of an element was achieved by rotating the element by a specified angle. The rotation technique is only valid for circular polarized (CP) reflectarray elements. For linear polarized reflectarray, the variable-size technique and patches with variable-length stubs are in common use. One advantage of the element rotation technique is that all the array elements are of the same size and no physical overlapping between elements would occur as opposed to the variable size technique for the linear polarization. A recent work proposed a single-layer reflectarray which supported tri-band operations [24]. Elements of different frequency bands were all placed on the same substrate. The polarizations of two of the three frequency bands were circularly polarized and the third one is linearly polarized. Since the two circularly polarized operations used the rotation technique and only the linearly polarized operation uses the variable size technique to achieve the required element reflection phase, physical overlapping among elements is unlikely to happen even three different elements are placed on the same substrate. For future advanced space applications, multi-band

operation is an imperative trend for the reflectarray design.

CP antennas are attractive to radars, satellite communications, and other modern wireless communication systems. A CP signal is less susceptible to the multi-path effect and is more effective in a non-line-of-sight transmission path. Planar antenna technology has primarily focused on the microstrip patch antennas. However, the microstrip patch antenna inherently has small impedance bandwidth and even smaller axial ratio (AR) bandwidth (AR < 3 dB) when it is configured as a CP radiator. The microstrip slot antenna (MSA) keeps the planar and light properties of the microstrip patch antenna. However, its impedance bandwidth is generally wider than the conventional microstrip patch antenna. The MSAs can be fed through the striplines [25], microstrip lines [26], and the coplanar waveguides (CPW) [27, 28]. The stripline-fed slot antennas have unidirectional radiation patterns, but may possibly cause the undesired parallel-plate modes. The CPW-fed technique has advantages over the microstrip-fed technique including lower dispersion loss and uniplanar configuration which eases the alignment problem during the fabrication.

The annular ring is one of the simplest structures and has contributed excellent results in the RF and millimeter wave applications [29]. Therefore using annular ring slots as the radiating elements can reduce the design complexity. A CPW line can feed a pair of annular ring slots simultaneously and achieves a very wide impedance bandwidth. Thus this configuration is beneficial for the construction of arrays.

The feature of the wide impedance bandwidth makes the MSA a suitable candidate for the broadband CP antenna. Perturbation to the radiating element is essential to the

generation of circular polarization. It is also well known that adding parasitic elements to the main radiating element can increase the bandwidth of the antenna. Thus a simple and intuitive method to design a broadband CP antenna is to choose the radiating element as a perturbed annular ring slot coupled with parasitic ring slots. In the case of array applications, the sequential rotation technique described in [30] can be applied to obtain a much wider impedance and 3-dB AR bandwidth.

Polarization diversity and frequency reuse are other methods that are equivalent to increasing the bandwidth of an antenna. Reconfigurable antennas can provide the desired diversified functionality. Depending on the design methodology, the reconfigurable antennas can have the frequency, pattern, or polarization reconfigurability. The piezoelectric transducer (PET) provides a good mechanism for achieving reconfigurability. Its movement is controlled by an external DC voltage and it does not consume DC power. It has the advantages of low loss, wide band, and easy implementation.

Dual linear polarized antenna or array is similar to the CP antenna. It can avoid the required precise alignment between two antennas in the single linearly polarized systems. It is also a good example of the frequency reuse and polarization diversity. In simultaneous transmit-receive applications, dual-polarized antennas with two-port connections offer an alternative to the commonly used bulky circulator or separate transmit and receive antennas. As mentioned earlier, the dual-layer structure supports the dual-band operation and antennas of the two frequency bands share the same aperture, which means more space is saved. With all these features, a dual-band and dual-

polarized antenna array fabricated on ultra-thin substrates should be suitable for airborne applications.

## 2. Dissertation organization

The contents covered in this dissertation include dual-band beam scanning reflectarray, low sidelobe level aperture coupled microstrip feed array, a new dual-band reflectarray configuration, wideband circularly polarized microstrip slot antenna and array, polarization reconfigurable microstrip antenna, and dual-band dual-polarized antenna array for airborne applications. This dissertation has seven chapters.

Chapter II presents the design of a dual-band (Ku/Ka band) beam scanning reflectarray for the planet cloud/precipitation radar application. The basic operation mechanism of the reflectarray is briefly introduced. Low sidelobe level aperture coupled microstrip arrays are designed to illuminate the reflectarray and provide the beam scanning capability. The reflectarray emulates the cylindrical/parabolic type of reflector antenna. New reflectarray elements are proposed to achieve the wide phase variation characteristic.

Chapter III introduces a new dual-band (C/K band) reflectarray configuration. Perforated patches loaded by slots at the ground plane are used as the radiating elements at C-band and rectangular patches directly loaded by slots are used at K-band. Radiating elements of both frequency bands are print on the same substrate to eliminate the blockage effect from the top layered occurred in the case where elements of two frequency bands are printed on separate substrates. No physical contacts between elements will occur as the sizes of the elements are changing.

Chapter IV proposes a novel wideband CP annular ring microstrip slot antenna and array. Firstly, two types of CPW-fed annular ring slot antennas are introduced to show the wideband characteristic of the MSA. Then a wideband CP MSA operating at the second resonant mode is presented. The proposed antenna element is arrayed with a triangular arrangement and sequential rotation technique to achieve a wider 3-dB AR bandwidth.

Chapter V describes a new method to achieve the polarization diversity for microstrip patch antenna. The proposed reconfigurable microstrip antenna can operate in both right-hand and left-hand CP modes. The PET provides the reconfigurability and is controlled by an external DC voltage. Two dielectric perturbers are attached to the PET and create perturbations for the patch to achieve circular polarization.

Chapter VI introduces a dual-band (S/X band) dual-polarized planar array antenna for airborne applications. The array antenna utilizes a dual-layer configuration to achieve dual-band operation. Circular patches are used as the radiating elements of the X-band array and are fed at two orthogonal points on the perimeter to obtain dual-linear polarization. The square ring microstrip antenna is used as the unit element of the S-band array and it also reduces the blockage effect. The feed points of the two polarizations are placed at orthogonal edges of two individual rings so that the coupling between two ports can be significantly reduced.

Finally, a summary of the research accomplishments in this dissertation and recommendations for further studies are provided in Chapter VII.

# CHAPTER II

# OFFSET LINEAR-ARRAY-FED KU/KA DUAL-BAND BEAM SCANNING REFLECTARRAY FOR PLANET CLOUD/PRECIPITATION RADAR*

## 1. Introduction

Spaceborne radar is a crucial technology to the research in the meteorology and topography of the Earth and other planets in the solar system. Recently, in order to obtain more accurate information of global rainfall, cloud density and surface topography of the Titan, JPL/NASA proposed the Titan Cloud Precipitation Radar and Altimeter (TCPRA) which features wide-swath scanning capability and improved observation resolution. Cylindrical reflectors fed by linear phased array antennas have found use in the area of radar applications. A prototype model of the advanced precipitation radar antenna utilizing parabolic cylindrical reflector made of a polymer membrane material is presented in [30]. An offset cylindrical reflector has been designed for the applications of automotive radar [31]. The analysis of line-source-fed single layer

microstrip reflectarray is reported by Sze [32]; however, only the numerical study is presented.

This chapter presents a 0.5-m Ku/Ka band dual-frequency shared-aperture linear-array-fed microstrip reflectarray antenna as a demonstration model for the next generation of JPL/NASA TCPRA. Most of the reflectarrays either have fixed beam directions or their main beams can be scanned at only one frequency by integrating tuning or switching devices with the reflectarray element. The reflectarray antenna in this work is capable of scanning the main beam at both frequency bands. In the recent work [30], the scannable cylindrical reflector has the ripple problem on the reflector membrane surface due to the improper material and the imperfect tension force. This problem can cause the degradation in the radiation patterns. An alternative solution is the linear-array-fed flat microstrip reflectarray which emulates the cylindrical reflector and provides advantages of lightweight, easy deployment, minimum surface distortions, and the wide angle cross-track scanning. An offset feed configuration is used to reduce the aperture blockage and the same dual-layer configuration is used for the reflectarray as reported in [13]. The reflectarray is printed on thin membranes to facilitate in-space large aperture folding or inflatable mechanism. Conventional weather radars utilize single-linear polarization technique to measure the precipitation reflectivity. However, this technique has limitations in accuracy and does not support the hydrometeor classification. On the other hand, radars using dual-linear polarization technique can obtain more detailed and accurate information of the precipitation and precisely identify the hydrometeor types. To meet the dual-linear polarization requirement, symmetric reflectarray elements of

variable sizes are used for the present design to obtain the required phase correction for each element. However, the phase correction is only required in one direction for this application. For the demonstration purpose, the feed arrays are only single-linear polarized. Two single-linear polarized aperture coupled microstrip feed arrays are designed at each frequency band to illuminate the reflectarray and provide the beam steering capability along the plane containing the feed array axis. In the final implementation, the feed arrays will have the electronic scanning capability to steer the main beam. The reflectarray was designed to have a cross polarization of -30 dB and a peak sidelobe level (SLL) of -25 dB with cross-track scanning angles of $0^o$ and $20^o$.

The concept of the dual-band circularly polarized reflectarray using the dual-layer configuration was introduced in the previous studies for communication applications [12-14]. However, the main beam direction of the reflectarray was fixed and the beam scanning was not possible. To utilize the reflectarray in radar applications, the beam scanning capability is normally required. The novelty of this work is that the proposed reflectarray antenna can achieve a wide cross-track scanning angle at both frequency bands with the use of two sets of feed arrays. The feed arrays designed in this work show very good results and are essential parts for the beam scanning. Moreover, a different phase control technique and new element types are chosen to achieve phase coherence and support dual-linear polarization. The new types of reflectarray elements proposed in this chapter also yield very wide and linear phase variation curves.

## 2. Basic reflectarray operation theory

The descriptions of the operation theory of the reflectarray in this section are referenced from [21]. Figure 1 shows the geometry of a microstrip reflectarray. A feed antenna is placed at the focal point to illuminate the reflectarray. When the wave from the feed antenna is incident on the reflectarray surface, the elements of the reflectarray will reradiate the incident energy into the space. However, as can be seen from Figure 1, the incident path length ($D_1$, $D_2$, …, $D_n$) for the field propagating from the feed antenna to the elements are different. Therefore the reradiated field will not be coherent. The key to the reflectarray design is to adjust the reflection phases of the elements to compensate for the path length differences so that the reradiated field from each element would be collimated towards one specific direction.

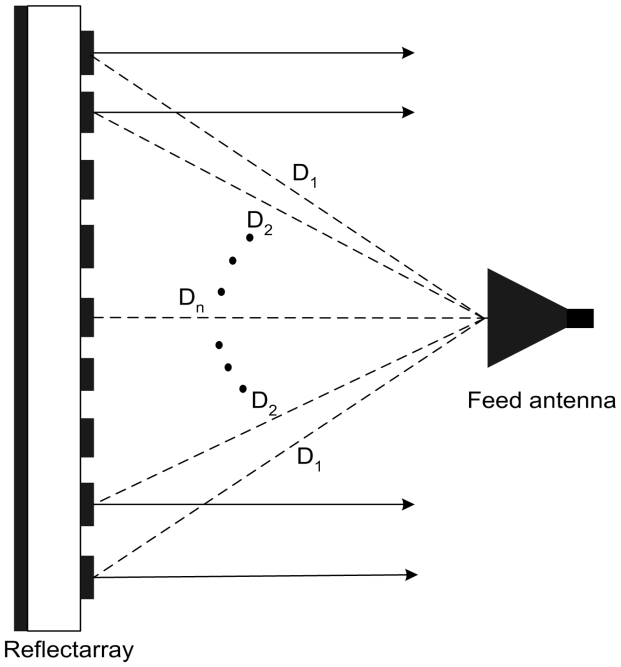


Fig. 1. Geometry of a microstrip reflectarray.

Figure 2 shows a reflectarray aperture illuminated by a feed antenna located at $r_f$. The reradiated field from an element on a rectangular reflectarray aperture with M x N elements in an arbitrary direction, $\hat{u}$, will be of the form

$$E(\hat{u}) = \sum_{m=1}^{M}\sum_{n=1}^{N} F(\vec{r}_{mn}\cdot\vec{r}_f)A(\vec{r}_{mn}\cdot\hat{u}_o)A(\hat{u}\cdot\hat{u}_o)\exp\left\{-jk_o\left[\left|\vec{r}_{mn}-\vec{r}_f\right|+\vec{r}_{mn}\cdot\hat{u}\right]+j\alpha_{mn}\right\} \qquad (1)$$

Where $F$ is the pattern function of the feed antenna, $A$ is the pattern function of the reflectarray element, $r_{mn}$ is the position vector of the mnth element, $\hat{u}_o$ is the desired main-beam angle, and $\alpha_{mn}$ is the required phase delay provided by the element.

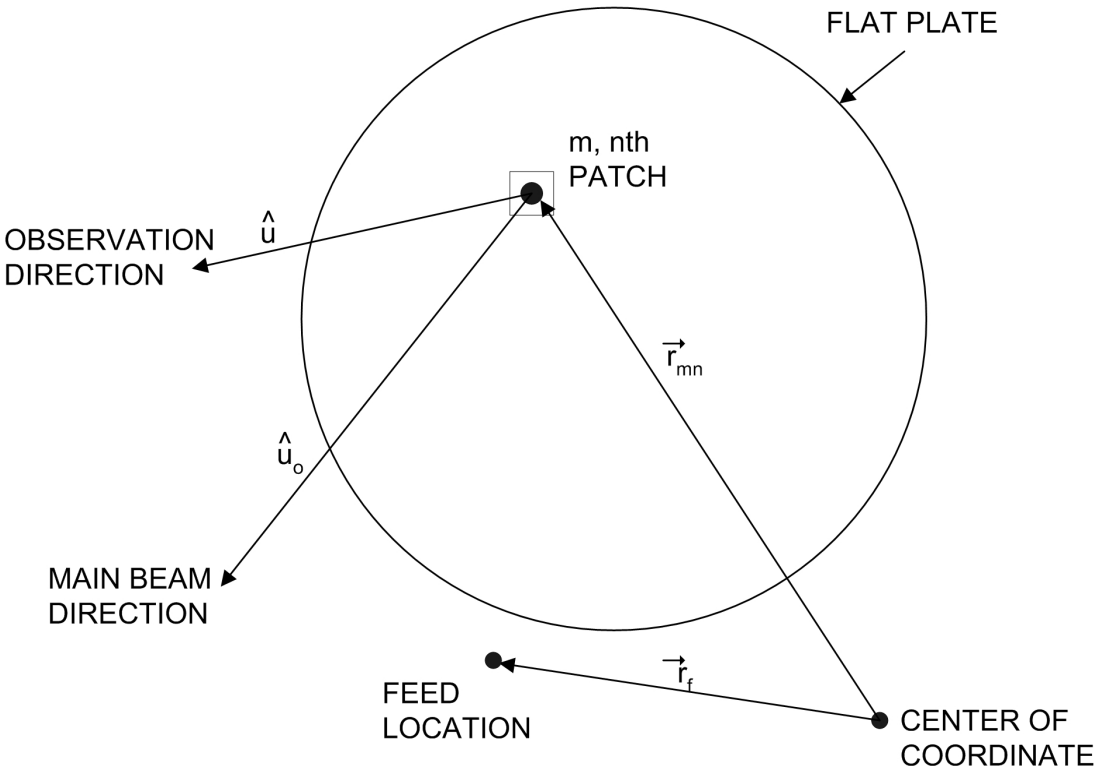


Fig. 2. Coordinate system for reflectarray pattern analysis [21].

Equation (1) is valid for a rectangular array with M x N elements. For an array with circular aperture, the elements outside the circular aperture should not be included in the summations. To achieve a phase coherent beam in the desired main beam angle, the following equation should hold

$$\alpha_{mn} - k_o \left[ \left| \vec{r}_{mn} - \vec{r}_f \right| + \vec{r}_{mn} \cdot \hat{u}_o \right] = 2n\pi, \qquad n = 0, 1, 2, \cdots \tag{2}$$

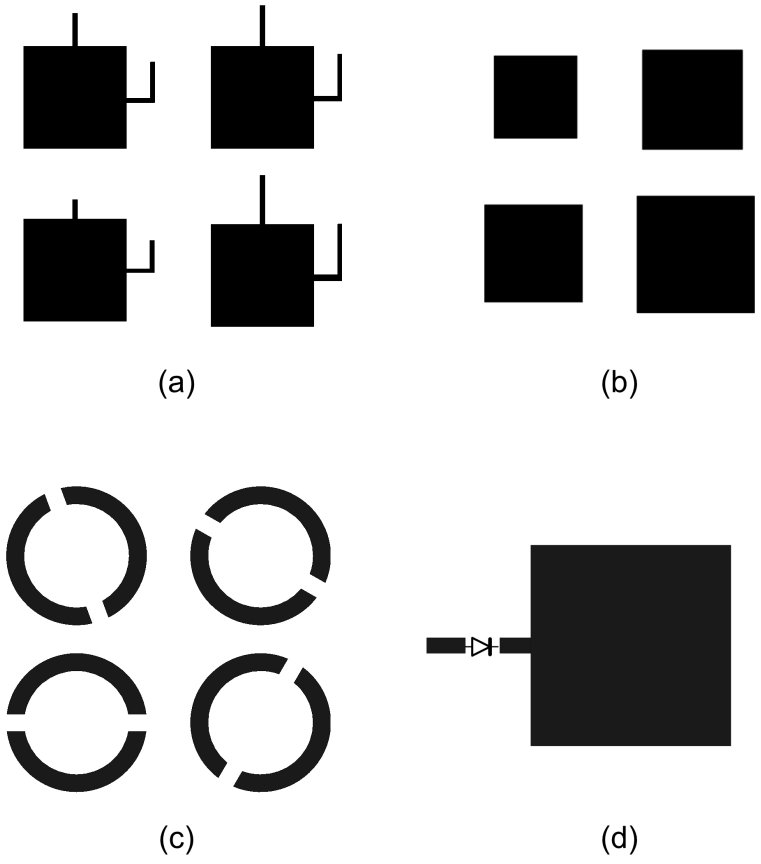


Fig. 3. Examples of the element types of different reflectarray phase control techniques: (a) variable stub length (b) variable element dimensions (c) angular rotation (d) integration with tuning devices.

There are several methods to control the reflection phase of the elements. Figure 3 illustrates four commonly used methods. The first method is to use microstrip patches with different feeding stub lengths. By adjusting the length of the stub, the reflection phase of the element could be controlled. The second reflection phase control method is to use elements with different dimensions. For a circularly polarized element, its reflection phase can be controlled by the rotation angle of the element. It is also possible to control the reflection phase by integrating MEMS devices, oscillators, and varactor diodes into the reflectarray elements. However, the last method always increases the design complexity and manufacturing cost of the reflectarray.

## 3. Design and performance of the feed arrays

Two horizontally polarized aperture coupled microstrip arrays with main beam directions at broadside and $20^{o}$ off broadside, which will be named as the "broadside feed array" and the "scanned feed array", serve as offset feeds to illuminate the reflectarray at each frequency band. The challenges in the feed array design are to achieve the -25 dB peak sidelobe level with the presence of the complicated feeding networks. The feed arrays are mounted on the supporting arm and placed along the focal line of the reflectarray. Each array has 2 elements in the vertical direction and 32 elements in the horizontal direction. Figure 4 shows the schematic layout of the feed array and the unit aperture coupled patch element. The design parameters and dimensions are also given in Figure 4. Photos of the Ku band feed arrays are shown in Figure 5. A large microstrip feed array often suffers from high insertion loss due to the

presence of the lengthy feeding networks. The problems associated with this high feed loss, in a future practical system, will be mitigated by using distributed transmit/receive (T/R) amplifier modules. The feeding networks also produce spurious radiation, which degrades the performance of sidelobe and the cross polarization levels. In consideration of the harmful effects of the feeding networks, aperture coupled microstrip array configuration is selected for the feed array. The feeding networks are isolated from the patch layer by the ground plane. Thus the spurious radiation from the feeding networks will be reduced to the minimal extent and the design of the feed lines can be more flexible.

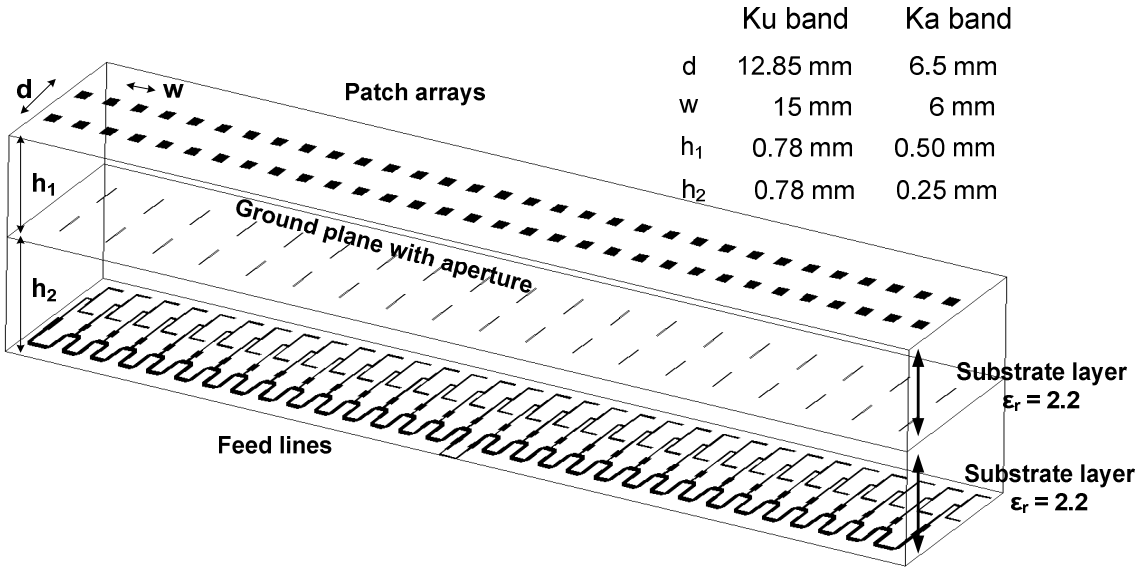


(a)

Fig. 4. Geometry of the aperture coupled feed antenna array element (a) 2 by 32 aperture coupled patch array (b) layout and dimensions of the aperture coupled patch element.

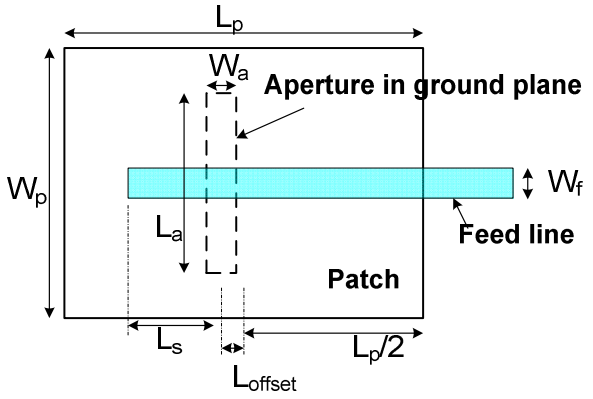


Parameters of the aperture coupled patch element

| Parameters (in mm) | $W_p$ | $L_p$ | $W_a$ | $L_a$ | $L_s$ | $L_{offset}$ | $W_f$ |
|---|---|---|---|---|---|---|---|
| Ku-band | 4.35 | 5.8 | 0.65 | 3.36 | 2.815 | 0 | 0.675 |
| Ka-band | 1.7 | 2.256 | 0.3 | 1.5 | 1.128 | 0.05 | 0.3 |

(b)
Fig. 4. Continued.

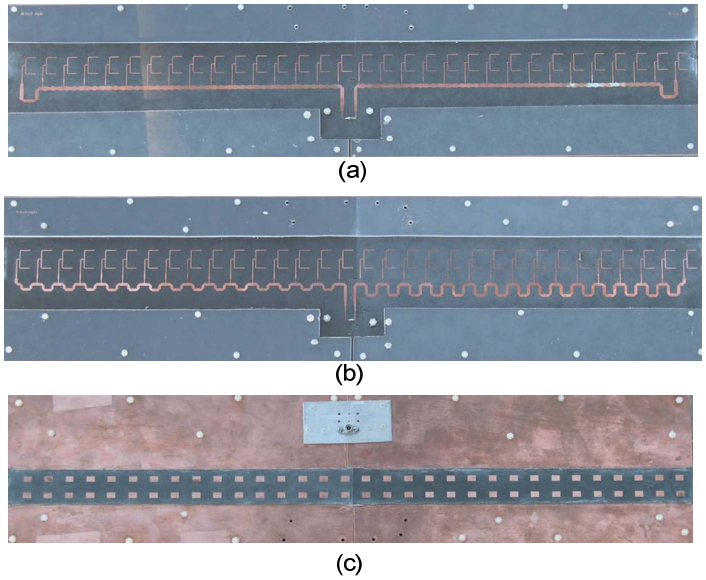


Fig. 5. Photos of Ku band feed array (a) feed lines of broadside feed array (b) feed lines of scanned feed array (c) radiating patches.

A. Design approaches and analysis

Two linearly polarized feed arrays are required at each frequency band with main-beam location at $0^o$ and $20^o$. The criteria to avoid the grating lobes can be written as

$$kd + kd\sin\theta_o < 2\pi - (2\pi / N) \tag{3}$$

From this equation, the element spacing is presumably selected to be 0.7 free space wavelengths at both bands with the total number of element equal to 32. To have less than – 25 dB side lobe level, a -30 dB Dolph-Tchebyscheff distribution is adopted. The excitation coefficients are obtained using the formula given by Elliott [33]:

$$I_n = I_{-n} = \sum_{p=n}^{N/2} (-1)^{(N/2)-p} \frac{N-1}{N+2(p-1)} \frac{(N/2+p-1)!}{(2p-1)!(N/2-p)!} \frac{(2p-1)!}{(p-n)!(p+n-1))!} a^{2p-1} \tag{4}$$

$$a = \cosh\left(\frac{1}{N-1}\cosh^{-1} b\right) \tag{5}$$

$N$ is the total number of elements of the array and $I_n$ is the excitation coefficient of the $n^{th}$ element from the center of the array. To determine the value of $a$, the desired main beam to side lobe level ratio $b$ needs to be specified in voltage ratio. For this design, its value is 31.62. Figure 6 shows the required amplitude distribution for 16 elements of the one half part of the array. The distribution is symmetric on both sides of the feed array with respect to the feed point at the center. With symmetry applied to the other half part of the array elements, the array factor is simply expressed as

$$AF_{2M} = \sum_{n=1}^{M=16} I_n \cos[(2n-1)\frac{\pi d}{\lambda}\cos\theta] \tag{6}$$

where $d$ is the element spacing, $\lambda$ is the free-space wavelength, and $\theta$ is the beam scanning angle.

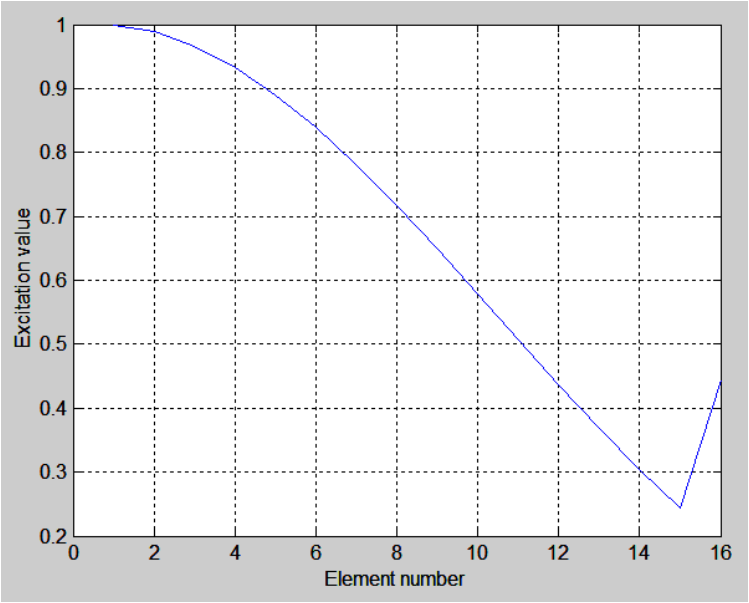


Fig. 6. Required amplitude distribution for -30 dB side lobe level.

To determine an expression for the conductance for a given Dolph-Tchebyscheff distribution, let's say the power absorbed by the last element be $P_N$. The element conductance is assumed to be proportional to the square of the amplitude excitation coefficient. That is, $g_n = KI_n^2$, where $K$ is the constant of proportionality. Since the power after the last element is the load power, $P_L$, the incident power must be $P_N + P_L$. The normalized conductance can therefore be expressed as

$$g_N = \frac{P_N}{P_L + P_N} \tag{7}$$

The power incident on the next to last element is $P_L + P_N + P_{N-1}$. The conductance is

$$g_{N-1} = \frac{P_{N-1}}{P_L + P_N + P_{N-1}} \tag{8}$$

Continuing with this analysis, an expression can be found for any conductance in the array

$$g_n = \frac{P_n}{P_L + \sum_{i=n}^{N} P_i} = \frac{P_n}{1 - \sum_{i=1}^{n-1} P_i} \tag{9}$$

Where the second expression in equation (7) results from the fact that the sum of the radiated and load power is set equal to one. This allows the determination of the constant of proportionality, $K$, between $I_n$ and $P_n$. Solving for $K$ and with the normalization of the power, we get

$$K = \frac{1 - P_L}{\sum_{n=1}^{N} I_n^{\,2}} \tag{10}$$

and

$$g_n = \frac{K I_n^{\,2}}{1 - \sum_{n=1}^{N} K I_n^{\,2}} \tag{11}$$

The resulting input impedances looking into the sub-arrays (2 by 1 array) at the input of the main feed line are calculated with $P_L$ equal to zero and Figure 7 shows the calculated values versus the element index.

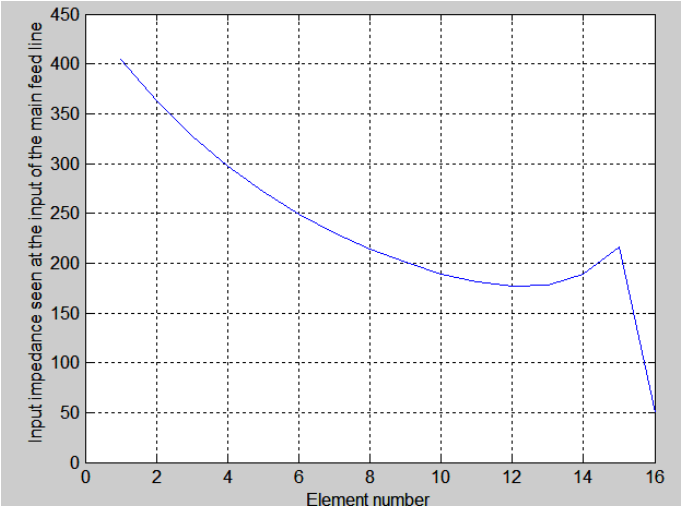


Fig. 7. Input impedances looking into the sub-arrays input of the main feed line versus element index.

Figure 8 shows an array factor power pattern of a 32-element broadside Dolph-Tschebyscheff array. The mainbeam angle is at $90^{o}$ which refers to the broadside direction of the array.

Low dielectric constant substrates are selected to reduce the possibility of surface wave excitation and increase the efficiency. The substrate material used is RT/duroid 5880 with a dielectric constant of 2.2. The array element spacing is properly chosen to avoid creating grating lobes. In this study, the length of the Ku band feed arrays is close to the side length of the reflectarray. However, the length of the feed arrays at Ka band is scaled down by the frequency ratio of (14/35) so that its beamwidth in E-plane is similar to that at Ku band.

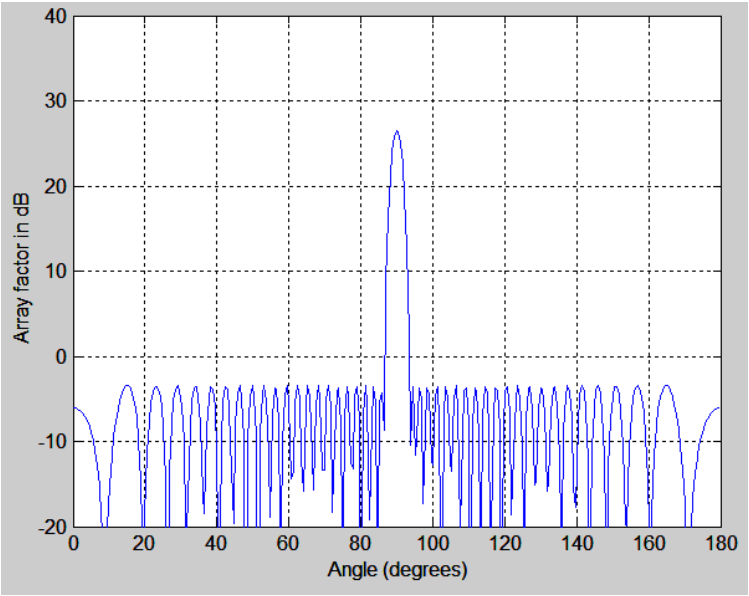


Fig. 8. Array factor of a 32-element Dolph-Tschebyscheff array.

For the broadside feed array at both frequency bands, the transmission line connecting each sub-array is designed to provide a progressive phase shift that is a multiple of $360^o$. For the scanned feed array, a linear phase taper has to be applied across the array. Due to the center-fed configuration, one half part of the array has a progressive phase shift of $86.2^o$ between adjacent sub-arrays from the center sub-array to the one at the end, whereas the other half part needs a progressive phase shift of $-86.2^o$ from the center to the other end. Such an arrangement will yield a single main beam at either $20^o$ or $-20^o$ off broadside other than two main beams at $\pm 20^o$. The main meander connecting transmission lines have a characteristic impedance of 50Ω. The simulations of the feed arrays are performed by using Zeland's IE3D to show and prove the design concepts.

B. Ku band feed arrays

The measured return loss at 14.1 GHz is 12 dB for the broadside feed array and is 12.3 dB for the scanned feed array. Figure 9 shows the typical normalized radiation patterns of both feed arrays. For the broadside feed array in Figure 9(a), the peak SLLs in the E-plane are -17.2 dB/-15.2 dB (left/right) and the average SLL is below -25 dB. The average SLL is defined as a measure of the power in the pattern excluding $\pm 10^o$ from the main beam peak. The half power beamwidth (HPBW) of the main beam is $2.8^o$. The cross-polarization level is -27.5 dB near the main beam region and below -30 dB outside. For the scanned feed array, the main beam in E-plane is located near $20^o$ with an HPBW of $3.95^o$ as shown in Figure 9(b). The peak SLLs are -22 dB/-26 dB (left/right) and the average level is below -25 dB. Lower than -30 dB cross polarization level within

the main beam is observed. The measured peak gain is 17.4 dBi for the broadside feed array and 16.9 dBi for the scanned feed array. The directivity of each array is calculated based on measured co-polarized patterns in the E-plane and H-plane. It is obtained by taking the ratio of the radiation intensity in a given direction to the total power radiated by the antenna divided by $4\pi$. The loss factor of the array, defined as the difference between the directivity and the measured peak gain, is 7.1 dB for broadside array and 8.1 dB for scanned array. The feed lines are covered by the microwave absorbers in the measurement to minimize the back radiation. It should also be noted that in order to obtain a low sidelobe level, the symmetry of the amplitude distribution on both sides of the feed array should be retained and the progressive phase shift errors need to be minimized. Ku band feed arrays are cut into two sections due to the size limitation of the panel in the etching facility. The two sections are then combined together and probe-fed at the center of the combined microstrip line. It is found out that the probe is very sensitive to fabrication and alignment errors and combining the two panels aggravates these problems. For Ka band feed array, only one panel is sufficient because of the short length. This is the reason that the radiation pattern performances of the Ka band feed arrays as discussed below are in general better than those of the Ku band feed arrays.

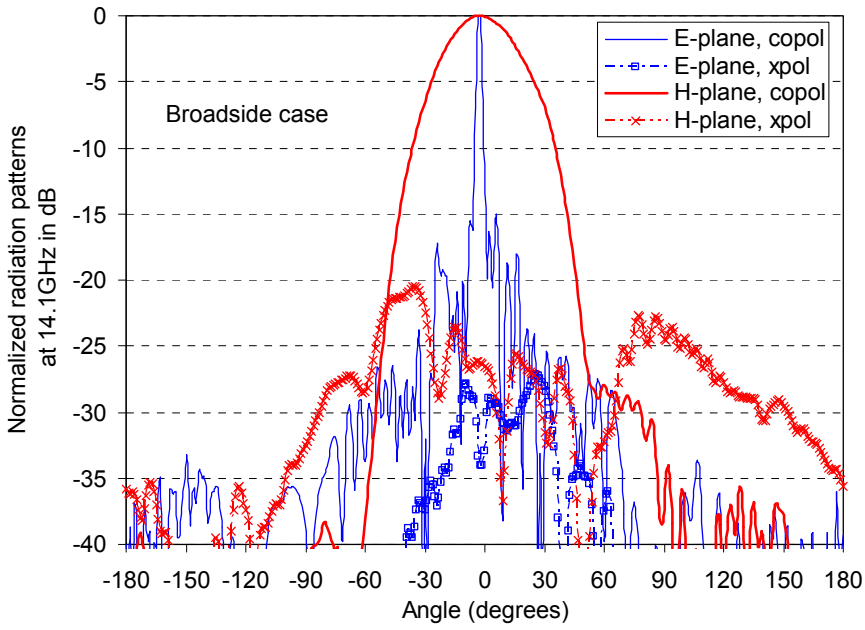


(a)

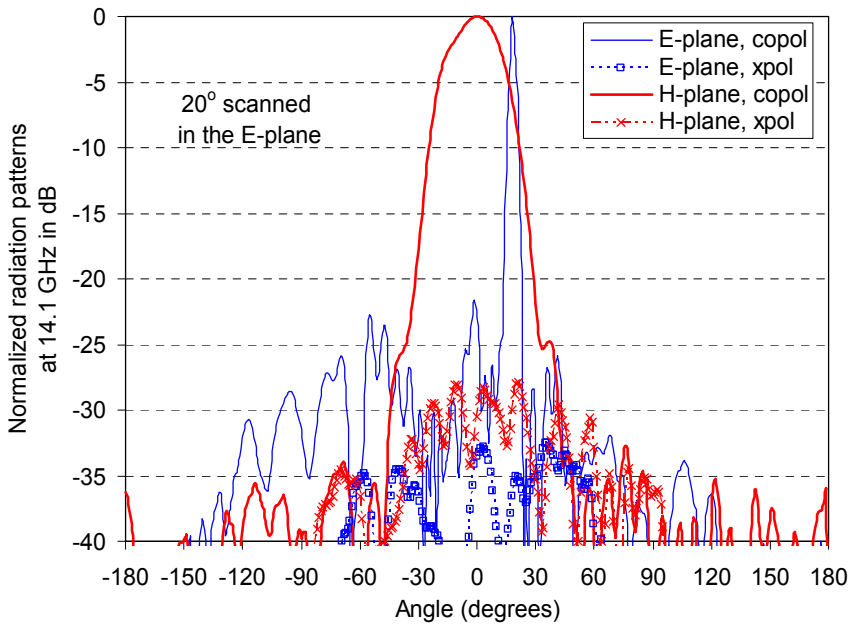


(b)

Fig. 9. Measured normalized feed array patterns in two-principal planes at Ku band (a) broadside (b) 20° scanned.

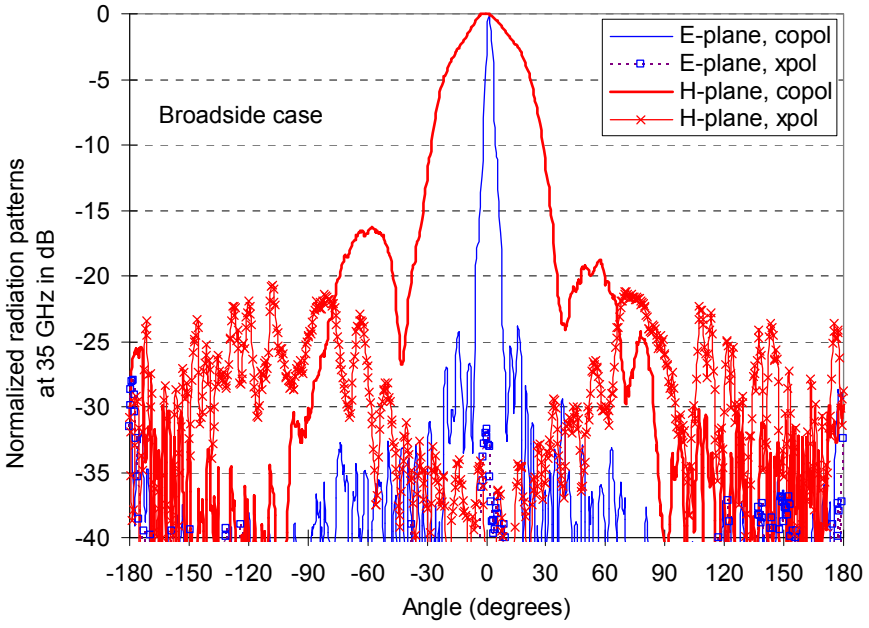


(a)

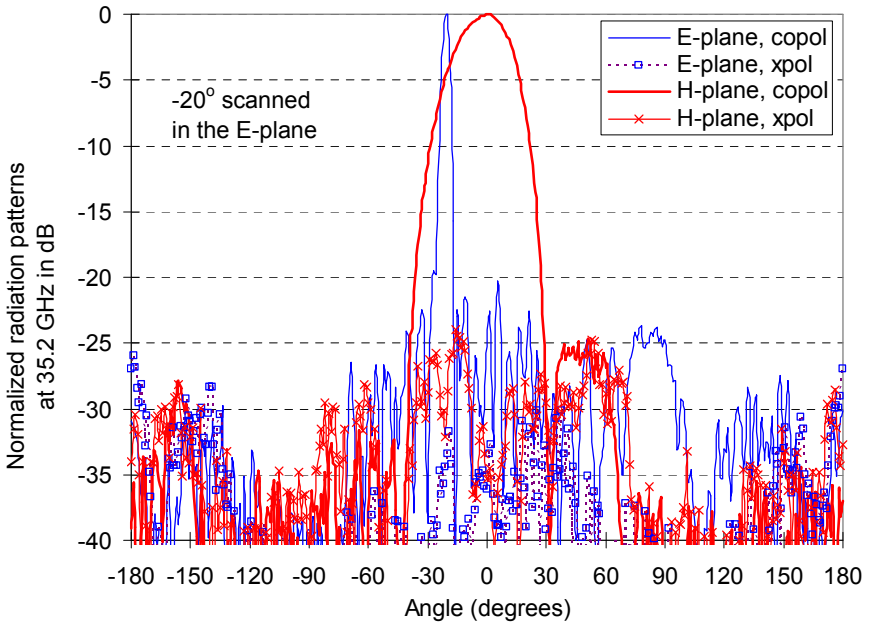


(b)

Fig. 10. Measured normalized feed array patterns in two-principal planes at Ka band (a) broadside (b) -20° scanned.

C. Ka band feed arrays

The measured return loss at 35 GHz is 17 dB for the broadside feed array and is 12 dB for the scanned feed array. Well-behaved feed array patterns are observed at Ka band. Typical normalized radiation patterns for the broadside feed array at 35 GHz are shown in Figure 10(a). For the broadside feed array, the peak SLLs in the E-plane are -24 dB with an average level well below -30 dB. The half power beamwidth (HPBW) of the main beam is $3.52^{o}$. The cross polarization levels within the main beam are lower than -30 dB in both E- and H-planes. The measured peak gain and the loss factor of the array are 17.45 dBi and 7.03 dB. Figure 10(b) shows the normalized radiation patterns for the scanned feed array at 35.2 GHz. The measured beam peak in E-plane is located near $-20^{o}$, which is close to the desired scan angle. The reason that the angle is $-20^{o}$ instead of $20^{o}$ is because the feed line is printed on the substrate in the opposite direction to that of the Ku band feed array. The HPBW is $3.71^{o}$. The peak SLLs are -22.5 dB/-20.5dB (left /right) and the average level is below -25 dB. The measured peak gain and the loss factor are 18.82 dBi and 6.22 dB.

## 4. Reflectarray design

The reflectarray has dual-layer configuration with Ku band layer on top of Ka band layer to support dual-frequency operation. The schematic drawing and the close-up picture of the reflectarray elements with their dimensions at both bands are shown in Figure 11. Double ring elements are used for Ku band, while a ring with an inner circular patch are used for Ka band. These element configurations are selected to achieve

a wider range of the reflection phase variation. The ring-patch combination at Ka band provides a more linear phase variation. However, it can not be used in Ku band because the circular patch will block the Ka band incident wave. The element spacing is 0.56 free-space wavelength at Ku band and 0.64 free-space wavelength at Ka band. Substrates used for the reflectarray are Rogers R/flex 3000 liquid crystalline polymer (LCP) materials with $\varepsilon_r = 2.9$ and 0.0508 mm in thickness. As shown in Figure 11(b), the element sizes are dependent on the variables $R_1$ and $R_2$. The reflection phase of each element changes with these variables and is simulated with Ansoft's HFSS using the H-wall waveguide approach mentioned in [34]. While the size of a reflectarray element differs from that of its neighboring elements, this simulation approach assumes an infinite periodic array environment with normal incident wave to optimize the element sizes. A foam layer ($\varepsilon_r = 1.06$) is inserted below both reflectarray layers to support the structure and to reduce the rapid reflection phase change near resonance.

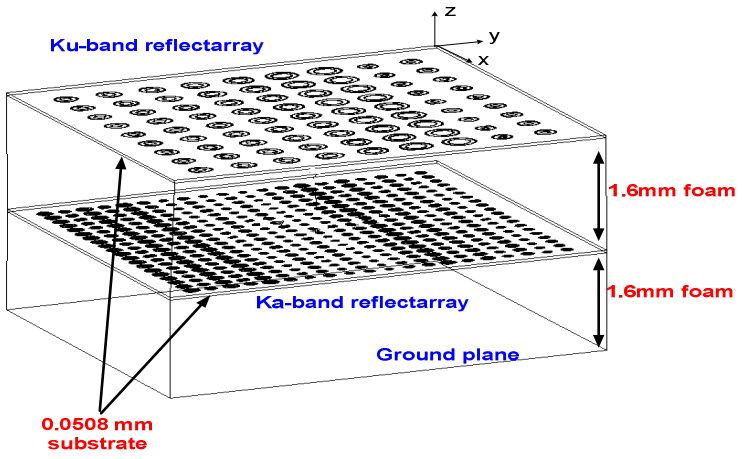


(a)

Fig. 11. Schematic and close-up views of the reflectarray (a) dual layer configuration (b) unit reflectarray elements (c) close-up view of fabricated reflectarrays.

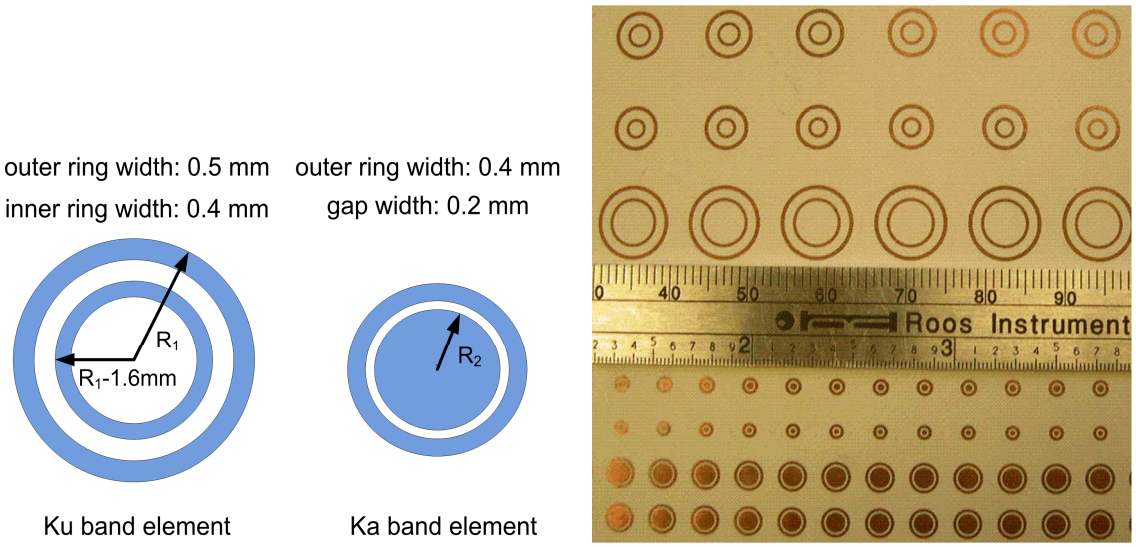


(b) (c)

Fig. 11. Continued.

Figure 12 shows the simulated reflection phases against the element size controlling variables at two frequency bands. Since the element unit cell dimensions at Ka band are only 5.5 mm x 5.5 mm, the range of the size variation for a single array element is limited. Thus accommodating elements with variable sizes into unit cells to achieve a sufficient phase variation range is a big challenge in the reflectarray design. Three different curves at Ka band are compared in Figure 12(b). Neither the ring nor the circular patch alone can provide a sufficient phase variation range for a practical reflectarray design. With the proposed ring-patch combination, it is found that the resulting phase curve is very linear and provides a sufficient phase range. As shown in Figure 11(c), the sizes of elements within a column are individually varied corresponding to their required reflection phase. However, element sizes are kept constant within a row.

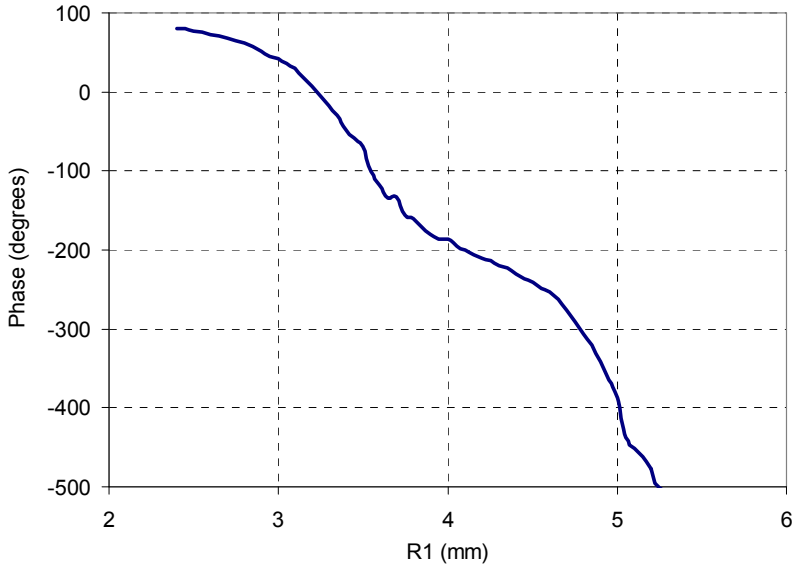


(a)

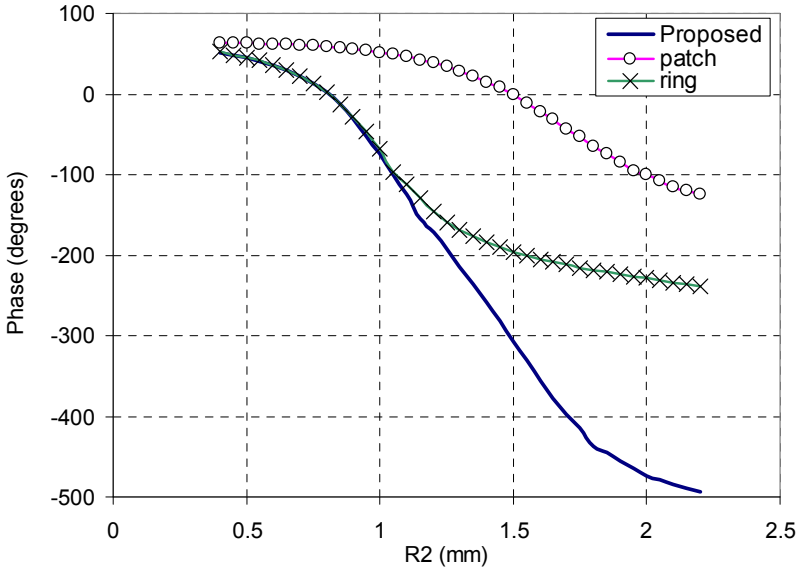


(b)

Fig. 12. Simulated reflection phases versus the element size controlling variables at two frequency bands. (a) Ku band (b) Ka band.

Both the Ku and Ka band reflectarray layers have a size of 0.5 m x 0.5 m. Since the reflectarray emulates the cylindrical reflector antenna, it only focuses the energy in the vertical direction (H-plane). The definitions of the E and H-planes of the reflectarray are depicted in section 5. In the horizontal direction (E-plane or cross-track plane), the reflectarray acts as a mirror and the beam focusing is done by the feed arrays which also enable the beam steering functionality in the same plane. Therefore the main beam of the reflectarray in the E-plane is expected to occur in the direction of broadside with broadside feed arrays and $20^{o}$ or $-20^{o}$ off broadside with scanned feed arrays depending on the fabrication direction. The pattern characteristics in the E-plane also resemble the E plane pattern characteristics of the feed array. The offset feed configuration is adopted to avoid the blockage of the feed array. It is well known that the beam squint effects can be minimized by choosing the incidence angle of the feed array close to the main beam scan angle [7]. Therefore the H-plane main beam scan angle is designed to be $20^{o}$ for both frequency bands, which can be achieved by controlling the phase variations of elements in the vertical direction of the reflectarray. The square aperture of the reflectarray is used to reduce the spillover loss from the wide beam scanning [30]. The excitation amplitude across the aperture has significant influence on the directivity and SLL of the reflectarray radiation patterns. A trade-off exists between the directivity and the SLL. The uniform excitation amplitude for the reflectarray aperture gives the highest directivity and SLL. Tapering the excitation amplitude reduces the sidelobe levels. The sidelobe levels in both principal planes are controlled separately. In the E-plane of the reflectarray, since the feed array gives a severely tapered illumination, very low sidelobe

levels can be expected. In the H-plane, the feed arrays are designed to illuminate the reflectarray with edge tapers of -13 dB at Ku band and -15 dB at Ka band. According to [35], when the aperture in the vertical direction is illuminated with a cosine on a pedestal field distribution with -10 dB edge illumination, the lowest achievable SLL in the vertical plane for a cylindrical reflector is -20 dB assuming a uniform line source in the horizontal direction. Thus, with the -13 dB and -15 dB edge illumination for the reflectarray, it is expected that SLL of lower than -20 dB can be achieved in the H-plane.

## 5. Experimental results of the system

Measurements of the reflectarray are conducted in the anechoic chamber at Texas A&M University with the range of 10 meters. For the purpose of simplicity, in the following descriptions, the reflectarray with the broadside feed array is named “case 1” and the reflectarray with the scanned feed array is named “case 2”. The schematic views and the photos of three different measurement settings are shown in Figure 13. A diagram in Figure 13(c) shows the anticipated beam directions of the reflectarray and the measurement cuts for the E and H-plane. The B-o-S plane is $20^{o}$ off the reflectarray’s broadside direction and represents E-plane cuts of case 1 and case 2; the B-o-y (y-z) and S-o-y planes represent respectively the H-plane cuts of case 1 and case 2. The theoretical main beam angles for all states are listed in Table 1.

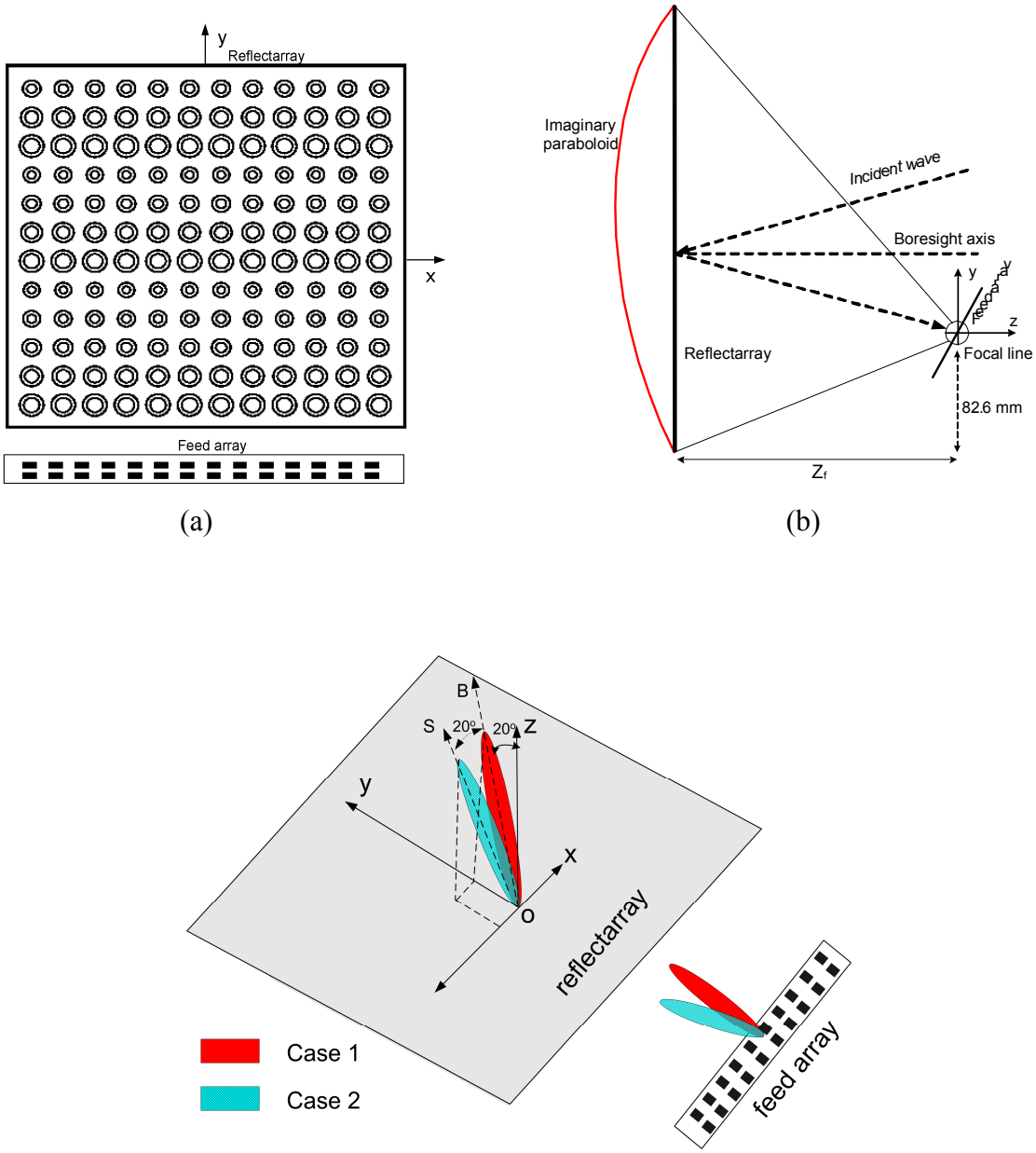


Fig. 13. Schematic of the system and photos of three different reflectarray measurement setups. (a) front view, top: reflectarray, bottom: feed array (b) side view (c) diagram showing the main beam directions (d) H-plane measurement for case 1 (e) H-plane measurement for case 2 (f) E-plane measurement.

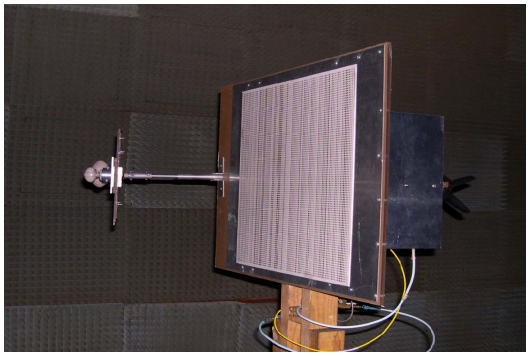

(d)

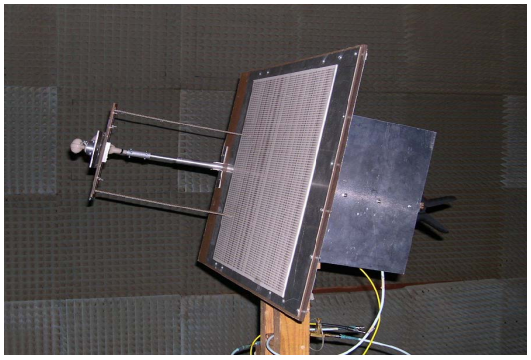

(e)

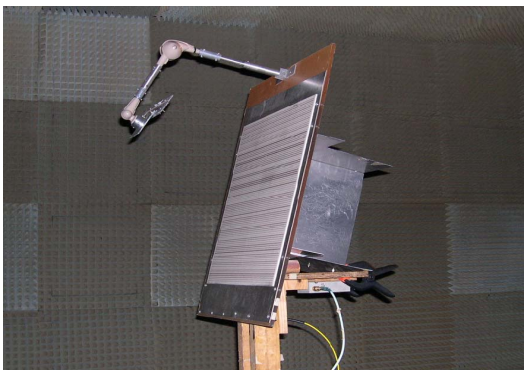

(f)

Fig. 13. Continued.

TABLE 1. Theoretical main beam angles of the reflectarray

| parameters | E-plane | | H-plane | |
|---|---|---|---|---|
| | case 1 | case 2 | case 1 | case 2 |
| Ku band | $0^o$ | $20^o$ | $20^o$ | $20^o$ |
| Ka band | $0^o$ | $-20^o$ | $20^o$ | $20^o$ |

As can be seen in the diagram, some of the measurement cuts take place in planes other than the reflectarry's two principle planes (x-y and y-z planes) so that the measurement cuts can pass through the main beam peaks. In the H-plane measurement, the reflectarray aperture sits vertically on the rotatable mount in the chamber with broadside feed array, whereas with the scanned feed array it is tilted by $20^{o}$. In the E-plane measurement, it is tilted by $20^{o}$ with both the broadside and scanned feed array. In Figure 13(d)-(f), only the reflectarray with the Ka band feed array is shown and the exposed ground plane is covered by absorbing materials to minimize the harmful effects during the measurements. The pattern measurements with scanned feed array are very time consuming due to accuracy in the alignment process because the base of the fixture has to be raised up by the designed angle on one side. The measurement settings for Ku band are similar to those shown in Figure 13. The focal line is located at a distance $Z_f$ above the reflectarray. $Z_f$ is equal to 261.5 mm at Ku band and 331.4 mm at Ka band in the current design.

A. Ku band results

It should be noted that the range of the anechoic chamber at Texas A&M University is smaller than the generally required distance for far-field distance. Measuring the antenna in an insufficient far-field range could yield some detrimental effects on the radiation patterns including filling the nulls between sidelobes, increase in SLL and decrease in gain. It is believed that the measurement results will be improved if an outdoor far-field range is available. Normalized radiation patterns at 14.1 GHz are given

in Figure 14 and Figure 15. Major pattern characteristics including SLL, cross polarization level and beamwidth, etc. are summarized in Table 2. In case 1, the main beam peak is at boresight for the E-plane and is at $22.5^{o}$ for the H-plane. Cross polarization levels are less than -30 dB outside the main beam region. The measured peak gain is 28 dBi. Based on the measured HPBW in both planes, the estimated directivity is calculated to be 35.4 dB using the equation in [36]. The maximum directivity calculated from the aperture size is 38.4 dB. The aperture efficiency of the reflectarry is calculated by comparing the measured gain and the maximum reflectarray directivity. The loss factor of the feed array has to be compensated to calculate the pure reflectarray efficiency. The aperture efficiency for this case is calculated to be 45.4 %. In case 2, the main beam peaks occur at $17^{o}$ for the E-plane and at $-22.5^{o}$ for the H-plane. The measured peak gain for this case is 28.6 dBi and the calculated aperture efficiency is 67.5 %. It is observed that the measured beam angles depart from those listed in Table 1, showing the misalignment of feed arrays to the true focal line. The minus sign in the H-plane beam angle of case 2 indicates that the reflectarray aperture is placed in a reverse position in favor of locating the measurement cuts during the experiments. Two reasons account for the slightly degraded pattern performance at Ku band: First, the gravitational loading of the heavier feed array makes the supporting arm slant and the feed array deviated from the focal line leading to degraded H-plane patterns. Secondly, two panels are combined at Ku band. The fabrication and alignment errors of the feed array cause the E-plane patterns to be not as good as those at Ka band. However, the E-plane patterns at Ku band still verify the cross-track scanning capability of the reflectarray.

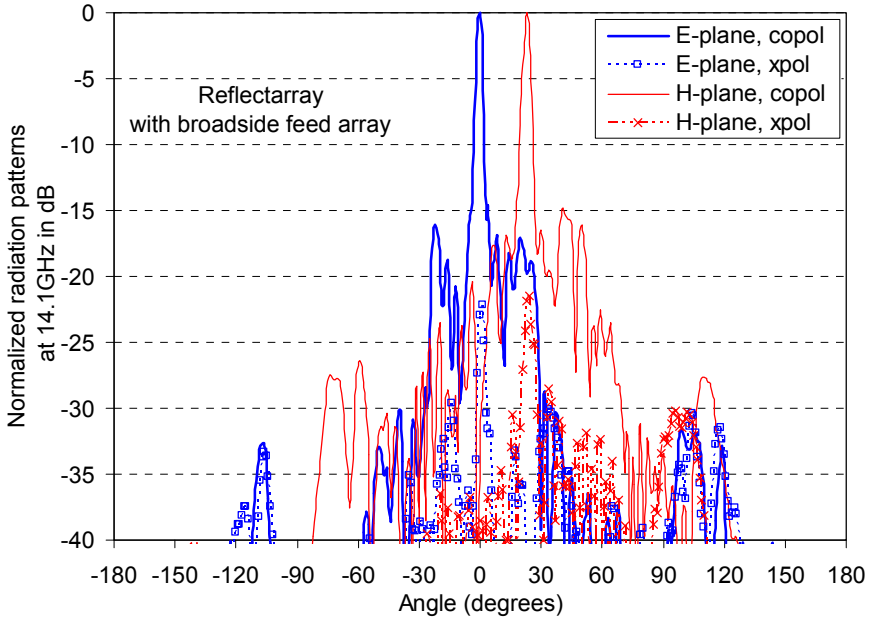


Fig. 14. Measured normalized radiation patterns of case 1 at 14.1 GHz.

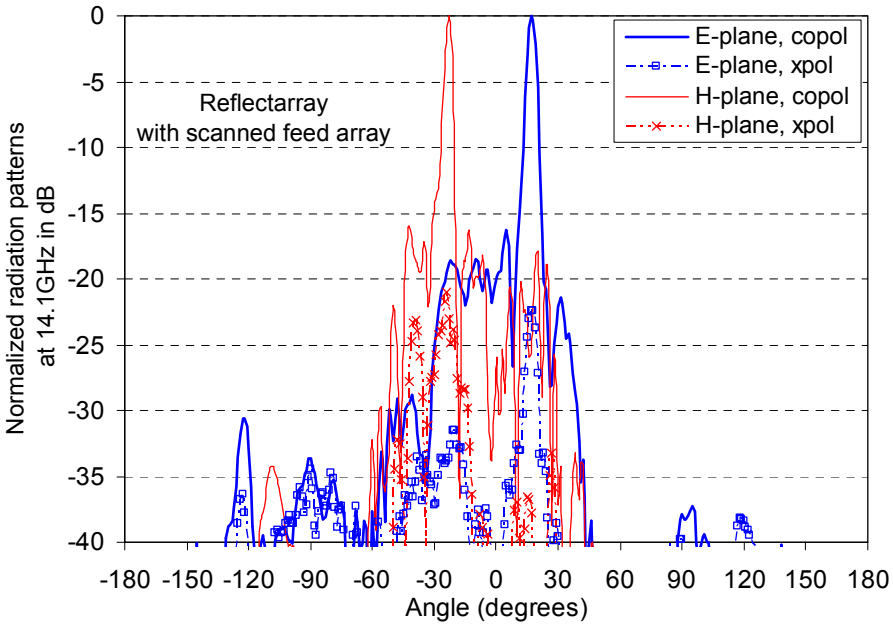


Fig. 15. Measured normalized radiation patterns of case 2 at 14.1 GHz.

B. Ka band results

Normalized radiation patterns of case 1 at 35 GHz are shown in Figure 16. The main beam peak is at boresight for the E-plan and at 21$^{o}$ for the H-plane. Good SLLs and cross polarization levels are observed and summarized in Table 2. Except for the near-in peak sidelobes and the cross polarization levels inside the main beam region, all other SLLs and cross polarization levels are well below -30 dB. The measured peak gain for this case is 29.9 dBi. Normalized radiation patterns of case 2 at 35.2 GHz are shown in Figure 17. The main beam peaks of the E-plane and H-plane are located at -23$^{o}$ and 18.5$^{o}$. Again, the discrepancy between the measured and theoretical main beam angles is primarily due to the inaccurate manual operation of the antenna alignment during the measurements. The measured peak gain is 31.4 dBi. Other pattern characteristics can be seen in Table 3. As expected, similarities are observed between the E-plane patterns of the reflectarray and its feed array in each case. Therefore the cross-track scanning capabilities of the reflectarray using feed arrays are successfully demonstrated and verified at Ka band as well. Though the measurements are not able to be done in the good far-field range, the measured patterns shown here are considered very well-behaved especially at Ka band. Ideally, the maximum reflectarray directivity calculated based on the physical aperture area is 46 dB at 35 GHz. However, since the length of the Ka band feed arrays are shrunk down to have similar beamwidth to Ku band in the E-plane pattern, it is more reasonable to consider the aperture size in the horizontal direction to be the length of the feed array. The calculated maximum directivity then becomes 42 dB. Because the range of the antenna chamber is not long enough to support

the far field measurements at Ka band, the aperture efficiencies at Ka band are estimated. Since in the previous few projects, the reflectarray measured in the far-field range at JPL picked up 3 to 4 dB higher in gain as compared to that measured in the antenna chamber at Texas A&M University, the aperture efficiencies of the two cases at Ka band are estimated by adding 3 dB to the measured gains. The aperture efficiency is estimated to be 61.73 % for the case 1 and 71.29 % for the case 2 after adding 3 dB to the measured gain.

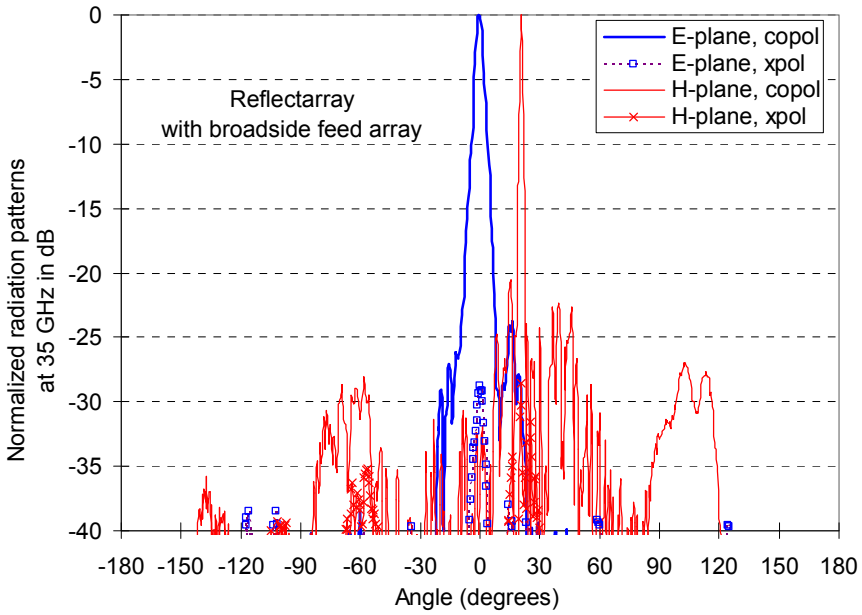


Fig. 16. Measured normalized radiation patterns of case 1 at 35 GHz.

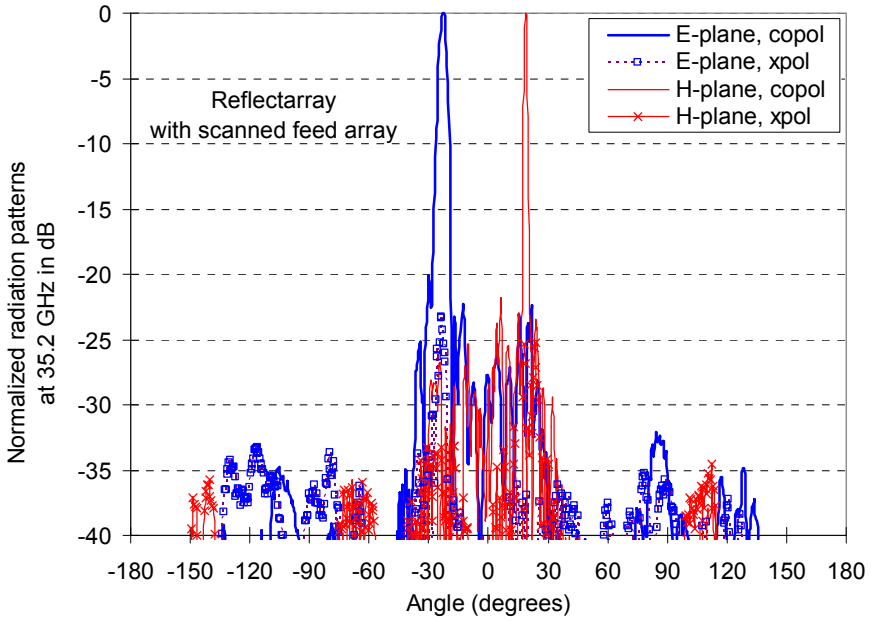


Fig. 17. Measured normalized radiation patterns of case 2 at 35.2 GHz.

TABLE 2. Summary of the reflectarray performance at Ku-band

| Parameters | Ku-band case 1 | | Ku-band case 2 | |
|---|---|---|---|---|
| Scan plane | E | H | E | H |
| Frequency | 14.1 GHz | | 14.1 GHz | |
| Estimated directivity (dB) | 35.4 | | 33.6 | |
| Beamwidth | 2.74° | 3.4° | 4.3° | 3.3° |
| Peak SLL (left/right) (dB) | -16.1 /-16.9 | -17.3 /-15 | -16.2 /-21.4 | -16.3/-16.5 |
| X-pol (dB) | 23.2 | 23 | 23.7 | 22.8 |

TABLE 3. Summary of the reflectarray performance at Ka-band

| Parameters | Ka-band case 1 | | Ka-band case 2 | |
|---|---|---|---|---|
| Scan plane | E | H | E | H |
| Frequency | 35 GHz | | 35.2 GHz | |
| Estimated directivity (dB) | 38.2 | | 38.1 | |
| Beamwidth | $3.7^{o}$ | $1.34^{o}$ | $3.9^{o}$ | $1.3^{o}$ |
| Peak SLL (left/right) (dB) | -27.1 /-24 | -20.7 /-22.4 | -20.1 /-22.5 | -21.8 /-23.5 |
| X-pol (dB) | 29.5 | 30 | 29 | 28 |

## 6. Discussions

The effects of the element phasing methods on the performance of the dual-layer reflectarray are discussed. Microstrip ring elements with gaps are used to achieve circular polarization for the dual-band reflectarrays in [12-14]. Variable angular rotation technique serves as the phase control mechanism. All elements in each frequency band are identical in dimensions but with different rotation angles. The dimensions of the ring elements for the two frequency bands are very different. This leads to the fact that elements in one layer are rather transparent to those in the other layer. Thus the reflection phase of an element suffers little with the presence of the elements in the other layer and the gain degradation due to the phase errors can be minimized. In the current work, in order to meet the requirement of the dual-linear polarization, elements of variable sizes are used for the phase correction. This technique has the benefits of simple

placement of elements, larger bandwidth, and lower cross polarization levels. However, because the reflectarray consists of different sized elements in each layer, some of the Ku band elements have dimensions close to those of Ka band elements and vice versa. In addition, the two frequency bands are closer to each other than those in previous studies. Therefore there are some interactions existing among those elements and the accuracy of the reflection phase deteriorates. It is expected that the gain and the efficiency of the reflectarray can be reduced due to the resulting phase errors. Up to 1 dB gain drop in comparison with the previous study is observed for the dual layer measurements. The SLL and cross polarization levels are not significantly degraded.

The antenna measured here used one frequency feed at a time for the reason of simplicity, while in the actual system both frequency feeds need to be placed in front of the reflectarray aperture. There is a concern of mutual interactions between the two feeds. One advantage of the developed reflectarray is that the two Ku and Ka-band layers can each be designed to have its own focal line location. These two focal line locations, in the real applications, can be optimized to minimize the interactions and perturbation between the two feeds.

## 7. Conclusions

An offset linear-array-fed reflectarray antenna emulating the cylindrical parabolic reflector has been developed which has features of dual-band (Ku and Ka) and dual-linear polarized operation. Two horizontally polarized aperture-coupled microstrip antenna arrays are designed at each band with one beam pointing at broadside and the

other beam pointing at $20^{o}$ to illuminate the reflectarray and achieve the cross-track scanning. The feed arrays show deep SLL suppression and low cross polarization levels. The dual-band beam scanning capability of reflectarray has been successfully demonstrated and well-behaved radiation patterns are observed. A slightly high gain drop occurs for the dual layer measurements for both frequency bands. Further study should focus on reducing these relatively high gain drops, improving the rigidity of the supporting arm, and measuring the patterns in a range with true far-field distance.

# CHAPTER III

# NEW DUAL-BAND REFLECTARRAY CONFIGURATION*

## 1. Introduction

A microstrip reflectarray, often used in space missions, is a light, flat, and high gain antenna and is intended to replace the traditional bulky parabolic reflectors. The basic concept of a reflectarray antenna is to control the phase of the wave re-radiated from its elements so that the reflected wave can achieve a cophasal wave front. Methods to control the phase of the re-radiated wave include using elements with variable sizes [4], patches with different stub lengths [5], slots with variable lengths at the ground plane or loaded on the patch [37,38], and the variable rotation angle technique [8].

Inherited from the microstrip antennas, the reflectarray antenna generally has a narrow bandwidth. There are two possible solutions to overcome the bandwidth limitation. One is to design the reflectarray using element with a wider phase variation range [39]. The other is to operate the reflectarray at multiple frequency bands in a shared aperture [13]. This chapter introduces a new dual-band (C/K band) reflectarray configuration. The two frequency bands selected here are only for demonstration purpose. Other combinations of frequency bands can also be used in the proposed configuration. As mentioned in Chapter II, the measured gain drops in a dual-layer dual-

band reflectarray configuration due to the blockage effect of the top layer. The radiating elements of the two frequency bands introduced in this chapter are printed on the same layer and therefore the blockage effect can be eliminated. In addition, the elements at the two frequency bands do not have a chance to physically interfere with each other as their sizes are changed to obtain required phases.

## 2. Geometry and analysis of the reflectarray elements

Perforated patches loaded by slots at the ground plane are used as the radiating elements at C-band and rectangular patches directly loaded by slots are used at K-band. Radiating elements of both frequency bands are on the same substrate layer. Figure 18 shows the geometry of a part of the reflectarray. The K-band elements are embedded in the perforated openings of the C-band elements. A similar configuration was introduced in [40] for a dual-band dual-polarized antenna array. Ansoft HFSS is used to simulate the phase response of the reflected wave. The effects of the presence of the elements of the other frequency band are also taken into account in the simulation. The proposed reflectarray utilizes two substrate layers (RT/Duroid 5880, $\varepsilon_r = 2.2$) with thicknesses of 0.787 mm for the top layer and 0.508 mm for the bottom layer. The ground plane is placed in between the two substrates and the metallization on the back of the bottom layer is used to prevent the power leaking to the back side of the reflectarray.

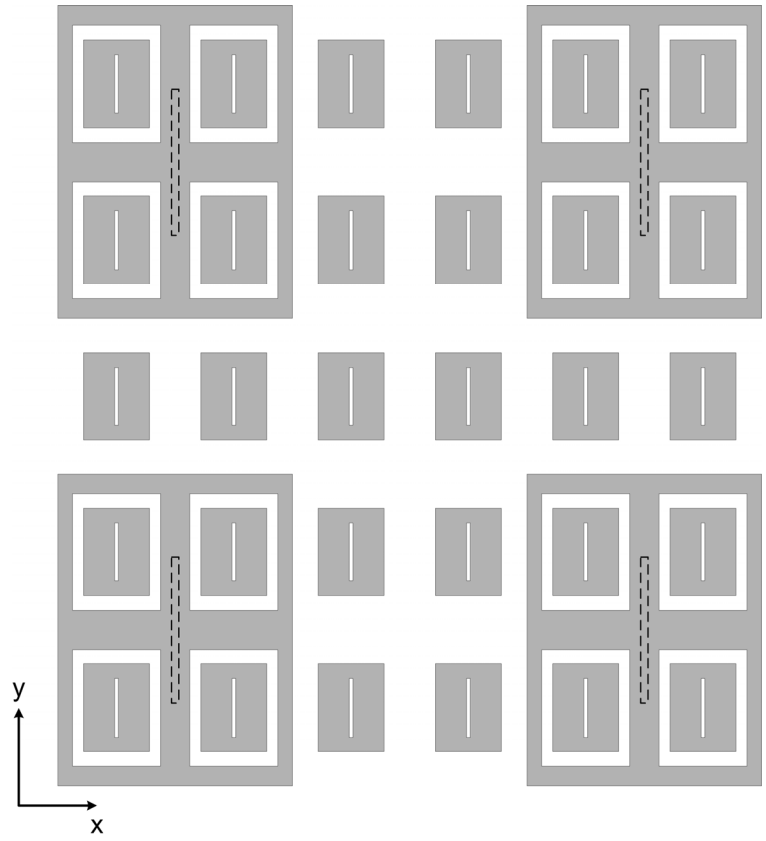


(a)

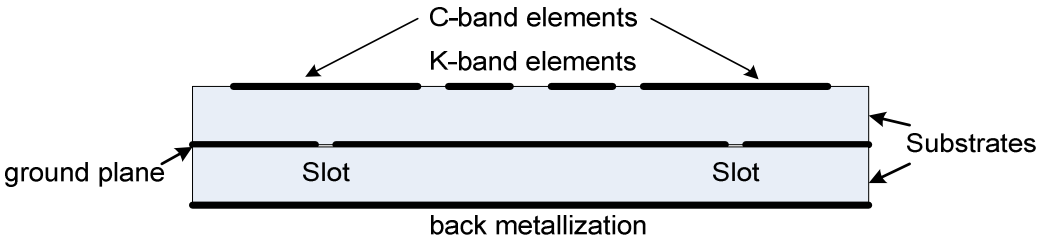


(b)

Fig. 18. Part of the proposed dual-band reflectarray geometry. (a) top view, (b) side view.

A. C-band perforated element design

Perforated patch elements are proposed as the array elements for a reflectarray operating at 5 GHz. The schematic of a unit cell is shown in Figure 19(a). The array

element is designed to be polarized in the x- direction. Four same perforations are used on the patch and reduce the required resonant length at 5 GHz. The resonant length of the perforated patch is 12 mm (around 0.28 $\lambda_g$), where $\lambda_g$ is the guided wavelength in the substrate. Other dimensions of the perforated patch can be found in Figure 19(a). The unit cell dimensions, which are also equivalent to the array element spacing, are 24 mm (0.4 $\lambda_o$) x 24 mm, where $\lambda_o$ is the free space wavelength. Each perforated patch is inductively loaded with a slot on the ground plane. The resonant length of the slot changes as the width of the slot. Figure 20 shows the reflection phase curve for various slot widths. The width of slots in this design is selected to be 0.4 mm because this width minimizes power leaking into the lower half space and still provide a good phase variation range.

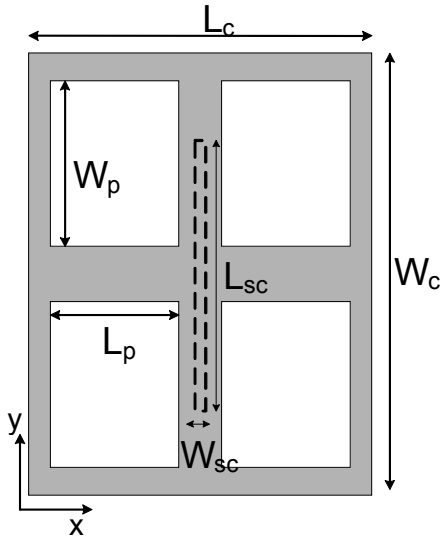


(a)

Fig. 19. Schematics of the reflectarray elements. (a) C-band. $L_C$ = 12 mm, $W_C$ = 16 mm, $L_P$ = 4 mm, $W_P$ = 6 mm, $W_{SC}$ = 0.4 mm, (b) K-band. $L_K$ = 3 mm, $W_K$ = 5 mm, $W_{SK}$ = 0.2 mm.

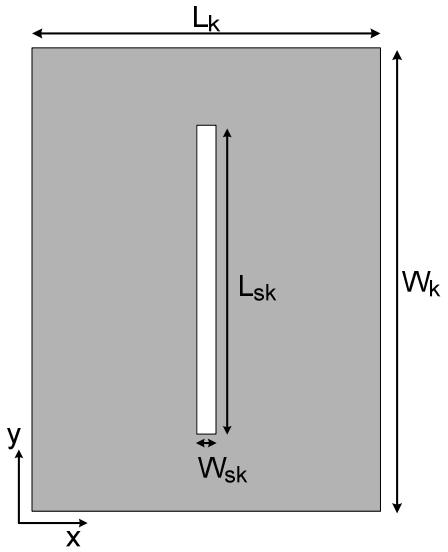


(b)

Fig. 19. Continued.

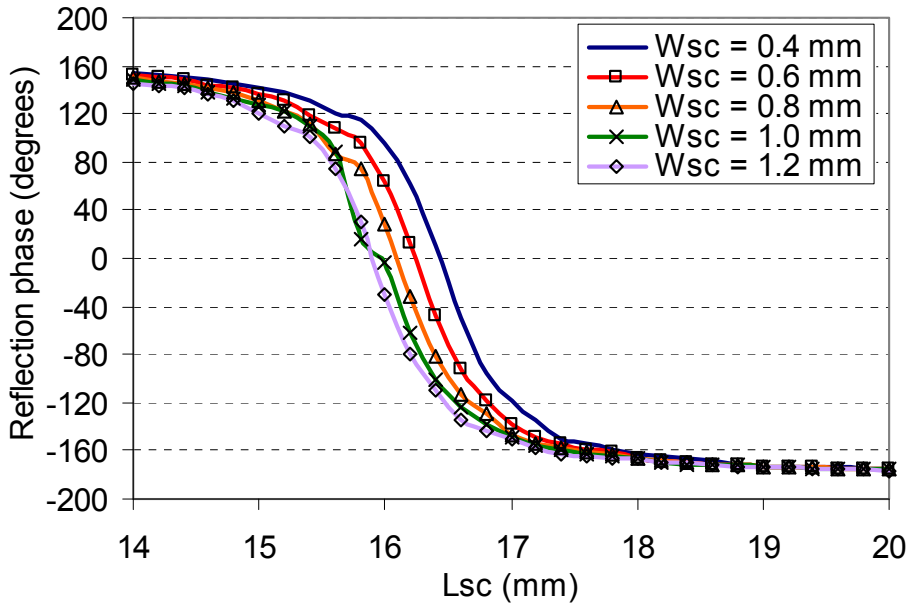


Fig. 20. The reflection phase curves of different slot widths.

As mentioned earlier, the bottom substrate with back metallization can prevent the power leaking into the lower half space. However, an additional substrate layer (bottom layer) is required for this purpose. This will increase the volume of the reflectarray. A study on the effects of different thicknesses of the bottom substrate is explored. Figure 21 shows the loss for different thicknesses when the wave is incident on the reflectarray and reflected back. For each thickness, the maximum loss occurs when the length of the slot is equal to its resonant length. It can be seen that the loss is higher for a thinner substrate. After considering the tradeoffs between the volume of the reflectarray and the loss in the substrate, the thickness of the second layer is selected to be 0.508 mm.

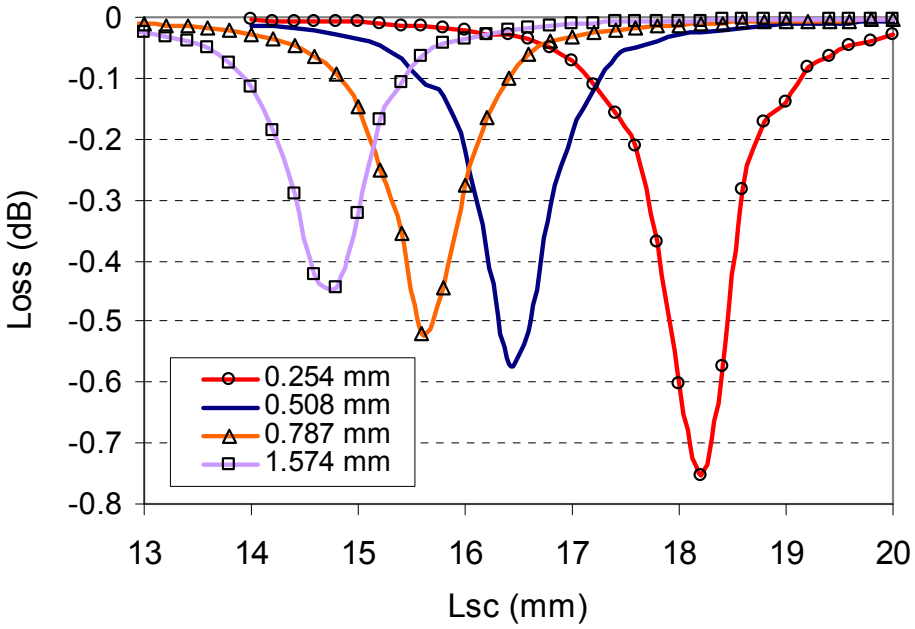


Fig. 21. The relations between the thickness of the bottom substrate and the loss.

By changing the length of the slot while keeping the dimensions of the patch the same, the phase of the reflected wave will change accordingly. The effect of the K-band

elements on reflection phase curve of the C-band elements is also studied. Figure 22 shows the simulated results of the phase variation with different slot lengths. It is observed that the presence of the K-band elements hardly affects the phase curve of the C-band elements. This shows that the perforated patch is a good candidate element type for dual-band reflectarray. A total phase variation of 330$^{o}$ is obtained with the slot length variation from 14 to 19 mm.

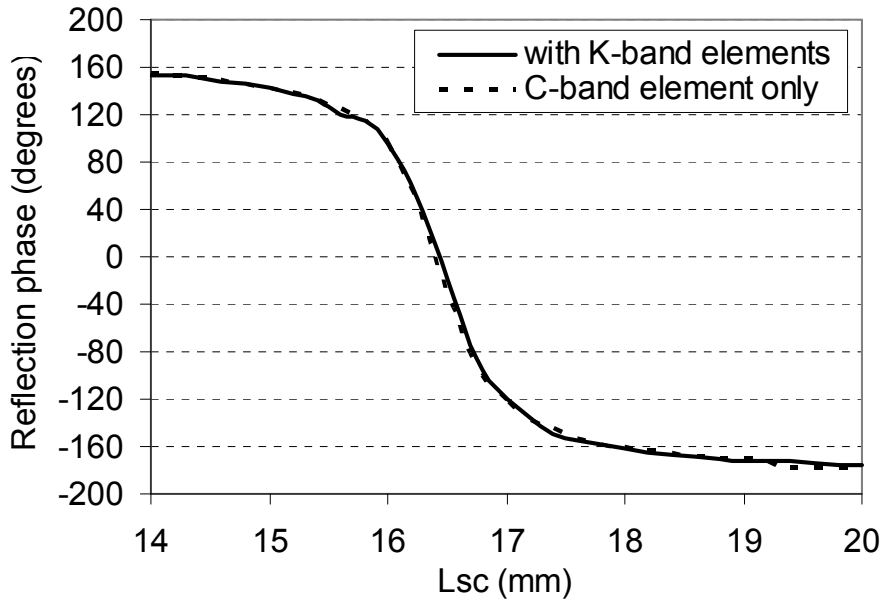


Fig. 22. Simulated reflection phase curves of the C-band element.

B. K-band element design

A rectangular patch directly loaded with a slot on its surface is selected as the reflectarray element at 20 GHz. The patch structure is shown in Figure 19(b). Prior to the adoption of the current structure, the performance of the structures that use patches

loaded with slots on the ground plane were also examined. However, no resonance was found as the slot length changed possibly due to the presence of much larger slots used at 5 GHz. The element spacing is 6 mm (0.4 $\lambda_o$) in x- direction and 8 mm (0.53 $\lambda_o$) in the y- direction. The clearance between the edge of the embedded patch and the edge of the perforated opening is 0.5 mm. This value is chosen for the better C-band phase range. Patches with different slot lengths re-radiate the incident wave with different phases. As can be seen in Fig. 18, the neighboring environments of the K-band elements in the shared reflectarray aperture can roughly be categorized into two kinds. One is that the element is embedded in the opening of the perforated patch. The other is that the element is located outside the perforated patch. Both cases are simulated and the results are shown in Figure 23.

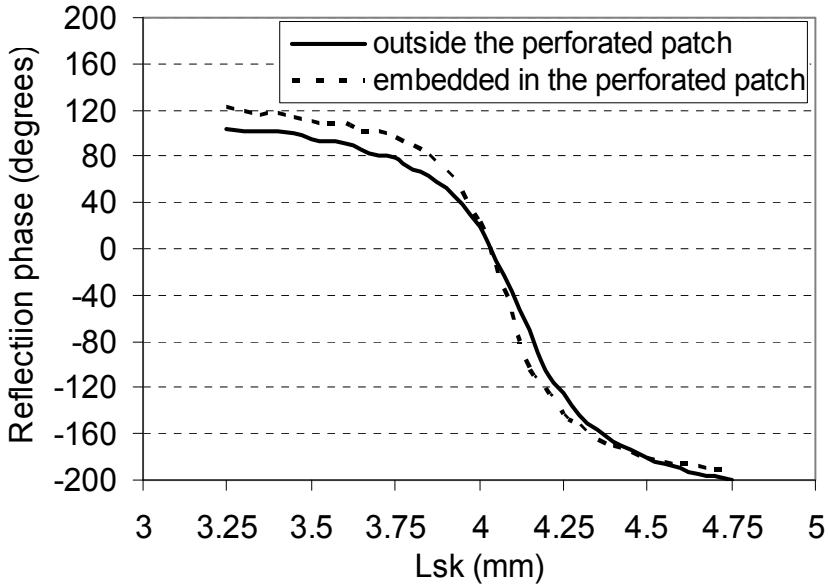


Fig. 23 Simulated reflection phase curves of the K-band element.

## 3. Conclusions

This chapter presents a new configuration for dual-band linearly polarized reflectarray. Simulated phase responses are given in the paper. The radiating elements at two frequency bands are printed at the same layer. No physical contacts between elements will occur as the sizes of the elements are changing. Top layer blocking effects of the dual-layer configuration are also eliminated. The proposed configuration should be a suitable candidate for the dual-band reflectarray.

# CHAPTER IV

# BROADBAND CIRCULARLY POLARIZED ANNULAR RING MICROSTRIP SLOT ANTENNA AND ARRAY*

## 1. Introduction

Circularly polarized (CP) antennas are attractive to radars, satellite communications, and other modern wireless communication systems. A CP signal is less susceptible to the multi-path effect and is more effective in a non-line-of-sight transmission path. Planar antenna technology has primarily focused on the microstrip patch antennas. However, the microstrip patch antenna inherently has small impedance bandwidth and even smaller axial ratio (AR) bandwidth (AR < 3 dB) when it is configured as a CP radiator. Microstrip slot antennas (MSAs) provide a solution to the problem of the limited bandwidth. The advantages of the MSA include low profile, being able to produce unidirectional and bidirectional radiation patterns with larger bandwidth, and being less sensitive to the fabrication tolerances [41]. The MSAs can be fed through the striplines [25], microstrip lines [26], and the coplanar waveguides (CPW) [27, 28]. The stripline-fed slot antennas have unidirectional radiation patterns, but may possibly cause the undesired parallel-plate modes. The CPW-fed technique has advantages over the

microstrip-fed technique including lower dispersion loss and uniplanar configuration which eases the alignment problem during the fabrication.

Previous research has studied numerous configurations of the MSA with CP operation. A coplanar waveguide-fed wide slot antenna with 18 % AR bandwidth was presented [42]. Ring type slot antennas using symmetric slot notches to achieve CP operation have been investigated in [43, 44]. However, the CP bandwidth in [43] was only 3.2% and the simulated and measured results in [44] did not agree very well. It is also desired that an antenna array could achieve wide AR bandwidth. Huang [45] used linearly polarized elements with the sequential rotation technique to construct a circular polarized array. Hall etc. [46] had discussed the detailed design considerations on the use of circular polarized elements with the sequential rotation technique to enhance the AR bandwidth. Many circularly polarized antenna arrays have been proposed following these two design methods [47, 48]. The annular ring is one of the simplest structures and has contributed excellent results in the RF and millimeter wave applications [29]. Therefore using annular ring slots as the radiating elements can reduce the design complexity.

This chapter first introduces two new and simple CPW-fed dual-annular-ring microstrip slot antennas which can eliminate the possible alignment problem with the conventional dual annular ring antenna [49]. Both inductive and capacitive configurations are presented. The CPW line simultaneously feeds two annular slots, which may be found favorable in the construction of an array configuration.

Then a simple and effective method to design a singly microstrip line fed broadband

CP annular-ring slot antenna is proposed. The second resonant mode of a perturbed annular slot antenna is utilized to create the broadband CP radiation. Detailed design considerations of the antenna are provided. The antenna elements are then arrayed in a triangular arrangement with the sequential rotation technique to further broaden the AR bandwidth. Using the equilateral triangular arrangement can help reduce the required number of elements for an array to have no spurious beams formed in the array pattern [50]. This arrangement can therefore compensate for the relatively large size of the antenna element due to the use of the second resonance when the elements are used in an array configuration. Simulated and experimental results of both the single antenna element and the equilateral triangular array are provided in this chapter. The performances of the AR bandwidth for two arrays using different power dividers are also discussed.

## 2. CPW-fed dual annular ring microstrip slot antennas

### A. Antenna structure and design considerations

Geometries of the proposed antennas are shown in Figure 24. The antennas are fabricated on the RT/Duroid 6006 substrates with a dielectric constant of 6.15 and thickness of 0.635 mm. The CPW lines feed the slots inductively in Figure 24(a) and capacitively in Figure 24(b). The gap width (g) and the central strip width (w) of the CPW feed line are 0.3 mm and 2 mm to achieve a characteristic impedance of 50 Ω. The width of the annular slots is adjusted during the optimization process to achieve a good impedance matching. Two short tapered slot lines serve as the transitions between the CPW feed line and annular ring slots for better matching. The simulated result of the

capacitive case shows that the electromagnetic energy coupled from the CPW feed line to the annular slots is very weak. Therefore, an additional tuning stub is used to enhance the coupling and aid the impedance matching for the capacitive case. The resonant frequency is determined by the average circumference of the annular slots. Unlike the CPW-fed single annular slot antenna mentioned in [27], of which the average circumference of the slot is 1.5 $\lambda_g$ ($\lambda_g$ is the guided wavelength of the slot line), the average circumferences of the proposed antennas are 1 and 1.12 $\lambda_g$ at 5.8 GHz for the inductive and capacitive case respectively. The values of other design parameters are: $R_{in1}$ = 5.2 mm, $R_{out1}$ = 6.8 mm, $R_{in2}$ = 6 mm, $R_{out2}$ = 7.5 mm, $d_1$ =7.8 mm, $d_2$ = 8.5 mm, t = 3.85 mm. Zeland's full-wave simulation tool, IE3D [51], is used to simulate and optimize the performance of the proposed antennas. Infinite ground plane is used in the simulation.

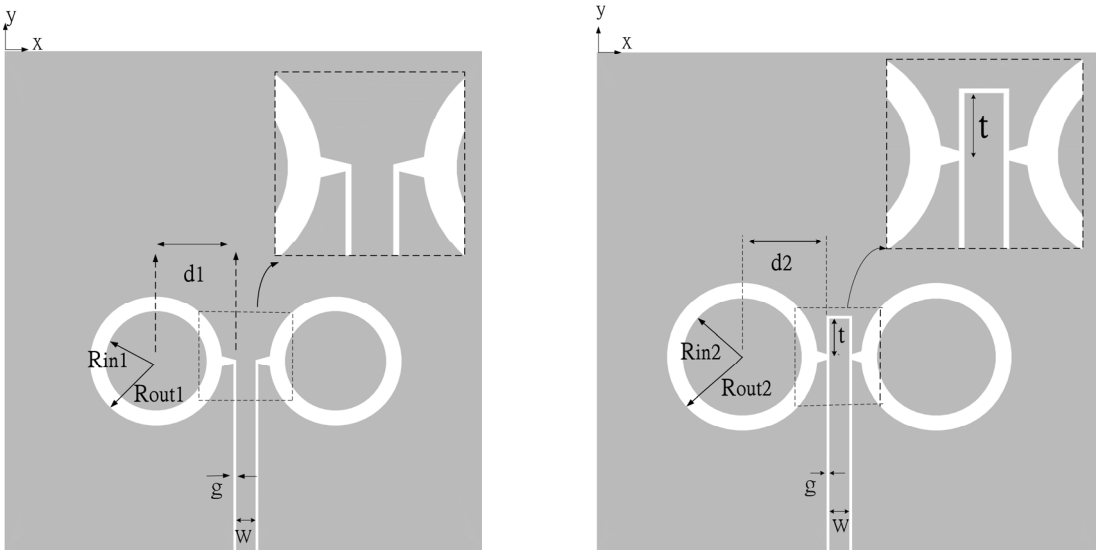


Fig. 24. Configurations of the CPW-fed dual-annular-ring slot antennas: (a) inductive configuration (b) capacitive configuration.

B. Experimental results

Two prototype antennas are fabricated and tested. The dimensions of the ground plane are 30 mm x 25 mm. The simulated and measured VSWR results of both configurations are shown in Figure 25. The measured impedance bandwidth defined by VSWR < 2 for the inductive case is from 5.1 to 6 GHz (16% bandwidth) and is from 5.36 to 5.8 GHz (7.8% bandwidth) for the capacitive case. As can be seen from these results, the achievable impedance bandwidth for the inductive case is about twice wider than that of the capacitive case. The measured results agree well with the simulated results. The slight discrepancy of the center resonant frequency may arise from two reasons: One is that the dielectric constant of the substrate used for fabrication is higher than its nominal value given by the manufacturer. The other is that the fabricated antennas have finite ground planes. Normalized co-polarized radiation patterns measured at the two principal planes are shown in Figure 26. The radiation patterns have very low cross polarization levels (around -25 dB in the broadside direction). The measured broadside gain is about 5.4 dBi for the inductive case and 4 dBi for the capacitive case.

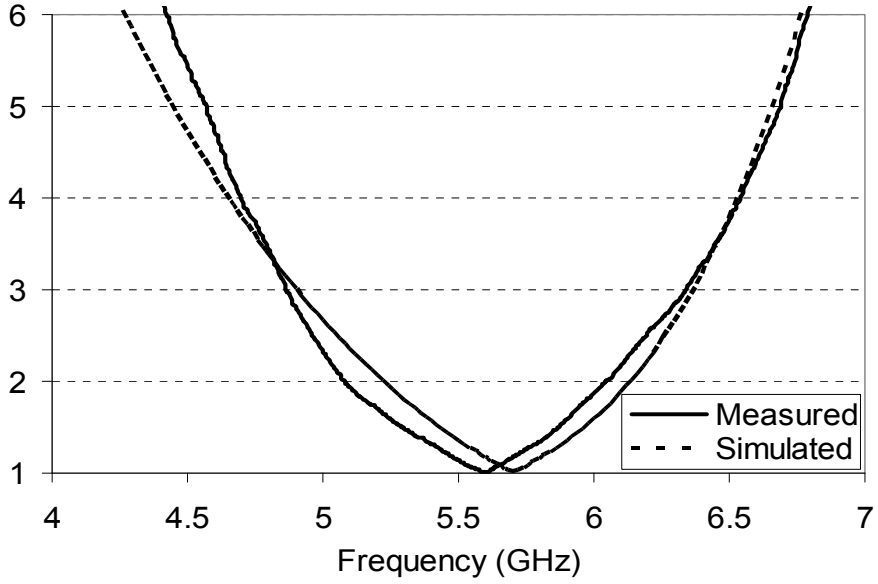


(a)

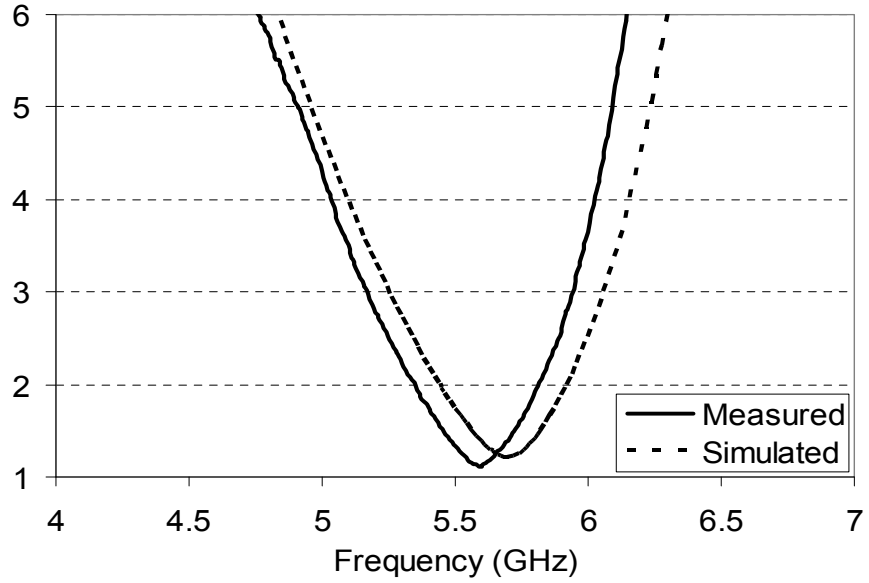


(b)

Fig. 25. Measured and simulated VSWR for both antennas: (a) inductive configuration (b) capacitive configuration.

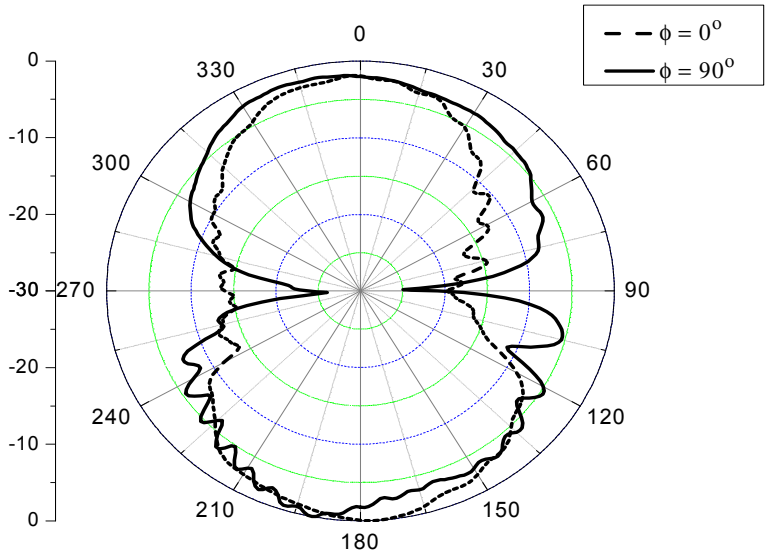


(a)

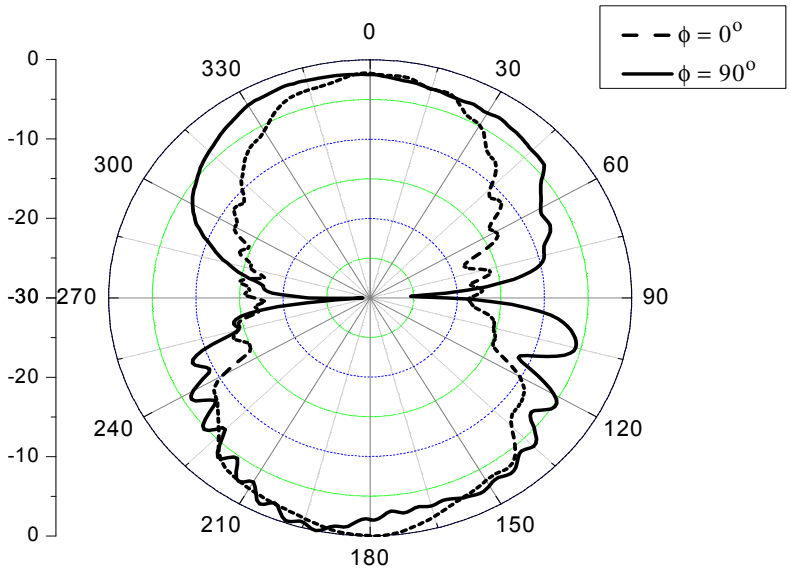


(b)

Fig. 26. Measured normalized co-polarized radiation patterns at two principal planes: (a) inductive configuration (b) capacitive configuration.

## 3. Circularly polarized annular ring microstrip slot antenna

### A. Antenna structure and design considerations

Figure 27 shows the geometry and dimensions of the proposed antenna. This antenna uses three interconnected concentric annular slots and the two outer annular slots serve as parasitic elements of the innermost annular slot to increase the impedance bandwidth of the second resonant mode. The mean circumference ($r_1$, $r_2$, and $r_3$) of the slot is defined as the average of the radii of outer and inner edge. Widths ($w_1$, $w_2$, and $w_3$) of the three annular slots are all selected to be smaller than $0.05\lambda_0$ (free-space wavelength). Small clearance ($p'_s$ are less than $0.01\lambda_0$) between two annular slots and the interconnecting slot sections can increase the energy coupling among slots. The second resonance of an annular ring slot antenna occurs at approximately 1.5 times of the first resonance frequency. Given the frequency of the second resonance, the frequency of the first resonance and the mean circumference of the innermost annular ring can be decided accordingly. It is found that the first resonant mode occurs when the mean circumference is about $0.75\lambda_0$ considering the effects of the substrate permittivity and the feed line that comprises of a 50-Ω microstrip line and a section of tuning stub.

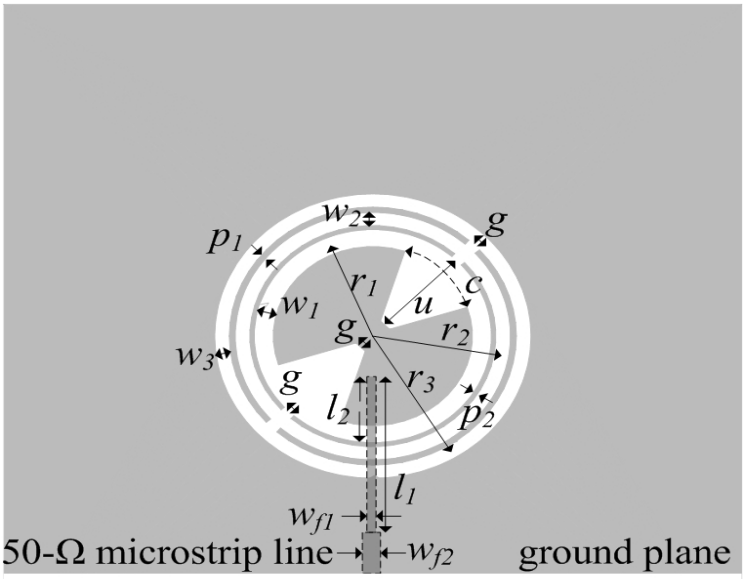


Fig. 27. Geometry and dimensions of the proposed antenna where $r_1 = 6.22$, $r_2 = 7.44$ , $r_3 = 8.6$ , $w_1 = 1.1$ , $w_2 = 0.84$, $w_3 = 0.84$ , $w_{f1} = 0.7$ , $w_{f2} = 1.46$ , $l_1 = 9.95$, $l_2 = 3.25$, $c = 6.7$ , $u = 4.68$, $g = 0.74$, $p_1 = 0.34$, $p_2 = 0.26$ (units: mm).

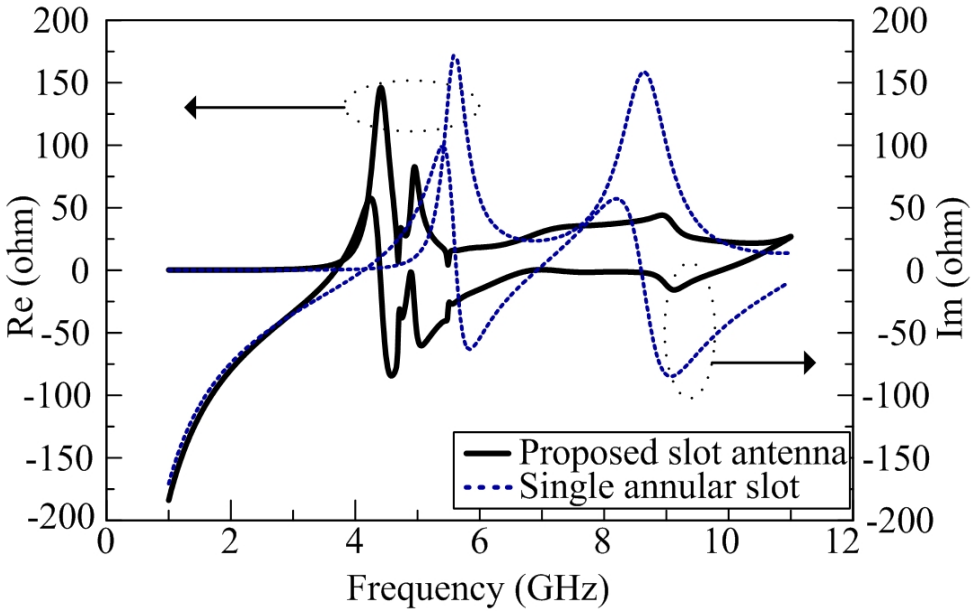


Fig. 28. The comparison of the input impedance between the proposed slot antenna and a single annular slot antenna.

Simulations reveal that interconnecting the concentric slots can smooth the curve of the imaginary part of input impedance at the second resonance and reduce their values close to zero over a wide frequency range. Two radial slot stubs located at 45$^o$ and 225$^o$ of the innermost annular ring slot can further flat the imaginary impedance curve and create a pure real input impedance. Most importantly, they can provide perturbations for the antenna to generate the circular polarization with wider bandwidth. A comparison of the input impedance curves between a single annular slot without perturbations and the proposed antenna can be seen in Figure 28.

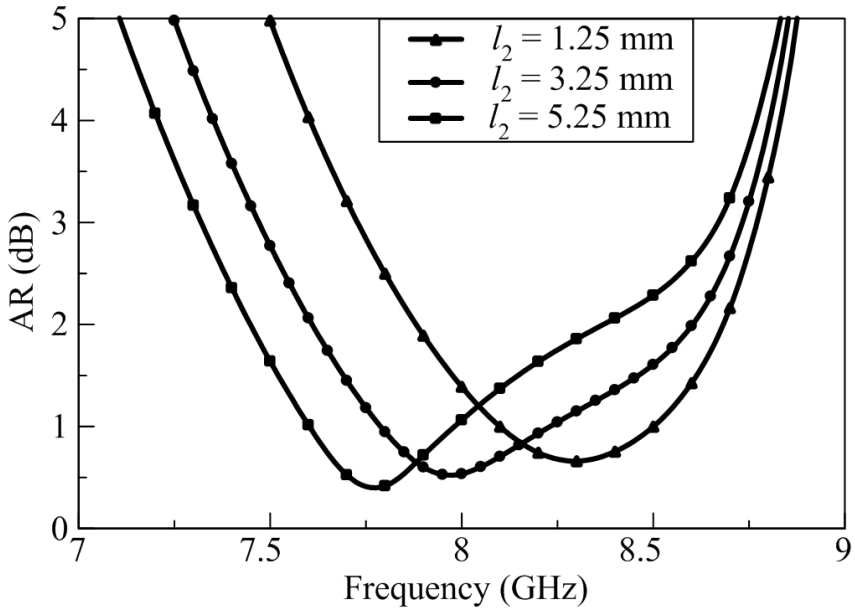


Fig. 29. Dependence of the frequency of minimum AR on $l_2$.

The minimum achievable value of the AR primarily depends on the size of the radial slot stubs. Detail dimensions of the radial stubs are described in Figure 27. The length ($l_2$) of the stub section within the innermost slot can fine tune the frequency of the

minimum AR. Dependence of the frequency of the minimum AR on $l_2$ is shown in Figure 29. The frequency of the minimum AR is observed to decrease as $l_2$ increases. Zeland's IE3D is used for the simulations and optimizations of the antenna. The electrical field distribution on the aperture of the slots is modeled as the magnetic current to save the computing time required for the simulations.

B. Experimental results of a single antenna element

A prototype antenna operating at the center frequency of 8 GHz is fabricated on the RT/Duroid 5870 substrate with a dielectric constant of 2.33 and thickness of 0.508 mm. The dimensions of the fabricated antenna's ground plane are 40 mm x 40 mm. Figure 30 shows the VSWR of the antenna. A measured bandwidth (VSWR < 2) of 32 % is obtained.

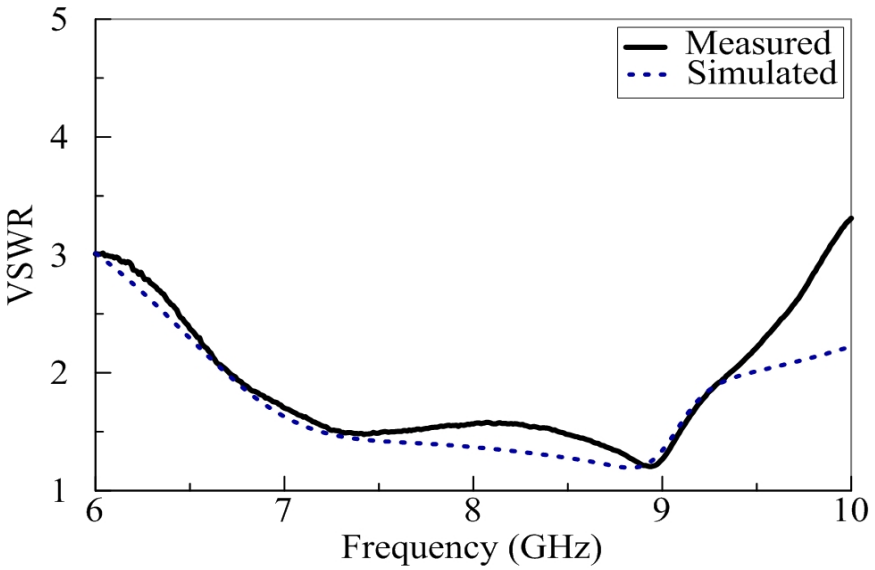


Fig. 30. The measured and simulated VSWR of the proposed antenna.

Measurements of the radiation patterns are carried out with the use of Narda linearly polarized pyramidal horn antennas in the anechoic chamber and the measured data are then post processed using the phase-amplitude method [52] to calculate the AR. The procedure of this method is briefly described below. The amplitude and the phase of the signal received by the antenna under test (AUT) are measured in a principal plane of the AUT. Then the transmitting linearly polarized horn is rotated $90^o$ and the measurement is repeated in the same principal plane of the AUT. Two sets of the measured complex data can be designated as $E_\theta$ and $E_\Phi$, which are the orthogonal patterns taken across the same principal cut of the AUT. These two sets of data are then post-processed. The right-hand CP (RHCP) and left-hand CP (LHCP) components can be represented as

$$E_R = \frac{1}{\sqrt{2}}\left(E_\theta + jE_\phi\right) \tag{12}$$

$$E_L = \frac{1}{\sqrt{2}}\left(E_\phi + jE_\theta\right) \tag{13}$$

If $|E_R| > |E_L|$ at the main beam angle, then the AUT is right-hand polarized and vice versa. The AR can be determined for any angle using

$$AR = \frac{\left|\,|E_R| + |E_L|\,\right|}{\left|\,|E_R| - |E_L|\,\right|} \tag{14}$$

The curve of the AR at the broadside direction against frequency can be seen in Figure 31 and the measured 3-dB AR bandwidth is 1.1 GHz (7.45 – 8.55 GHz) which is equivalent to 13.7% with respect to the designed center frequency. Minimum measured AR is 0.46 dB. Measured results match the simulated results very well. The antenna has a right-hand circular polarization (RHCP) and will have left-hand circular polarization

(LHCP) if the radial slot stubs are located at 135$^{o}$ and 315$^{o}$. The resulting CP co-polarized (RHCP) and cross-polarized (LHCP) radiation patterns at 8 GHz can be seen in Figure 32. The measured CP gain against the frequency is also shown in Figure 31. The gain variation is less than 1 dB with an average gain of 3.9 dBi within the AR bandwidth.

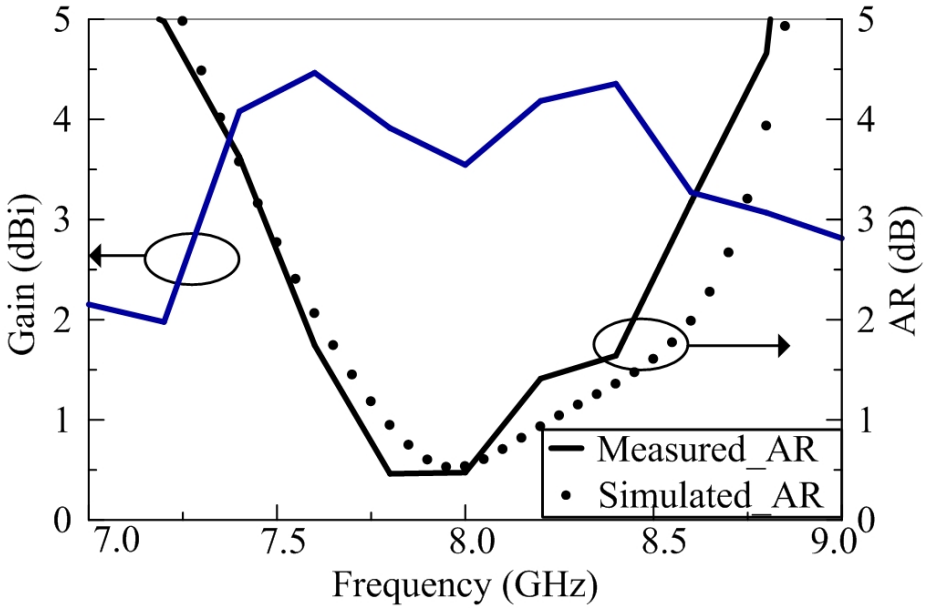


Fig. 31. The CP gain and AR of the proposed antenna.

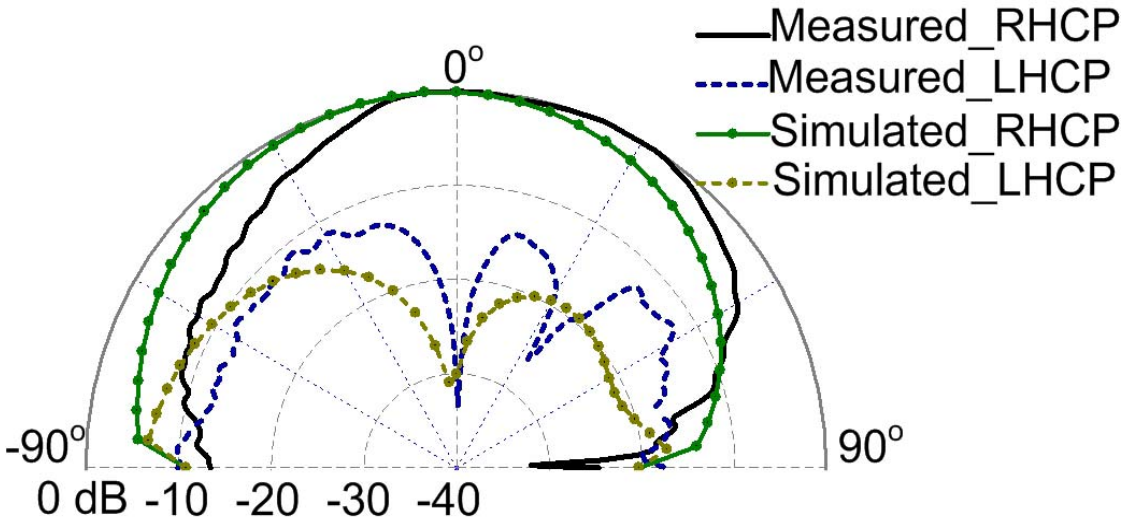


Fig. 32. CP radiation patterns of a single antenna element at 8 GHz.

## 4. Equilateral triangular array configuration

Three CP ring slot antenna elements are arrayed with an equilateral triangular arrangement. The triangular array arrangement can increase the maximum allowed element spacing at which the spurious beam begins to form [50]. The sequential rotation technique is applied to the array elements to achieve a wider CP bandwidth. Elements are sequentially rotated by angles of $0^{o}$, 120, and $240^{o}$ for element 1 to element 3, respectively. To compensate for the rotation angles, elements are excited by signals with phase shift of $0^{o}$, $-120^{0}$, and $-240^{o}$. These phase shifts are achieved by adjusting the length of the feed lines of each element. A three-way microstrip power divider proposed in [53] is used to feed the array. The feeding structure is integrated with the array and the schematic is illustrated in Figure 33.

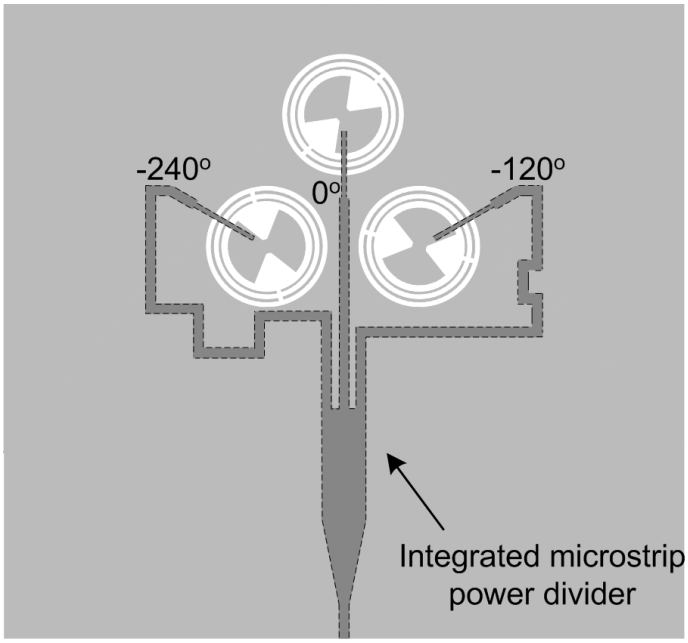


Fig. 33. Configuration of the three-element array fed with integrated microstrip power divider.

This array is fabricated on the same type of substrate given earlier for antenna elements. The measured VSWR in Figure 34(a) shows an impedance bandwidth of 40.5 %. Both measured and simulated results AR versus frequency are displayed in Figure 34(b) and show very good agreement. The 3-dB AR bandwidth approaches 1.7 GHz (6.95 – 8.65 GHz) and is equivalent to 21.8 %. Significant increase of the AR bandwidth has been achieved for the array as a result of the sequential rotation technique. Radiation patterns of the array are shown in Figure 35. The gain values within the 3-dB AR bandwidth are all greater than 5 dBi with the maximum equal to 6.6 dBi.

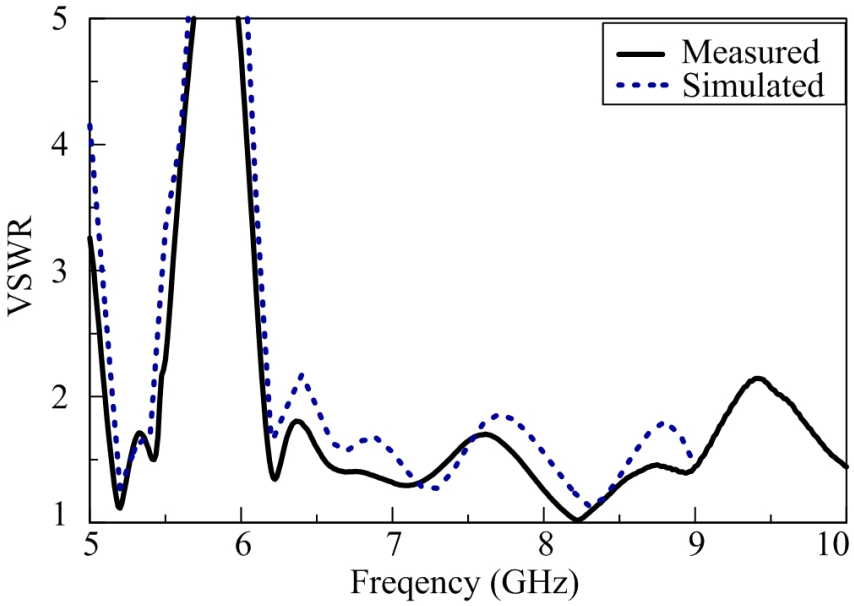


(a)

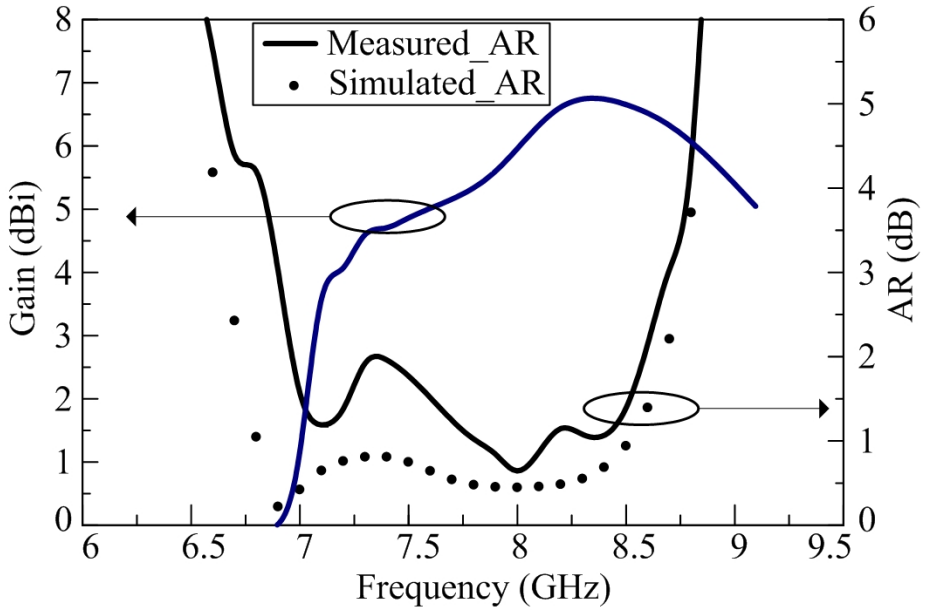


(b)

Fig. 34. Performances of the proposed array fed with integrated microstrip power divider: (a) VSWR (b) CP gain and axial ratio.

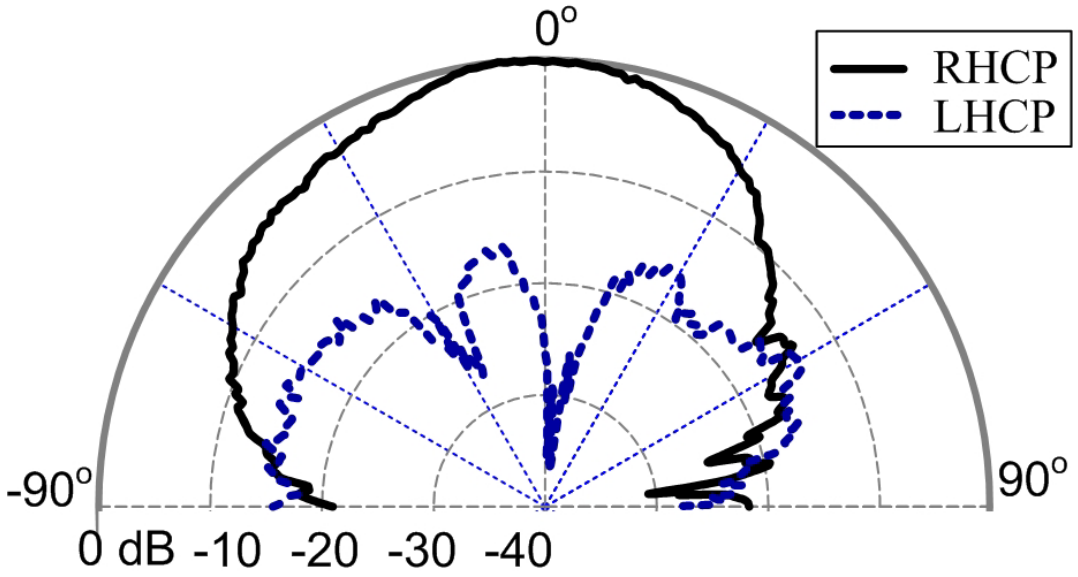


Fig. 35. CP radiation patterns of the array fed with integrated microstrip power divider at 8 GHz.

A second array fed with an external power divider manufactured by Narda is tested and compared with the first array. The comparison of the measured AR bandwidth between two arrays can be seen in Figure 36. Obviously, the second array has a wider 3-dB AR bandwidth up to 31% (6.65 – 9.1 GHz). This much wider bandwidth could be attributed to the wider bandwidth of the external power divider. Despite the difference in the AR bandwidth, both arrays have verified the wideband characteristic of the sequentially rotated triangular array arrangement.

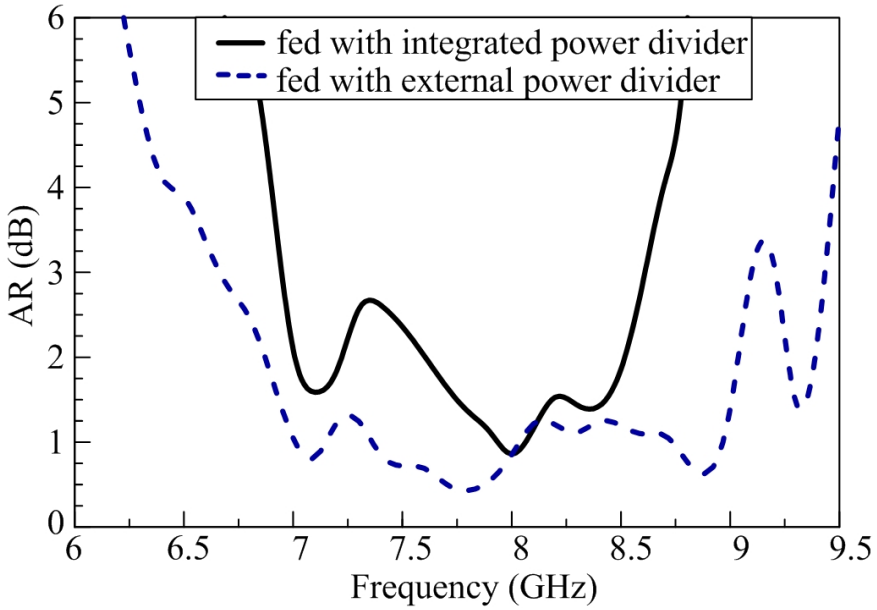


Fig. 36. Comparison of the AR between two arrays.

## 5. Conclusions

In this chapter, two new linearly polarized CPW-fed dual annular MSAs have been presented. The proposed antennas utilize very simple feeding structures and radiating elements but demonstrate very good performances. The use of the two slots facilitates the construction of an annular slot array. The inductive configuration is found to have better performance over the capacitive case with a wide impedance bandwidth of 16% and gain of 5.4 dB.

A broadband circularly polarized annular ring MSA operating around the second resonant mode has also been demonstrated. The antenna presents wide impedance and 3-dB AR bandwidths. An array has been built with three annular ring slot antenna elements with equilateral triangular arrangement. The arrangement significantly increases the 3-dB AR bandwidth. Measured results have well proved the proposed

concept with good agreement with simulated results. The antenna and array should be suitable for many wireless applications.

# CHAPTER V

# NOVEL RECONFIGURABLE MICROSTRIP ANTENNA WITH SWITCHABLE CIRCULAR POLARIZATION*

## 1. Introduction

Microstrip antennas have drawn lots of attention in the wireless communication systems recently. Generally, a microstrip antenna is designed to operate in a single polarization mode, such as linear polarization or circular polarization. Circular polarization is more attractive in the applications of wireless communications since the antennas of the transmitter and receiver do not need to be aligned. Polarization diversity is an interesting and essential feature for improving the signal reception performance in a multi-path fading environment [54]. Frequency reuse can also be achieved by utilizing the property of polarization diversity [55]. The antennas reported in [54] and [55] use the dual-fed configurations. Two input ports are needed to generate two different polarizations, resulting in a complicated feeding network. On the other hand, the singly-fed CP antenna has a simple feeding network. Several switchable circular polarized antennas using singly-fed configurations have been demonstrated. In [56], a dual

frequency and dual circular polarization antenna is introduced by incorporating a Schottky diode mounted across a slot on the patch as a switch. A slot antenna with switchable polarization was reported in [57] where PIN diodes are used to switch between different polarizations. More reconfigurable circularly polarized antennas with the use of PIN diodes to achieve the switching mechanism have been presented in [58] and [59]. Using the diode to achieve switching operation has been practically implanted. However, the biasing circuits need to be designed on the patch surface and large capacitors are required to maintain the RF connections.

The concept of the PET controlled phase shifter has been studied in [60]. The electromagnetic fields of the transmission line are perturbed by a dielectric perturber that changes the effective permittivity, propagation constant, and the phase shift of the transmission line. In this chapter, an antenna with switchable circular polarization using PET is developed. The PETs are deflected by two external voltages. Therefore, the dielectric perturbers attached to the PET can either touch or suspend above the substrate. The switching mechanism is controlled by the external DC voltages. Two PET-controlled perturbers are utilized to realize the antenna with switchable circular polarization. In comparison with the reconfigurable antenna using diodes, the PET-controlled switchable circularly polarized antenna utilizes a much simpler DC biasing circuit for its piezoelectric transducer. The proposed antenna operates in the 5.8 GHz frequency band and shows similar antenna performances including gain, axial ratio (AR) and radiation patterns for both right hand and left hand circular polarizations.

## 2. Antenna design and operation mechanism

The configuration of the proposed reconfigurable antenna is shown in Figure 37. A nearly square singly-fed microstrip patch is used as the radiating element. The patch has dimensions of 17mm x 16.75mm and is etched on a 0.381mm RT-Duroid substrate with a dielectric constant of 2.2. A typical method to generate CP is to truncate the corner of the patch.

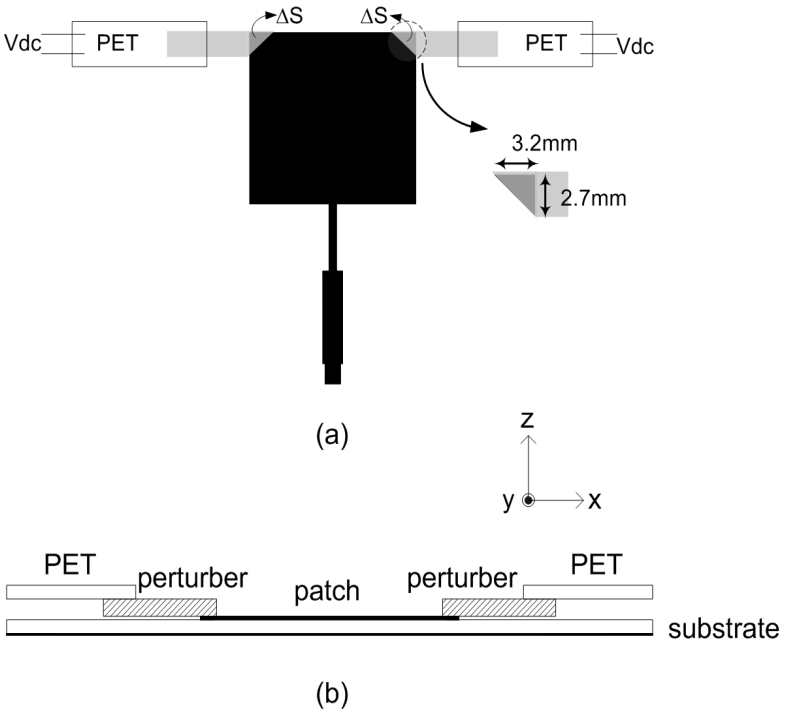


Fig. 37. Schematics of the proposed antenna: (a) top view (b) side view.

The mechanism of the CP operation for the proposed antenna can also be explained by the cavity model method. When both perturbers are lifted up, no perturbation is added, and a pair of degenerated modes ($TM^{z}_{010}$ and $TM^{z}_{100}$) are excited at the same

frequency. When one side of the perturber is pulled down to cover one corner of the patch, the perturbations will cause the two degenerated modes to split. With a certain amount of perturbations, the resonant frequencies of the two modes will be different and the radiation fields of the two modes will have the same amplitude but $90^{o}$ out of phase. The dielectric constant and thickness of the perturber have significant effects on the amount of perturbations. If the perturber's dielectric constant is low or the thickness is thin as compared with those of the patch substrate, a sufficient amount of perturbations cannot be achieved. Two dielectrics with a thickness of 1.27 mm and dielectric constant of 10.2 are attached to two PETs serving as the perturbers. The reason dielectric perturbers are used instead of metal is because of the lower loss showed in the experimental results of [60]. The PETs and perturbers are deflected vertically in the z-direction to yield the required perturbations. When the DC voltage of the right PET is ON and that of the left PET is OFF, the top right corner of the patch will be perturbed and LHCP will be generated. RHCP will be generated in the opposite situation. The states of the two PETs and their corresponding sense of CP are summarized in Table 4. It

TABLE 4. States of the external DC voltages of pets and their corresponding senses of CP

| Right PET | Left PET | Sense of CP |
|---|---|---|
| ON | OFF | LHCP |
| OFF | ON | RHCP |

is found from the simulation results that the perturbation areas ( $\Delta S$ ) affect the CP performance. There exists an optimum area of $\Delta S$ to achieve the best CP performance for a given patch size. The optimum area for the proposed antenna is found during the simulation. The corner with $\Delta S$ equal to 3.2mm x 2.7mm is covered by the perturber. Quarter-wavelength transformers are then used to match the antenna input impedance to 50Ω at the operating frequency. The simulation of the antenna is realized using IE3D [51]. Simulation results of the AR with different perturbed areas are shown and compared in Figure 38.

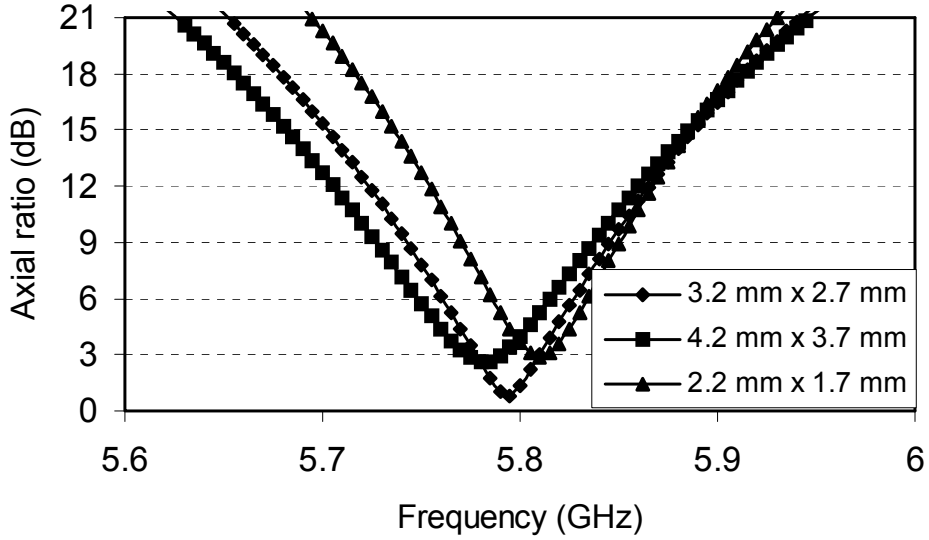


Fig. 38. Comparison of AR among different perturbed areas.

Other factors including dielectric constant, thickness, and the perturbed location of the patch are also found to have effects on the CP performance. Since the configuration of the antenna is completely symmetric in the x-direction, the performance of the RHCP

and LHCP should have very similar resonant frequency, return loss, gain, and AR performance. This is a desired feature for the polarization diversity applications. The basic design procedures for the proposed antenna are summarized as below: (i) Select the dielectric perturber with proper thickness and with dielectric constant larger than that of the antenna substrate. (ii) Determine the optimum perturbation location and area for best CP performance. (iii) Match the input impedance of the antenna to the feed line.

## 3. Experimental results

The antenna with the dimensions and features described above is fabricated and tested. During the measurements, the perturber needs to be flat and placed as close to the patch as possible. The CP performance will be affected by the gap size between the perturber and the patch surface. By adjusting the height of the PET and apply an external voltage to pull down the perturber, the air gap can be minimized. In the measurements, the external voltage is increased from 0V to 60V, which is required to make the perturber tightly contact the patch surface.

Figure 39 shows the simulated and measured return loss for both senses of CP. The antenna shows good impedance matching. Better than 20 dB return loss is observed. Due to the geometry symmetry, only boresight AR of LHCP is shown and compared with the simulated results in Figure 39. The AR of RHCP is very close to the AR of LHCP. The AR is measured using the phase-amplitude method described in [52]. The received amplitude and phase at the antenna under test (AUT) are measured across a principal plane with a linear polarized transmitting horn antenna. Then the horn is rotated $90^{o}$ and

the measurement is repeated across the same principal plane. Two sets of data for amplitude and phase are obtained to calculate the AR. Minimum AR of 0.485 dB is measured at 5.82 GHz. The frequency discrepancies between the simulated and measured results are mainly due to the fabrication tolerance and the flatness of the dielectric perturber.

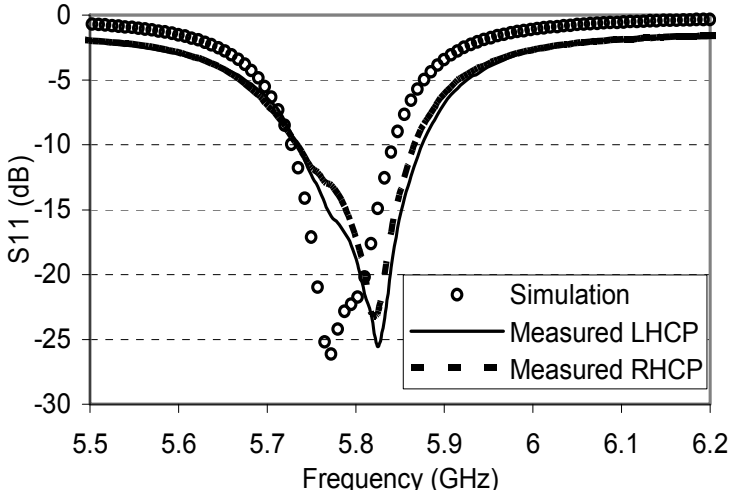


Fig. 39. Simulated and measured $S_{11}$ of the antenna.

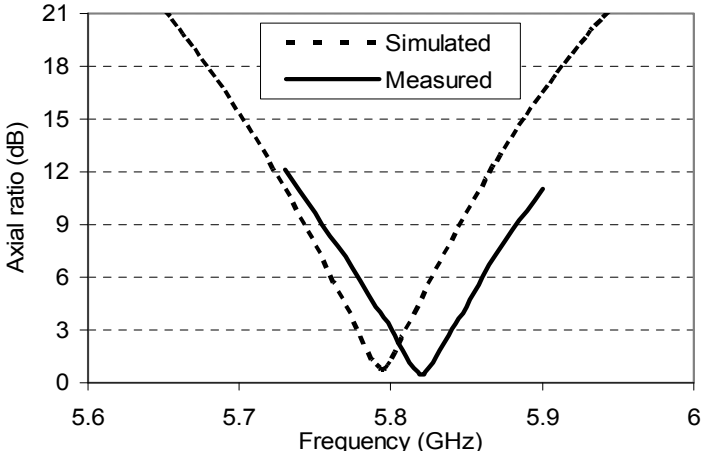


Fig. 40. Simulated and measured AR of the LHCP at the boresight.

Figure 41 shows the resulting LHCP co-polarization and x-polarization patterns at 5.82 GHz. The RHCP level is about 20 dB lower than the LHCP from -30º to 30º off the broadside, showing good CP performance near the boresight direction. The CP gain of 5.4 dBi at the boresight is calculated from the measured LP gain.

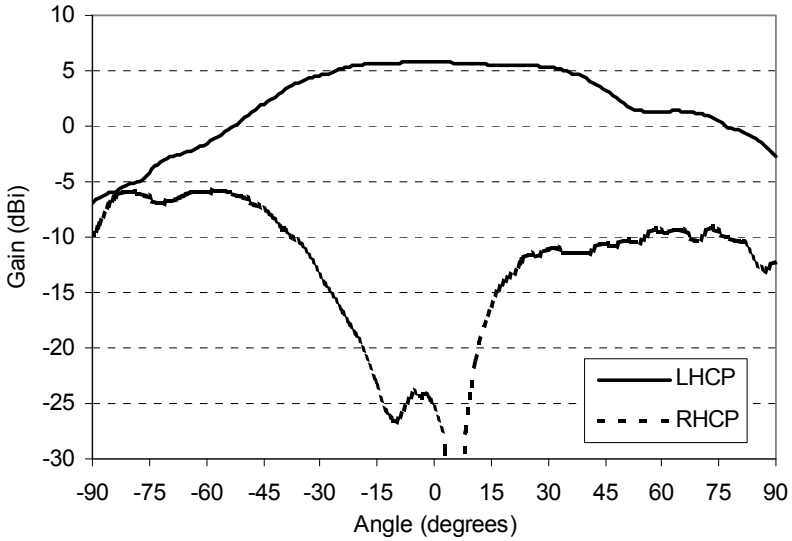


Fig. 41. Resulting CP co-polarization (LHCP) and x-polarization (RHCP) patterns at frequency of 5.82 GHz.

## 4. Conclusions

A piezoelectric transducer-controlled switchable circularly polarized antenna is proposed in this chapter. The antenna can have different senses of CP with a single feed by switching the external DC voltages of the PET. Compared with previous published switchable polarization antenna, the complicated DC biasing network is avoided in the design of the proposed antenna. Good agreements between simulation and measurements

are observed. The reconfigurability of the polarization senses makes the antenna suitable for practical applications requiring polarization diversity.

# CHAPTER VI

# DUAL-POLARIZED PLANAR ARRAY ANTENNA FOR S-BAND AND X-BAND AIRBORNE APPLICATIONS*

## 1. Introduction

Modern wireless communication systems demand low profile, lightweight, and relatively inexpensive antennas [61]. There have been increasing interests in the development of the dual-polarized antennas/arrays due to many advantages in the performance improvement for wireless communication and radar systems. The dual polarization avoids the requirement of precise alignment needed in single-polarized systems. The dual-polarized operation can also provide more information for radar systems, increase the isolation between the transmitting and receiving signals of the transceivers and transponders, and double the capacity of the communication systems by means of the frequency reuse [62-63]. In simultaneous transmit-receive applications, dual-polarized antennas with two-port connections offer an alternative to the commonly used bulky circulator or separate transmit and receive antennas. Furthermore, dual-polarized antennas can provide the polarization diversity, which prevents the system performance degradation from the multipath fading in complex propagation environments [64]. Compared with the space diversity, the polarization diversity

---

technique has the advantage of reducing the number and size of the antenna elements in the systems.

To create the dual-polarization, the antenna element has to be fed at two orthogonal points or edges such that two degenerated resonant modes can be excited for orthogonal polarizations, i.e., vertical and horizontal polarizations. Design techniques of the dual-polarized antennas can be classified into three main categories. One is to make an orthogonal arrangement of the radiation elements for two polarizations [65-66]. Another is to choose properly stacked structures of the radiating elements [67-68]. The other is to use special feeding techniques [69-70]. In general, symmetric structures tend to give better dual-polarization performance. At higher frequencies, to reduce the metallic loss of the patch, a dielectric resonator antenna can be used [71].

The dual-polarized antenna elements can be assembled to construct a high gain array. Although many dual-polarized antennas have been proposed, not all of them are good candidates for the array design due to their complex structures and feed-line networks. Many of them are bulky and heavy, and not suitable for airborne applications. On the other hand, the isolation is one of the important parameters to be considered in the dual-polarized array design. Most reported dual-polarized arrays achieve at least 20-dB isolation [72-75]. To minimize the coupling between the feed-line networks, a proximity/aperture coupling structure can be applied to prevent the radiation due to the microstrip line and radiator from degrading the polarization performance. The multi-layer structure can also be used to enhance the isolation, in which an isolation of better than 20-30 dB can be obtained with more complicated structures. However, most dual-

polarized antenna designs will result in a bulky array that is not suitable to be used in aircrafts, airships, or unmanned aerial vehicles (UAV).

In many airborne applications, the array antenna should have good isolation, high efficiency, and ease of integration with the aerial vehicles. A simple feed-line network with lower loss and high isolation is generally desired. Microstrip series-fed arrays have been shown to have a structure to enhance the antenna efficiency [61]. This is because the array feed-line length is significantly reduced compared to the conventional corporate feed-line network. Such arrays could be either traveling-wave or resonant arrays. A planar structure with a thin and flexible substrate is a good choice, which will not disturb the appearance of the aircraft and can be easily integrated with the electronic devices for the signal processing.

In this chapter, a dual-frequency dual-polarized array antenna is presented for the airborne antenna applications. For the dual-band operation, a multi-layer structure is adopted. The antenna arrays for the two frequencies are separated on different layers. To reduce the array volume and weight, a series-fed network is used. An ultra-thin substrate is chosen for the conformal purpose and the array can be easily placed on the aircraft fuselage or inside the aircraft. The parameters affecting the array characteristics are discussed, and measured return losses, radiation gains, and array patterns are presented.

## 2. Array design

Unlike most other operations, the electrical parameters of the substrate will be affected by the temperature and moisture variations occurring in airborne applications,

which affect the performance of the antennas. The magnitude of the transmitting power may also generate large amount of heat that results in a significantly increased temperature. Therefore, the choice of the substrate is an important factor in the airborne antenna design. The configuration of the antenna element determines the complexity of the array feed-line network that controls the size and mass of the array. Also, the configuration of the feed-line networks may incur different levels of port isolation and pattern polarization. Important design considerations of the dual-polarized airborne array antenna are summarized in Table 5. The goal is to design a low mass and conformal array antenna for airborne applications. An ultra-thin substrate is used to achieve the conformal antenna.

Table 5. Design considerations of the airborne array antenna

| Factor | Impact |
|---|---|
| Temperature | This is determined by the aerial condition and delivered power which will affect electrical parameters of the substrate. |
| Moisture | The effects due to moisture are similar to the temperature. |
| Electrical parameter | This controls the antenna performance and is mainly changed by large temperature variations. |
| Feed-line network | This determines the complexity of the array. Unsuitable antenna elements could result in bulky and heavy array. |
| Isolation | Port-to-port isolation and cross-polarization level can be enhanced by using well-designed feed-line networks such as proximity/aperture coupling and multi-layer configurations. |
| Coupling | For dual-frequency operation, the interference between antennas operating at different frequencies may affect radiation patterns and gain. |

The multi-layer array structure for the dual-band (S-band and X-band) operation is shown in Figure 42. The S-band antenna elements sit on the top layer and the X-band antennas are on the bottom layer. A foam layer ($h_2$) serves as the spacer and is sandwiched between the two substrate layers. One of the important design considerations of this multi-layer dual-band array is that the S-band antenna element should be nearly transparent to the X-band antenna elements. Otherwise, it may degrade the performance of the X-band antenna.

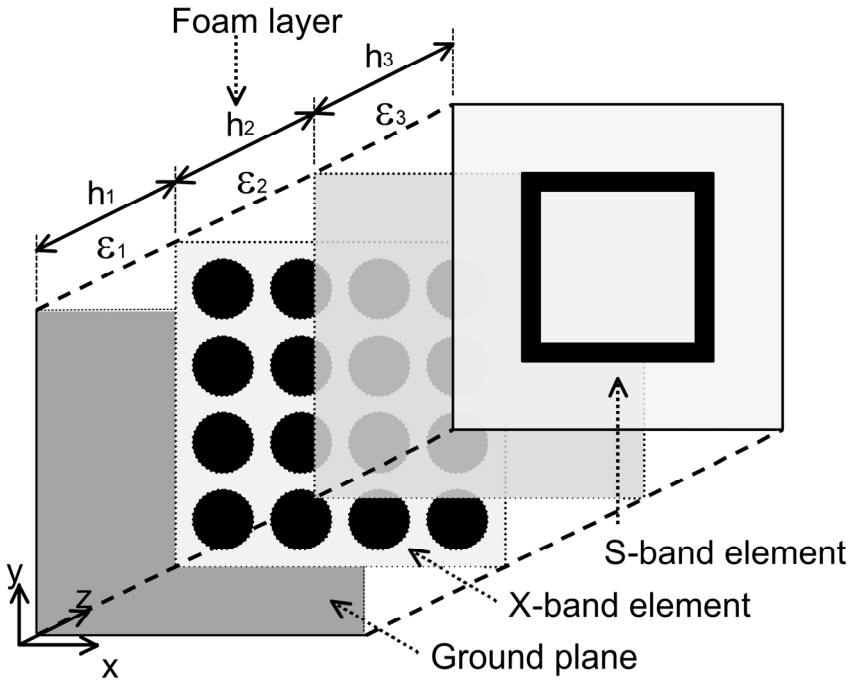


Fig. 42. Multi-layer structure of the dual-band dual-polarized array antenna.

Two RT/Duroid 5880 substrates ($\varepsilon_1 = \varepsilon_3 = 2.2$) and a foam layer ($\varepsilon_2 = 1.06$) form the multi-layer structure. The thicknesses of the substrates ($h_1$ and $h_3$) are both only 0.13 mm

(= 5 mil). These ultra-thin and flexible substrates make the array be easily attached on the aircraft fuselage or installed inside the aircraft. The foam layer has a thickness of $h_2$ = 1.6 mm. The dimensions of the array are optimized by using the full-wave electromagnetic simulator IE3D [51].

A. X-band antenna and subarray

The X-band array uses the circular patch as its unit antenna element. The patch radius $R$ for the dominant $TM_{11}$ mode at the resonant frequency ($f_r$ in GHz) can be calculated by [36]

$$R = \frac{F}{\left\{1 + \frac{2h}{\pi\varepsilon_r F}\left[\ln\left(\frac{\pi F}{2h}\right) + 1.7726\right]\right\}^{0.5}} \tag{15}$$

with

$$F = 8.791/(f_r\sqrt{\varepsilon_r}) \tag{16}$$

where $\varepsilon_r$ and $h$ (in cm) are the relative dielectric constant and thickness of the substrate, respectively. At the operation frequency $f_r$ = 10 GHz, an initial value $R$ of 5.82 mm calculated from (1) is used and the optimized value of 5.95 mm is obtained with the aid of IE3D.

The circular patches are fed with microstrip lines at the circumferential edge as shown in Figure 43(a). For a single circular patch, two microstrip feed lines are used to feed the circular patch to generate two orthogonal radiating $TM_{11}$ modes for dual-polarized operation. Two feed points are located at the edge of the patch and $90^o$ away from each other so that the coupling between these two ports could be minimized. The port isolation also depends on the quality factor of the patch. Increasing the substrate

thickness decreases the isolation [76]. Therefore, using thin substrates could improve the quality of isolation.

Figure 43(a) shows a 4x8 dual-polarized X-band array. V-port and H-port are input ports for the two orthogonal polarizations (vertical and horizontal). The array is composed of two 4x4 subarrays. The corporate-fed power divider lines split the input power at each port to the subarrays. Within each subarray, the circular patches are configured into four 4x1 series-fed resonant type arrays, which make the total array compact and have less microstrip line losses than that of the purely corporate-fed type arrays [41]. An open circuit is placed after the last patch of each 4x1 array. The spacing between adjacent circular patch centers is about one guided-wavelength ($\lambda_g$ at 10 GHz = 21.5 mm), which is equivalent to a $360^o$ phase shift between patches, such that the main-beam points to the broadside. Power coupled to each patch can also be controlled by adjusting the size of the individual patch to achieve a tapered amplitude distribution for a lower sidelobe design. Another advantage of using series-fed array configuration is that the array can be easily converted into a traveling-wave array with a matched termination at the end of the last elements if a steered beam array is needed.

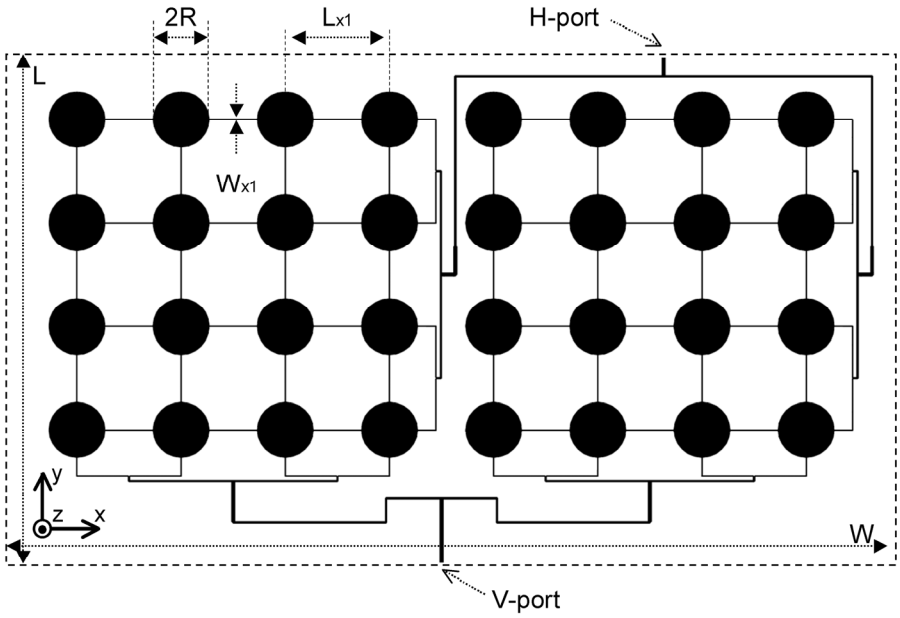


(a)

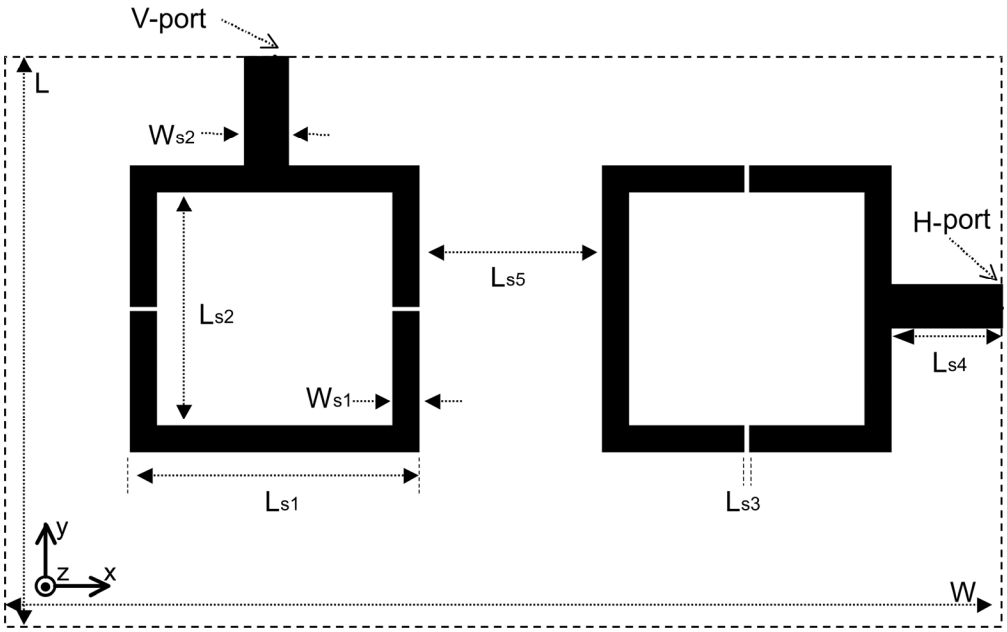


(b)

Fig. 43. Layouts of (a) X-band antenna and (b) S-band antenna, where $L$ = 106, $W$ = 183, $R$ = 5.82, $L_{x1}$ = 22, $W_{x1}$ = 0.17, $L_{s1}$ = 53.89, $L_{s2}$ = 44.6, $L_{s3}$ = 0.94, $L_{s4}$ = 19.31, $L_{s5}$ = 34.17, $W_{s1}$ = 4.9, and $W_{s2}$ = 7.8 (units: mm).

B. S-band antenna and subarray

The S-band antenna elements, as shown in Figure 43(b), are printed on the top substrate and are separated from the X-band elements by the foam layer. To reduce the blocking of the radiation from the X-band elements at the bottom layer, the shape of the S-band elements has to be carefully selected. A ring configuration is a good candidate since it uses less metallization than an equivalent patch element. Here, a square ring microstrip antenna is used as the unit element of the S-band array. Because antenna elements at both frequency bands share the same aperture, it is also preferred that the number of elements on the top layer could be as small as possible to minimize the blocking effects.

The stacked X-band and S-band array antennas are shown in Figure 44. As can be seen in the figure, the four sides of the square ring element are laid out in the way that they only cover part of the feed lines on the bottom layer but none of the radiating elements. Unlike the ordinary microstrip ring antenna, which has a mean circumference equal to a guided-wavelength, the antenna proposed here has a mean circumference of about $2\lambda_g$ ($\lambda_g$ at 3 GHz = 82.44 mm). Although the size of the proposed unit element is larger than an ordinary ring antenna, its gain is about twice higher because of its larger radiation aperture area.

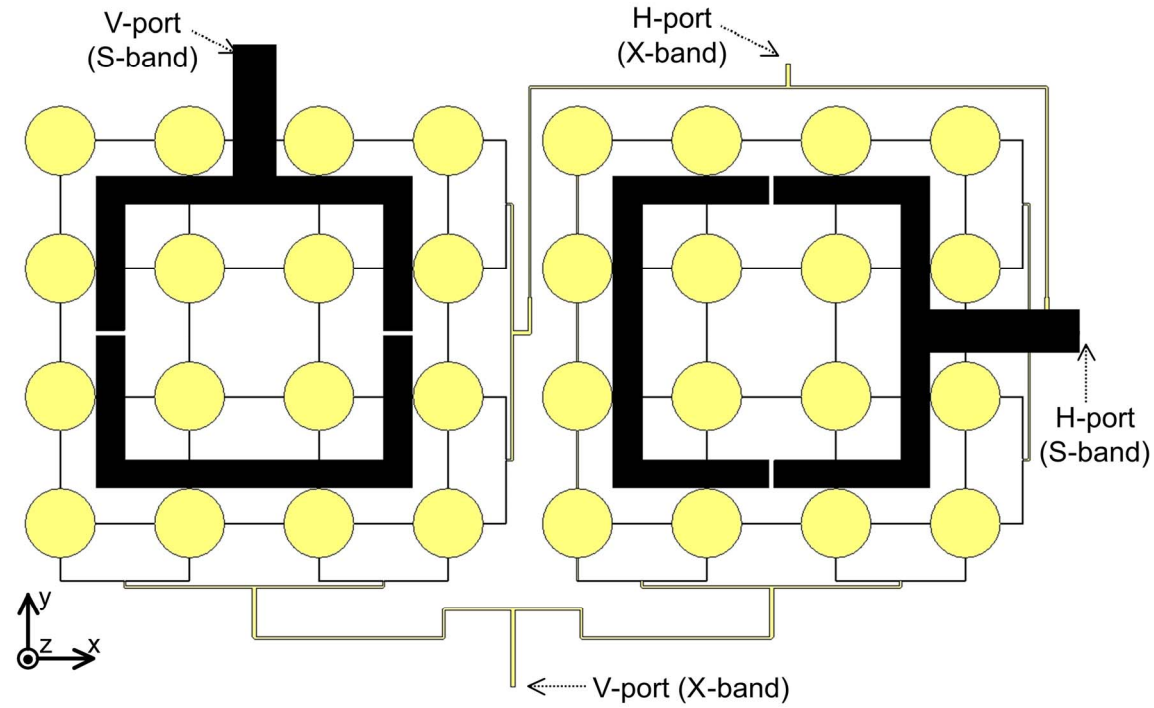


Fig. 44. Geometry of the dual-band dual-polarized array antenna.

The ring is loaded by two gaps at two of its parallel sides and these make it possible to achieve a 50 Ω input match at the edge of the third side without using a small value of $L_{s2}/L_{s1}$ as mentioned in [77]. For an edge-fed microstrip ring, if a second feed line is added to the orthogonal edge, the coupling between the two feeding ports will be high. The V-port and H-port feeds are therefore placed at two individual elements so that the coupling between two ports can be significantly reduced. Using separate elements seems to increase the number of antenna elements within a given aperture. However, this harmful effect could be minimized by reducing the number of elements with the use of larger sized microstrip rings. A design flow chart of the proposed antenna array is provided in Figure 45.

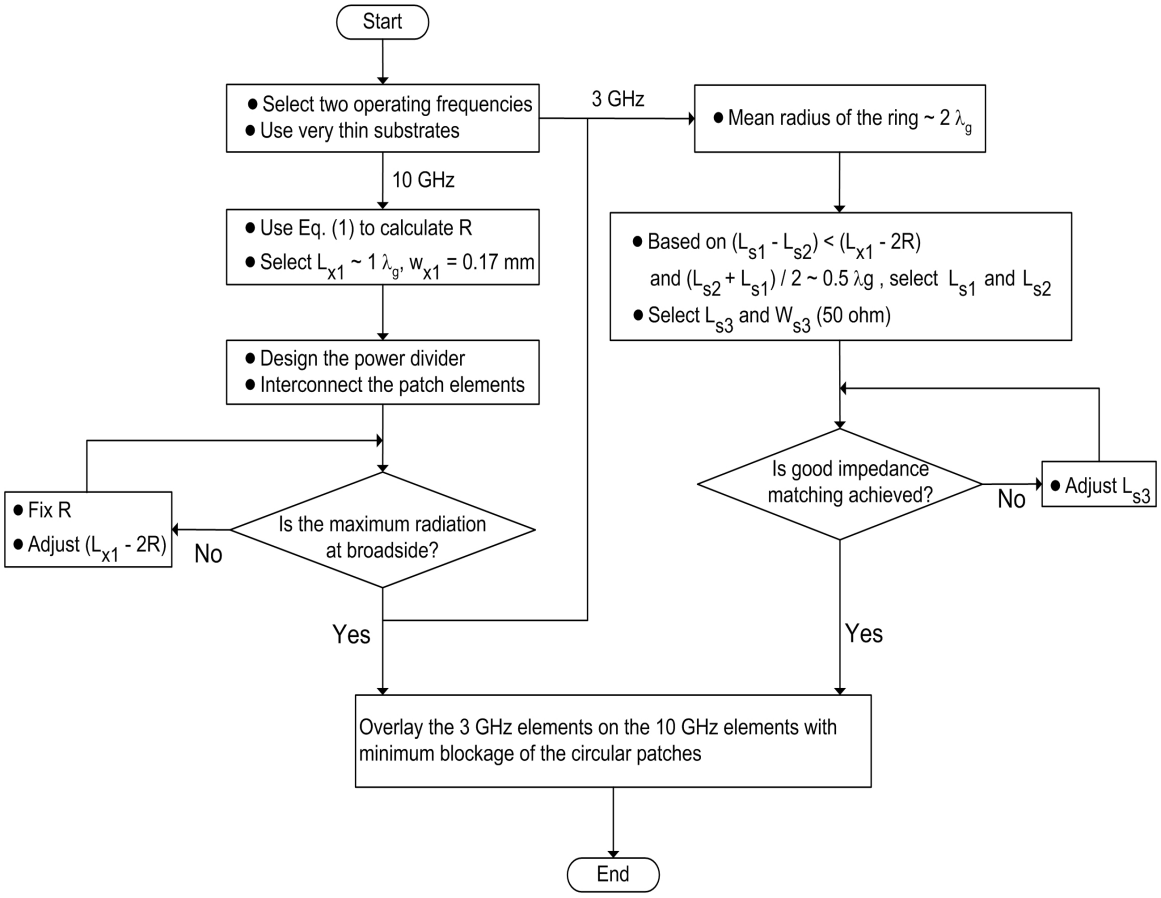


Fig. 45. Design flow chart of the proposed antenna array.

## 3. Measurement and discussions

A dual-band array prototype is fabricated and tested in the anechoic chamber of the Texas A&M University. The array is tested for one polarization at one frequency at a time while the other three ports are terminated with 50 Ω loads. Detailed simulated and measured results are given and discussed in the following.

A. X-band array

Figure 46 shows the return loss and the isolation of the X-band array. The measurements are carried out with the S-band layer on top of it. The center frequency of both polarizations is at around 9.95 GHz and the return losses ($S_{11}$ and $S_{22}$) are better than 22 dB. $S_{11}$ is the return loss for V-port and $S_{22}$ is for H-port. The isolation ($S_{21}$ or $S_{12}$) between the V- and the H- polarizations is better than 25 dB over a wide frequency band. These results are considered excellent for a dual-polarized array of which the feed-lines for both polarizations present at the same layer. These results are similar to those reported in [64], and the physical size of the array has been reduced due to the hybrid use of the corporate-fed and series-fed configurations.

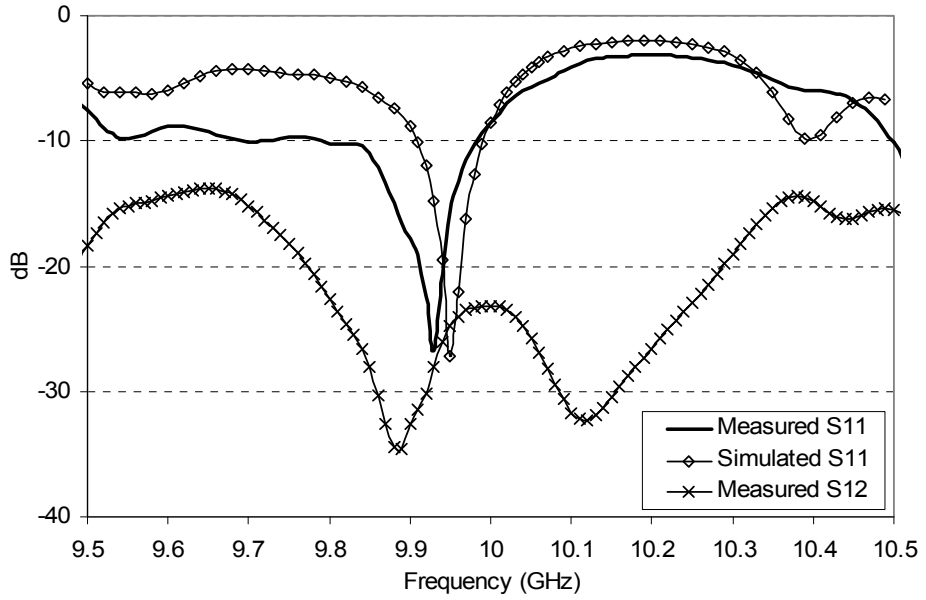


(a)

Fig. 46. S-parameters of the X-band array, where (a) port 1 is V-port feed for vertical polarization and (b) port 2 is H-port feed for horizontal polarization.

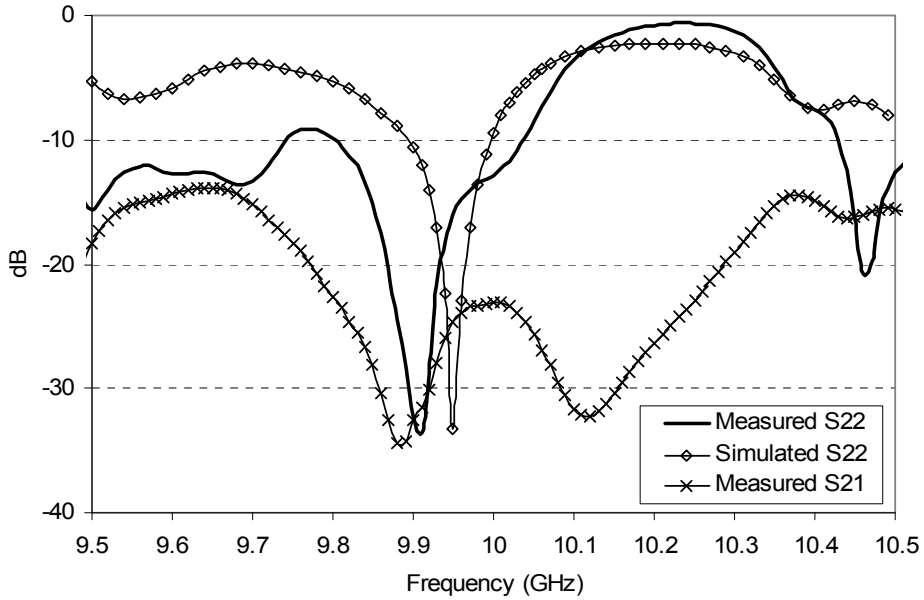


(b)

Fig. 46. Continued.

Normalized measured radiation patterns are shown in Figure 47. Well-defined patterns are observed. Cross-polarization levels in the E-plane and H-plane are 17 dB below the co-polarized beam peaks. It is noted that the dimensions of ground plane used for the array are about 18.3x10.6 $cm^2$, which are close to those of the array aperture. This can create strong edge diffraction and may account for the relatively higher cross polarization levels. Peak sidelobe levels are -10 to -13 dB, which are normal for the arrays with a uniform amplitude distribution. The asymmetric side-lobes of the H-port are caused by its feed-line network asymmetry with respect to the array center. The maximum measured gain is 18.3 dBi.

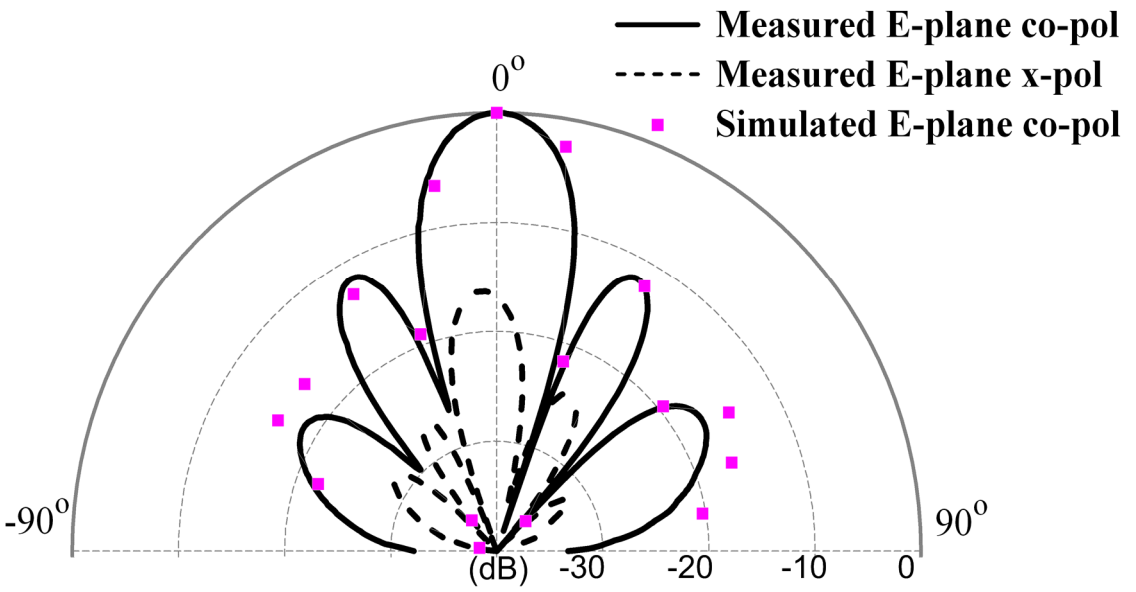


(a)

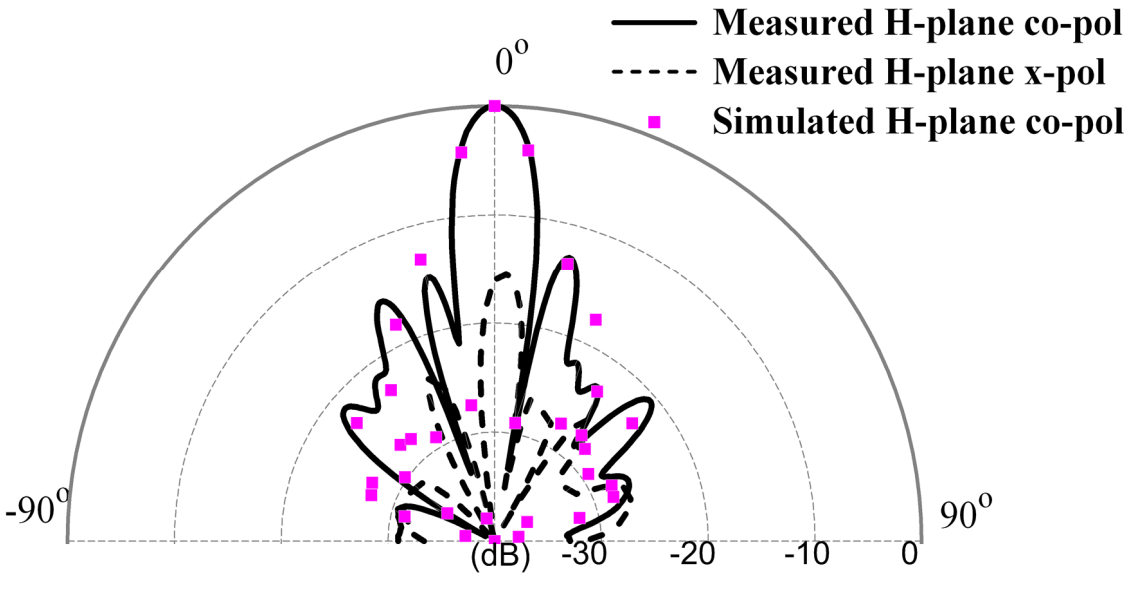


(b)

Fig. 47. Radiation patterns of the X-band array: (a) V-port feed, E-plane, (b) V-port feed, H-plane, (c) H-port feed, E-plane, and (d) H-port feed, H-plane.

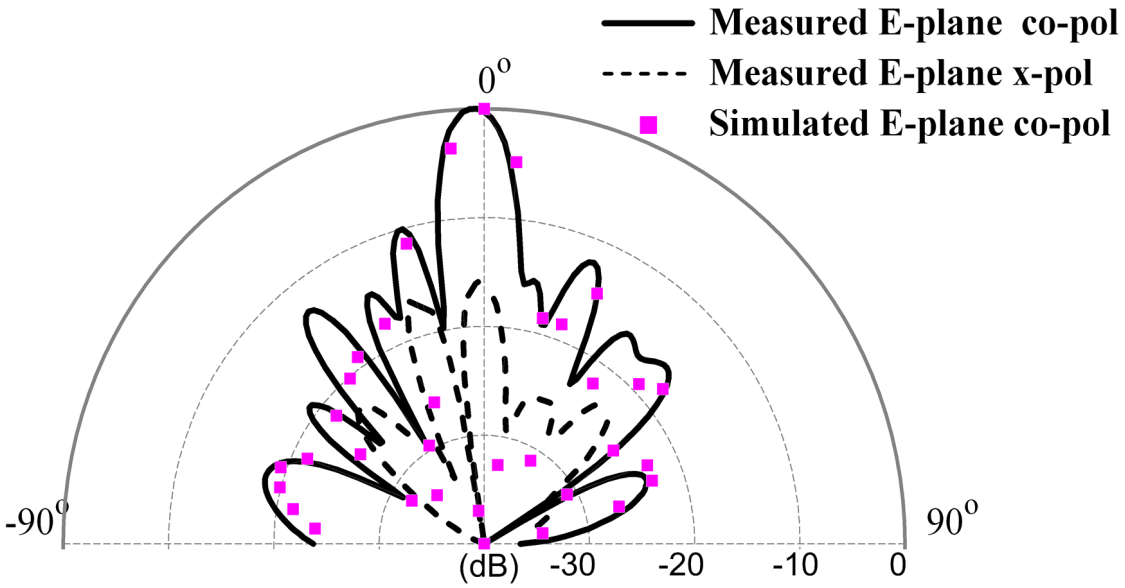


(c)

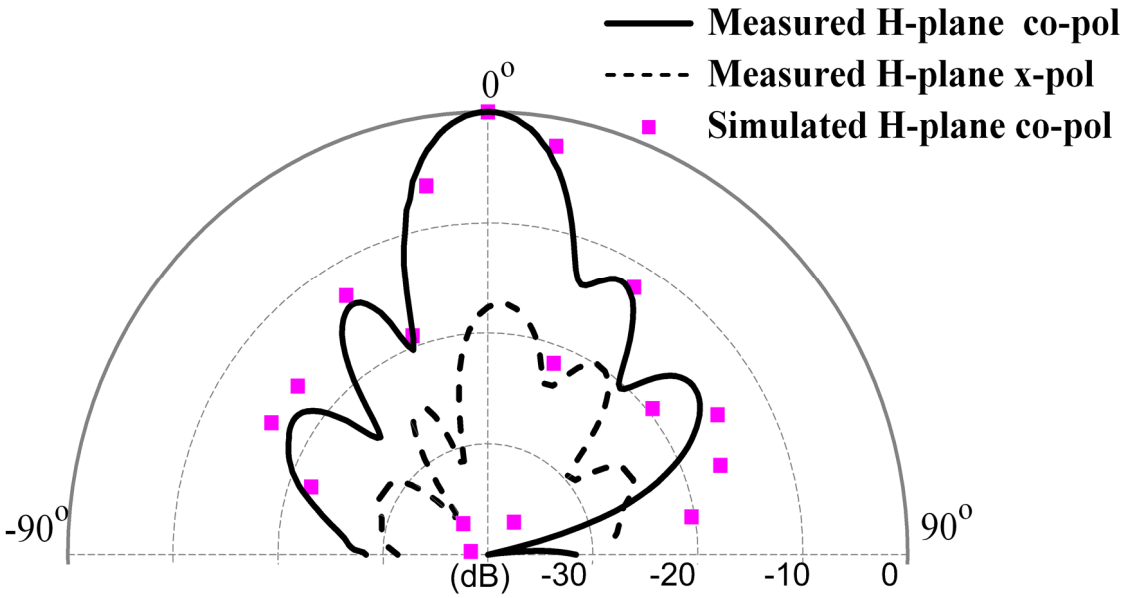


(d)

Fig. 47. Continued.

B. S-band array

The return loss of the S-band array is shown in Figure 48. The measurements are carried out with the X-band layer under the S-band layer. About 20 dB return loss is obtained at the resonant frequency of 2.96 GHz for both polarizations. Since two separate elements are used for two polarizations, the results show the port isolation is close to 30 dB.

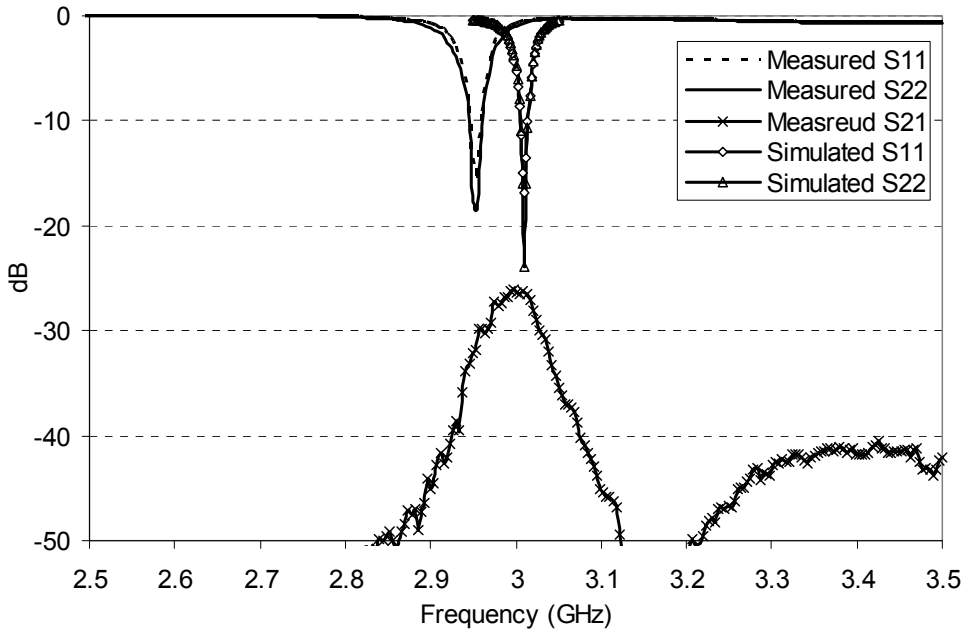


Fig. 48. S-parameters of the S-band antenna, where port 1 is V-port feed for vertical polarization and port 2 is H-port feed for horizontal polarization.

Normalized measured radiation patterns of both polarizations are shown in Figure 49. A typical single main-beam with a wide 3-dB beam-width is observed. Cross polarization levels are better than 20 dB. The maximum gain of the antenna is measured to be 9.5 dBi.

Simulated results of the return losses and radiation patterns from IE3D are also shown for comparison. Good agreements are observed for both frequency bands. Small discrepancies in the resonant frequencies may be attributed to the accuracy in the thickness dimension of the foam layer given by the manufacturer.

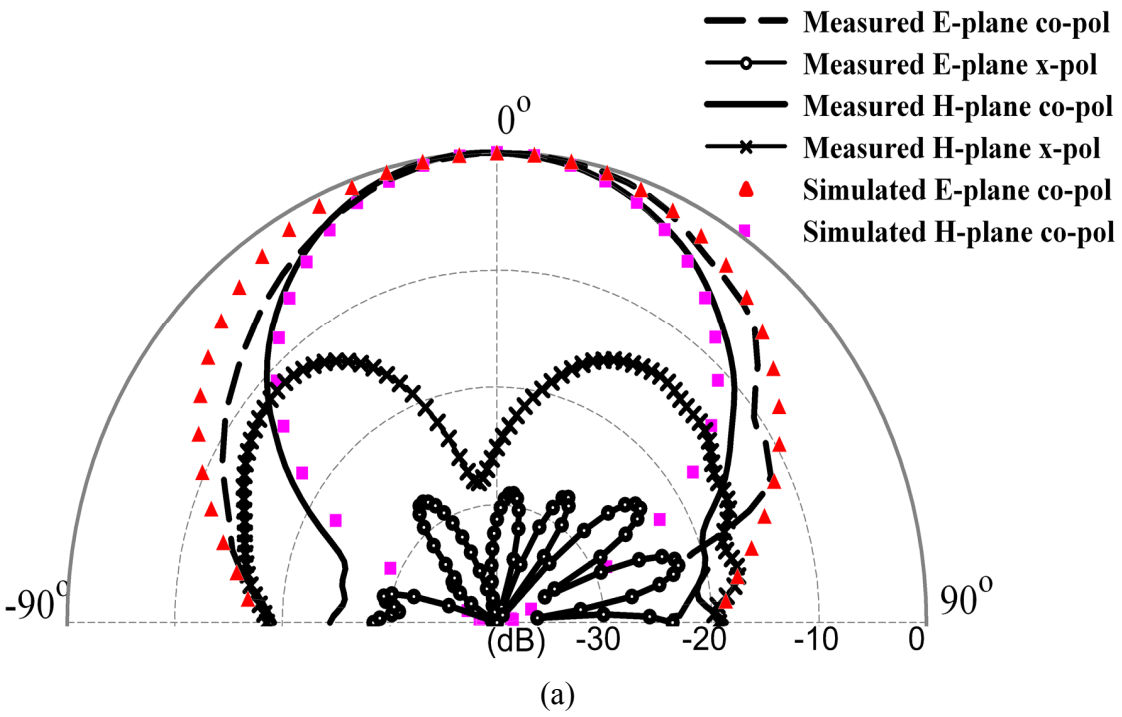


(a)

Fig. 49. Radiation patterns of the S-band array: (a) V-port feed and (b) H-port feed.

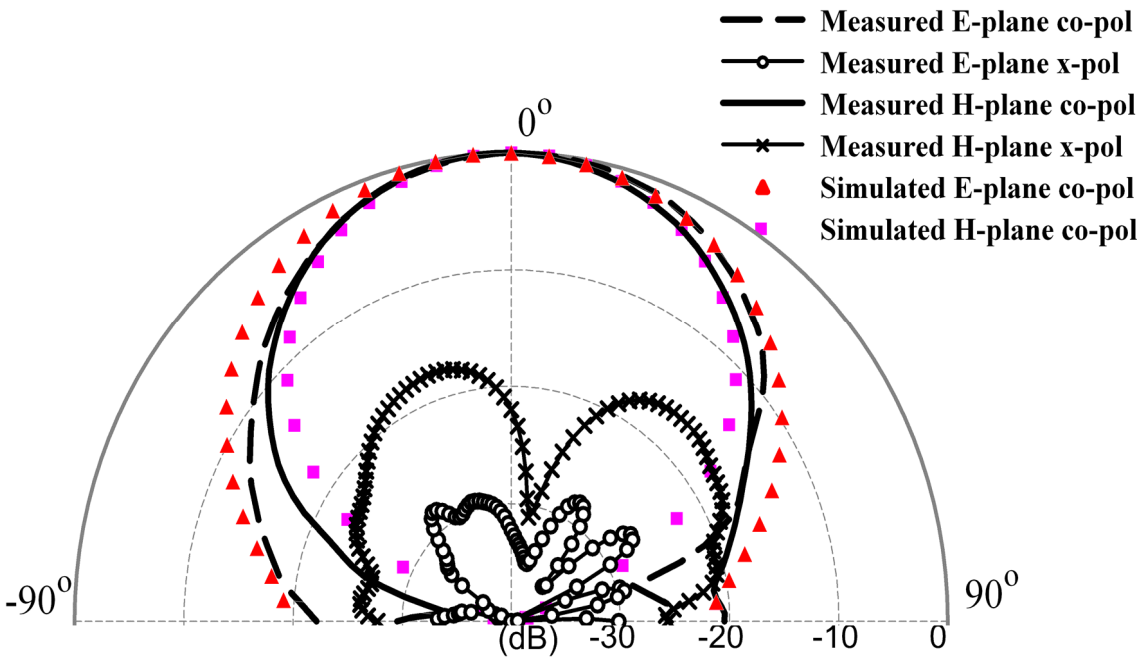


(b)

Fig. 49. Continued.

C. Mutual coupling effects of two layers

The results presented here for both X- and S-bands are measured with the concurrent presence of both antenna layers (dual-band operation). However, the measurements of the single layer without the presence of the other layer, i.e. single band operation, are also conducted to investigate the mutual coupling effects between the elements of different frequency bands. It is found that there are no distinct variations between the two measurements for the S-band array with or without the presence of the X-band array. For the X-band array, only small variations in the sidelobe levels are observed and the measured peak gain drops about 0.5 dB with the presence of the top S-band layer. Comparisons of the radiation patterns of the H-port are shown in Fig. 50. The S-band

layer presents little effects on the performance of the X-band layer. Therefore, the statement that one antenna layer is transparent to the other is confirmed.

## 4. Conclusions

A dual-frequency (S-band and X-band) dual-polarization array antenna has been developed. An ultra-thin structure is adopted for the purpose of aircraft uses. The conformal array can be installed on the airframe or inside the aircraft due to its small size and lightweight. The X-band array uses a series-fed configuration to save the space of the feed-line network. The S-band array adopts a larger radiation aperture to decrease the element number, reduce the blockage and enhance the radiation gain, while the V- and H-ports are put on two separate elements to achieve a high isolation. More subarrays can be assembled to obtain a higher gain with a narrower beam-width. The newly developed dual-frequency dual-polarization array antenna should be useful for future wireless communications, remote sensing, surveillance, radar systems, and UAV applications.

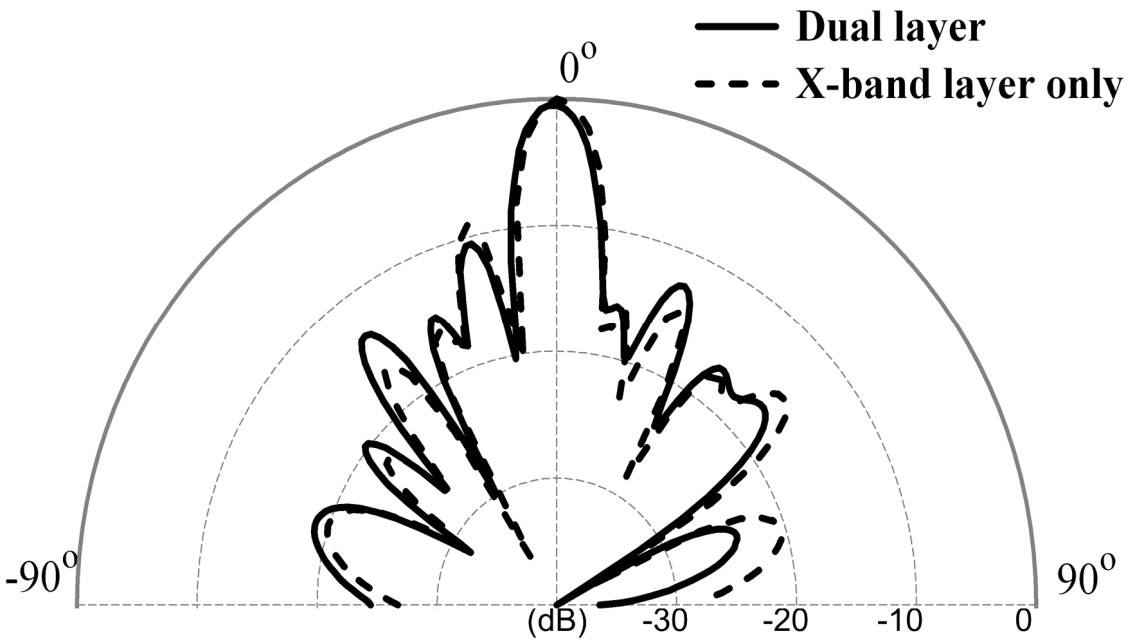


(a)

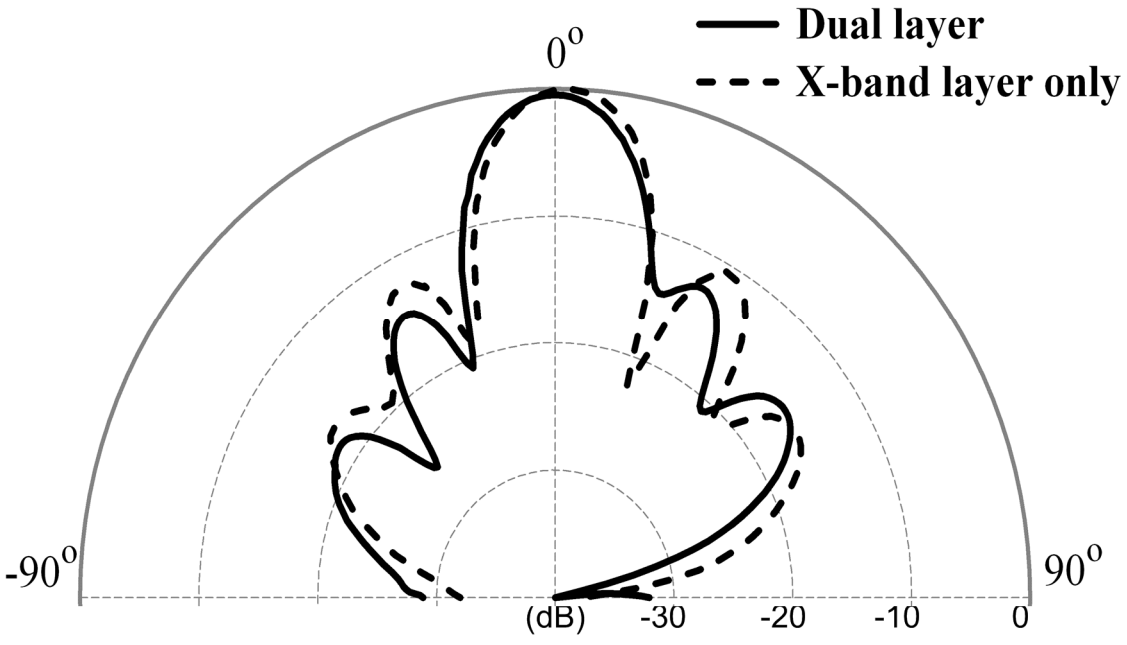


(b)

Fig. 50. Comparisons of the X-band radiation patterns of the H-port feed (a) E-plane and (b) H-plane.

# CHAPTER VII
# CONCLUSIONS

## 1. Summary

This dissertation covers the design concepts of the dual-band beam scanning reflectarray and techniques to improve the issue of the narrow bandwidth of the conventional microstrip antennas.

In Chapter II, a dual-band reflectarray which emulates the cylindrical/parabolic type reflector has been developed. The reflectarray uses a dual-layer configuration to support dual-band operation. To scan the main beam direction of the reflectarray, aperture coupled microstrip arrays with different main beam angles ($0^o$ and $20^o$) are used as feed arrays to illuminate the reflectarray and provide the beam scanning capability for the reflectrarray. These feed arrays have low SLL and cross-polarization levels. Measurement results show that the reflectarray has the beam scanning capability. The SLL and cross-polarization levels are close to the desired values of –25 dB and –30 dB, respectively.

Placing the elements of two frequency bands on the same substrate can eliminate the blockage effects arising from the presence of the top layer. Chapter III introduces a new configuration for the dual-band linearly polarized reflectarray. The array elements at C-band are perforated patches loaded with slots at the ground plane. Rectangular patches loaded with slots with the patches are used as the array elements at K-band. The dimensions of the radiating elements at each frequency band are unchanged. Reflection

phases are controlled by adjusting the length of the slots. No physical overlap between two elements will occur. The phase variation ranges at both frequency bands are larger than $320^{o}$, which is required for a practical design.

The broadband characteristic of the MSA has been shown in this Chapter VI. Annular ring structures provide simplicities for the design of the MSA. A broadband linearly polarized CPW-fed dual annular ring MSA and a broadband CP MSA using two additional parasitic annular ring slots have been presented. For the CPW-fed MSA, the impedance bandwidth is 16 % for the inductive case and is 7.8 % for the capacitive case. The CP MSA presents a 13.7 % 3-dB AR bandwidth. Three of the CP MSA elements are assembled into a triangularly arranged array with sequential rotation technique and yield a very wide 3-dB AR bandwidth. The array fed with an integrated microstrip power divider has a measured 3-dB AR bandwidth of 21.7 %. The array fed with an external commercial power divider approaches 31 %.

Polarization diversity is a method to reuse the frequency band and is equivalent to improving the bandwidth of the antenna. A reconfigurable single-fed CP microstrip antenna has been proposed in Chapter V for this purpose. The polarization of the antenna can be switched between RHCP and LHCP. The switching mechanism is achieved by using a PET.

Finally, a dual-band dual linearly polarized microstrip array is designed in Chapter VI. This array is fabricated on very thin substrates and is suitable for airborne applications. The measured gain is 18.3 dB at 9.95 GHz and is 9.5 dB at 2.96 GHz. The port isolation is better than 30 dB at 9.95 GHz and is better than 25 dB over a wide

frequency range. The port isolation is close to 30 dB at 2.96 GHz. It is also shown that the mutual coupling effects between top and bottom layer are negligible due to the use of the ring type elements at the top layer.

## 2. Recommendations for future research

Multi-band and polarization diversified antennas have been presented in this dissertation. It is recommended to further conduct research on a six-frequency-band reflectarray for the future large-aperture radiometer and imaging antenna at Medium Earth Orbit (MEO). The reflectarray uses the dual-layer configuration and each layer accommodates array elements of three frequency bands. Allocations of the frequency and polarization of each frequency band are listed in Table 6.

TABLE 6. Allocations of frequency and polarization of each frequency band

| Center frequency (GHz) | Polarization |
|---|---|
| 6.6 | Dual linear polarization (V and H) |
| 18.7 | Dual linear (V and H) and Dual CP (RHCP and LHCP) |
| 52.5 | Single linear (V) |
| 57.5 | Single linear (H) |
| 166 | Single linear (V) |
| 183.3 | Single linear (V) |

The reflectarray will consist of 2 thin substrate layers and 2 foam spacers. The preliminary plan for the layer configuration of the reflectarray and the layer allocation of elements at different frequency bands are illustrated in Figure 51.

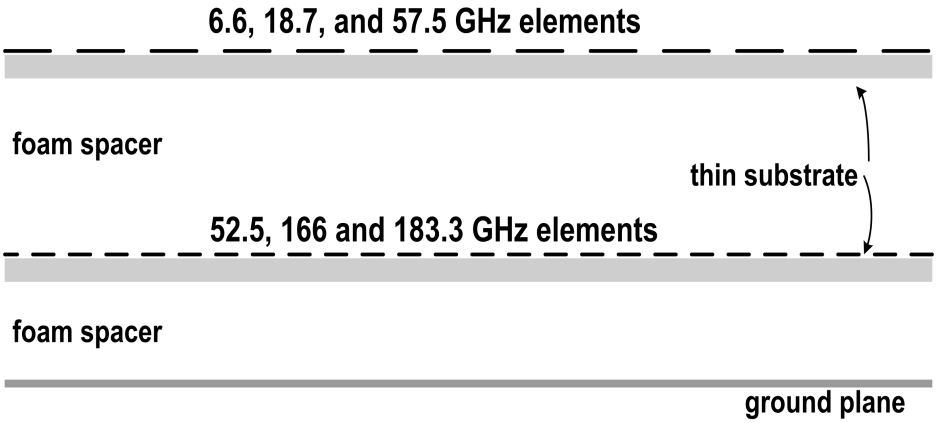


Fig. 51. Layer plan of the reflectarray.

Couplings among elements at different frequency bands are inevitable for multi-band reflectarray. Since this reflectarray covers six frequency bands, this problem will be more serious. Eliminating the coupling seems to be impossible. Minimizing the coupling might be a more practical research direction. The type and shape of the elements at each frequency band will have significant effects on the coupling effects. Possible element types at each frequency band are listed in Table 7. The element selection and design could be very critical especially at 166 and 183.3 GHz. Simple element shapes, i.e. rectangular patches or microstrip dipoles, are good candidates for the reflectarray elements at these two frequencies. The schematic of a possible arrangement of elements

in the top layer is illustrated in Figure 52. The element spacing in Figure 52 can be chosen to help reduce the coupling as long as the grating lobes are not generated.

TABLE 7. Element types at different frequency bands

| Frequency (GHz) | Element type |
|---|---|
| 6.6 | Ring or cross dipole |
| 18.7 | Cross dipole |
| 52.5 | Ring with gap or dipole |
| 57.5 | Ring with gap |
| 166 | Rectangular microstrip patch or dipole |
| 183.3 | Rectangular microstrip patch or dipole |

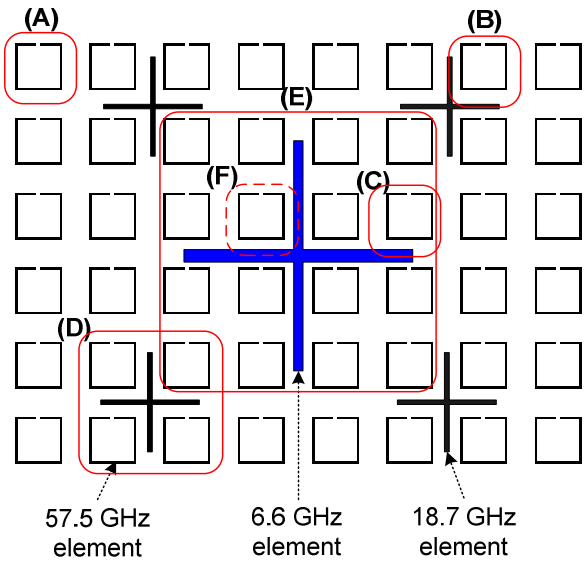


Fig. 52. A possible arrangement of the elements in the top layer.

Since the the couplings can not be eliminated, understanding the effects of the coupling is important. The effects of the coupling can be simulated with aid of HFSS. As can be seen in Figre 52, The red square boxes (A) to (F) represent the different cases of which the interferences of elements are needed to be investigated. The reflection phase curves for the design of the reflectarray will be more precise with the simulations of these cases.

Below are some considerations in implementing the reflectarray.

1. Because of the source power limitation and the required far field distances, at high frequency bands such as 166 and 183 GHz, it is not practical to implement the arrays with diameters of 0.75 meter. An alternate method is to implement the array with smaller dimensions so that measurements at these two frequency bands are possible.
2. The measurements of the reflection phase curves at 6.6, 18.7, 52.5 and 57.5 GHz are possible in our lab using network analyzer. These measurements will help to verify the accuracy of the simulations.
3. A computer program will be developed to automatically assigned the dimensions of each array element to save the developing time of the reflectarray.

# REFERENCES

[1] M. Thomas and G. Veal, "Highly accurate inflatable reflectors," Report AFRPL," TR84-023, May 1984.

[2] R.E. Munson, H. Haddad, and J. Hansen, Microstrip reflectarray antenna for satellite communications and RCS enhancement or reduction, U.S. Patent 4 684 952, Aug. 1987.

[3] J. Huang, "Reflectarray antenna," in *Encyclopedia of RF and Microwave Engineering*, Hoboken, NJ: Wiley, 2005 vol.5, pp. 4428-4436.

[4] D. M. Pozar and T. A. Metzler, "Analysis of a reflectarray antenna using microstrip patches of variable size," *IEE Electron. Lett.*, vol. 29, pp. 657-658, Apr. 1993.

[5] R. D. Javor, X. D. Wu, and K. Chang, "Design and performance of a microstrip reflectarray antenna," *IEEE Trans. Antennas Propagat.,* vol. 43, pp. 932-939, Sept. 1995.

[6] D. C. Chang and M. C. Huang, "Multiple polarization microstrip reflectarray antenna with high efficiency and low cross-polarization," *IEEE Trans. Antennas Propagat.*, vol. 43, pp. 829-834, Aug. 1995.

[7] D. M. Pozar, S. D. Targonski, and H. D. Syrigos, "Design of millimeter wave microstrip reflectarrays," *IEEE Trans. Antennas Propagat.*, vol. 45, pp. 287-296, Feb. 1997.

[8] J. Huang and R. Pogorzelski, "A Ka-band microstrip reflectarray with elements having variable rotation angles," *IEEE Trans. Antennas Propagat.*, vol. 46, pp. 650-656, May 1998.

[9] J. A. Encinar, "Design of two-layer printed reflectarrays using patches of variable size," *IEEE Trans. Antennas Propagat.*, vol. 49, pp.1403-1410, Oct. 2001.

[10] F. E. Tsai and M. E. Bialkowski, "Designing a 161-element Ku-band microstrip

reflectarray of variable size patches using an equivalent unit cell waveguide approach," *IEEE Trans. Antennas Propagat.*, vol. 51, pp. 2953-2962, Oct. 2003.

[11] B. Strassner, C. Han and K. Chang, "Circularly polarized reflectarray with microstrip ring elements having variable rotation angles," *IEEE Trans. Antennas Propagat.*, vol. 52, pp. 1122-1125, Apr. 2004.

[12] C. Han, C. Rodenbeck, J. Huang, and K. Chang, "A C/Ka dual frequency dual layer circularly polarized reflectarray antenna with microstrip ring elements," *IEEE Trans. Antennas Propagat.*, vol. 52, pp. 2871-2876, Nov. 2004.

[13] C. Han, J. Huang, and K. Chang, "A high efficiency offset-fed X/Ka-dual-band reflectarray using thin membranes," *IEEE Trans. Antennas Propagat.*, vol. 53, pp. 2792-2798, Sep. 2005.

[14] C. Han, J. Huang, and K. Chang, "Cassegrain offset subreflector-fed X/Ka dual-band reflectarray with thin membranes," *IEEE Trans. Antennas Propagat.*, vol. 54, pp. 2838-2844, Oct. 2006.

[15] J. Huang and A. Feria, "A one-meter X-band inflatable reflectarray antenna," *Microwave Opt. Technol. Lett.*, vol. 20, pp. 97-99, Jan. 1999.

[16] J. Huang and A. Feria, "Inflatable microstrip reflectarray antennas at X and Ka-band frequencies," in *IEEE Int. Symp. Antennas Propagat. Dig*., Orlando, Florida, July 1999, pp. 1670-1673.

[17] J. Huang and A Feria, H. Fang, "Improvement of the three-meter Ka-band inflatable refletarray antenna," in *IEEE Int. Symp. Antennas Propagat*. *Dig*., Boston, MA, July 2001, pp. 122-125.

[18] S. V. Hum, M. Okoniewski, and R. J. Davies, "Modeling and design of electronically tunable reflectarrays," *IEEE Trans. Antennas Propagat.*, vol. 55, pp. 2200-2210, Aug. 2007.

[19] L. Boccia, G. Amendola, and G. D. Massa, "A microstrip patch antenna oscillator for the reflectarray applications," in *Proc. IEEE AP-S Symp*., Jun. 2004, pp. 3927-

3930.

[20] J. P. Gianvittorio and Y. Rahmat-Samii, "Reconfigurable patch antennas for steerable reflectarray applications," *IEEE Trans. Antennas Propagat.*, vol. 54, pp. 1388-1392, May 2006.

[21] J. Huang, "Analysis of a microstrip reflectarray antenna for microspacecraft applications," TDA Progress Report 42-120, pp. 153-173, Feb. 1995.

[22] J. A. Encinar, "Design of two-layer printed reflectarrays using patches of variable size," *IEEE Trans. Antennas Propagat.*, vol. 49, pp. 1403-1410, Oct. 2001.

[23] P. De Vita, A. Freni, P. Pirinoli, and R. E. Zich, "A novel broadband single-layer printed reflectarray antenna," *IEEE Int. Symp. Antennas Propagat*. Dig., Honolulu, HI, June 2007, pp. 1449-1452.

[24] F. Yang, Y. Kim, A. Y, J. Huang, and A. Elsherbeni, "A single layer reflectarray antenna for C/X/Ka bands applications," *IEEE Int. Symp. Antennas Propagat*. Dig., Honolulu, HI, June 2007, pp. 1058-1061.

[25] C. Locker, T. Vaupel, T. F. Eibert, "Radiation efficient unidirectional low-profile slot antenna elements for X-band application," *IEEE Trans. Antennas Propagat.*, vol. 53, pp. 2765-2768, Aug. 2005.

[26] H. Tehrani and K. Chang, "Multifrequency operation of microstrip-fed slot-ring antennas on thin low-dielectric permittivity substrates," *IEEE Trans. Antennas Propagat.*, vol. 50, pp. 1299-1308, Sep. 2002.

[27] M. H. Yeh, P. Hsu, and J. F. Kiang, "Analysis of a CPW-fed slot ring antenna," *Proc. APMC2001 Intl. Conf.*, 2001, vol. 3, pp. 1267-1270.

[28] T. A. Denidni and M. A. Habib, "Broadband printed CPW-fed circular slot antenna," *IEE Electron. Lett.*, vol. 42, no. 3, pp. 135-136, Feb. 2006.

[29] K. Chang and L. H. Hsieh, "Microwave ring circuits and related structures," 2nd ed., John Wiley & Sons, New York, 2004.

[30] Y. Rahmat-Samii, J. Huang, B. Lopez, M. Lou, E. Im, S. L. Durden, and K. Bahadori, "Advanced precipitation radar antenna: Array-fed offset membrane cylindrical reflector antenna," *IEEE Trans. Antennas Propagat.*, vol. 53, pp. 2503-2515, Aug. 2005.

[31] P. Young-Jin and W. Wiesbeck, "Offset cylindrical reflector antenna fed by a parallel-plane luneburg lens for automotive radar applications in millimeter-wave," *IEEE Trans. Antennas Propagat.*, vol. 51, pp. 2481-2483, Sep. 2003.

[32] K. Y. Sze, "Analysis of line-source-fed single-layer microstrip reflectarrays," Ph.D. dissertation, Dept. Elect. Comp. Eng., Univ. Manitoba, Winnipeg, Canada, 2001.

[33] R. S. Elliott, *Antenna Theory and Design*, Englewood Cliffs, New Jersey: Prentice-Hall, 1981, ch. 5.

[34] F.E. Tsai and M. E. Bialkowski, "An equivalent waveguide approach to designing of reflect arrays with the use of variable size microstrip patches," *Microwave Opt. Technol. Lett*., vol 34, pp. 172-175, Aug. 2002.

[35] W. L. Stutzman and G. A. Thiele, *Antenna Theory and Design*, New York: Wiley, 1998, ch. 4.

[36] C. Balanis, *Antenna Theory Analysis and Design.* New York: Wiley, 2005.

[37] M. R. Chaharmir, J. Shaker, M. Cuhaci and A. Sebak, "Reflectarray with variable slots on ground plane," *IEE Proceedings Microwave Antennas Propogat*., vol. 150, pp. 436-439, Dec. 2003.

[38] D. Cadoret, A. Laisné, R. Gillard, and H. Legay, "A new reflectarray cell using microstrip patches loaded with slots," *Microwave Optical Technol. Lett*., vol. 44, no. 3, pp. 270-272, Feb. 2005.

[39] J. A. Encinar and J. A. Zornoza, "Broadband design of three-layer printed reflectarrays," *IEEE Trans. Antennas Propogat*., vol. 51, pp.1662-1664, July 2003.

[40] D. M. Pozar and S. D. Targonski, "A shared-aperture dual-band dual- polarized

microstrip array," *IEEE Trans. Antennas Propogat*., vol. 49, pp.150-157, Feb. 2001.

[41] R. Garg, P. Bhartia, I. Bahl, and A. Ittipiboon. *Microstrip Antenna Design Handbook*, Norwood, MA: Artech House, 2001.

[42] J.Y. Sze, K.L. Wong, and C. C. Huang, "Coplanar waveguide-fed square slot antenna for broadband circularly polarized radiation," *IEEE Trans. Antennas Propagat.*, vol. 51, no. 8, pp. 2141–2144, Aug. 2003.

[43] M. Haneishi, S. Saito, A. Matsui, and Y. Hakura, "A configuration of triplate-type circularly polarized planar antenna," *Trans. IEICE*, vol. J71-B, no. 11, pp. 1383-1385, Nov. 1988.

[44] X. Qing and Y.W.M. Chia, "A novel single-feed circular polarized slotted loop antenna," *IEEE Int. Symp. Antennas and Propagat. Dig.*, Orlando Florida, July 1999, pp. 248-251.

[45] J. Huang, "A technique for an array to generate circular polarization with linearly polarized elements," *IEEE Trans. Antennas Propagat.*, vol. 34, no. 3, pp. 1113-1124, Sept. 1986.

[46] P.S. Hall, J. S. Dahele, and J. R. James, "Design principles of sequentially fed, wide bandwidth , circularly polarized microstrip antennas," *IEE Proc*. Vol. 136, Pt. H, no. 5, pp. 381-389, Oct. 1989.

[47] J.-S. Row, C.Y.D Sim and K.-W Lin, "Broadband printed ring-slot array with circular polarization, *IEE Electron. Lett.*, vol. 41, no. 3, pp. 110-112, Feb. 2005.

[48] H. K. Kan and R. B. Waterhouse, "A small CP-printed antenna using $120^{o}$ sequential rotation," *IEEE Trans. Antennas Propagat.*, vol. 50, no. 3, pp. 398-399, Mar. 2002.

[49] Yang, J., Litva J., Wu, C., and Tam, T. 'Practical microstrip dual-ring antenna', *IEE Electron. Lett*., 1996, 32, (6), pp. 511-512.

[50] E. D. Sharp, "A triangular arrangement of planar-array elements that reduce the

number needed," *IRE Trans. Antennas Propagat.*, vol. 9, no. 2, pp. 126-129, Mar. 1961.

[51] IE3D, Zeland Software Inc., Fermont, CA.

[52] C.T. Rodenbeck, K. Chang, and J. Aubin, " Automated pattern measurement for circularly-polarized antennas using the phase-amplitude method," *Microw. J.*, vol. 47, no. 7, pp. 68-78, July 2004.

[53] L. Li and K. Wu, "Integrated planar spatial power combiner," *IEEE Trans. Microwave. Theory Tech.*, vol. 54, no. 6, pp. 1470-1476, June 2006.

[54] M. Kossel, R. Kung, H.Benedickter, and J.Hansen, "Circularly polarized, aperture-coupled patch antennas for 2.4 GHz RF-ID system," *IEEE Trans. Microwave Theory Tech*., vol. 47, no. 12, pp. 2242-2248, Dec. 1999.

[55] X.-X Yang and S.-S Zhong, "Analysis of two dual-polarization square-patch antennas," *Microwave Opt. Tech. Lett*., vol. 26, no. 3, pp. 153-156, Aug. 2000.

[56] N. Jin, F. Yang, and Y. Rahmat-Samii, "A novel patch antenna with switchable slot (PASS): dual frequency operation with reversed circular polarizations," *IEEE Trans. Antennas Propagat.*, vol. 54, no. 3, pp. 1031-1034, Mar 2006.

[57] M.K. Fries, M. Gräni, and R. Vahldieck, "A reconfigurable slot antenna with switchable polarization," *IEEE Microwave Wireless Comp. Lett.*, vol. 13, no. 11, pp. 490-492, Nov. 2003.

[58] H. Aïssat, L. Cirio, M. Grzeskowiak, J.-M. Laheurte, and O. Picon, "Reconfigurable circularly polarized antenna for short-Range communication systems," *IEEE Trans. Microwave Theory Tech*., vol 54, no 6, pp. 2856-2863, Jun. 2006.

[59] Y. J. Sung, T.U. Jang, and Y.-S. Kim, "A reconfigurable microstrip antenna for switchable polarization," *IEEE Microwave Wireless Comp. Lett.*, vol. 14, no. 11, pp. 534-536, Nov. 2004.

[60] T.-Y. Yun, and K. Chang, "Analysis and optimization of a phase shifter controlled

by a piezoelectric transducer," *IEEE Trans. Microwave Theory Tech*., vol. 50, no. 1, pp.105-111, Jan. 2002.

[61] A. Vallecchi and G. Gentili, "Design of dual-polarized series-fed microstrip arrays with low losses and high polarization purity," *IEEE Trans. Antennas Propagat.*, vol. 53, no. 5, pp.1791-1798, May 2005.

[62] S. Gao and A. Sambell, "Dual-polarized broad-band microstrip antennas fed by proximity coupling," *IEEE Trans. Antennas Propagat.*, vol. 53, no. 1, pp.526-530, Jan. 2005.

[63] X. Qu, S. Zhong, Y. Zhang, and W. Wang, "Design of an S/X dual-band dual-polarised microstrip antenna array for SAR applications," *IET Microwave, Antennas, and Propagations*, vol. 1, no. 2, pp.513-517, Apr. 2007.

[64] S. Zhong, X. Yang, S. Gao, and J. Cui, "Corner-fed microstrip antenna element and arrays of dual-polarization operation," *IEEE Trans. Antennas Propagat.,* vol. 50, no. 10, pp.1473-1480, Oct. 2002.

[65] G. Chattopadhyay and J. Zmuidzinas, "A dual-polarized slot antenna for millimeter waves," *IEEE Trans. Antennas Propagat.,* vol. 46, no. 5, pp.736-737, May 1998.

[66] K. Mak, H. Wong, and M. Luk, "A shorted bowtie patch antenna with a cross dipole for dual polarization," *IEEE Antennas and Wireless Propagat. Lett.*, vol. 6, pp.126-129, 2007.

[67] S. Gao and A. Sambell, "Dual-polarized broad-band microstrip antennas fed by proximity coupling," *IEEE Trans. Antennas Propagat.,* vol. 53, no. 1, pp.526-530, Jan. 2005.

[68] K. Ghorbani and R. Waterhouse, "Dual polarized wide-band aperture stacked patch antennas," *IEEE Trans. Antennas Propagat.,* vol. 52, no. 8, pp.2171-2174, Aug. 2004.

[69] D. Krishna, M. Gopikrishna, C. Aanandan, P. Mohanan, and K. Vasudevan,

"Compact dual-polarized square microstrip antenna with triangular slots for wireless communication," *IEE Electron. Lett.*, vol. 42, no. 16, pp.894-895, Aug. 2006.

[70] K. Wong and T. Chiou, "Design of dual polarized patch antennas fed by hybrid feeds," *IEEE Proceedings, 5th Int. Sym. Antennas, Propagation, and EM Theory*, Beijing, China, pp.22-25, Aug. 2000.

[71] Y. Guo and K. Luk, "Dual-polarized dielectric resonator," *IEEE Trans. Antennas Propagat.,* vol. 51, no. 5, pp.1120-1123, May. 2003.

[72] B. Lindmark, S. Lundgren, J. Sanford, and C. Beckman, "Dual-polarized array for signal-processing applications in wireless communications," *IEEE Trans. Antennas Propagat.*, vol. 46, no. 6, pp.758-763, Jun. 1998.

[73] A Parfitt and N. Nikolic, "A dual-polarised wideband planar array for X-band synthetic aperture radar," *IEEE Int. Symp. Antennas and Propagat. Dig.,* vol. 2, Boston, MA, pp.464-467, Jul. 2001.

[74] H. Wong, K. Lau, K. Luk, "Design of dual-polarized L-probe patch antenna arrays with high isolation," *IEEE Trans. Antennas Propagat.*, vol. 52, no. 1, pp.45-52, Jan. 2004.

[75] J. Skora, A. Sanz, and R. Fabbra, "Dual polarized phased array antenna for airborne L-band SAR," *IEEE MTT-S International Conference*, Long Beach, CA, pp.192-196, Jul. 2005.

[76] R. James and P. S. Hall, (Eds.), *Handbook of Microstrip Antennas*, Vol. 1, Peter Peregrinus, London, UK, 1989.

[77] P. M. Bafrooei and L. Shafai, "Characteristics of single- and double-layer microstrip square-ring antennas," *IEEE Trans. Antennas Propagat.*, vol. 47, no. 10, pp. 1633-1639, Oct. 1999.

# VITA

Shih-Hsun Hsu was born in Taiwan in 1978. He received a B.S. degree in electrical engineering from National Cheng-Kung University, Taiwan, and an M.S. degree in electrical and computer engineering from the University of Wisconsin - Madison, in 2000 and 2002, respectively. From August 2002, he started working towards his Ph.D. degree in electrical engineering at Texas A&M University, College Station, TX, and was advised and guided by Prof. Kai Chang in the Electromagnetics and Microwave Laboratory. His research interests include reflectarray antennas, advanced antennas and phased arrays, and microwave circuits. He can be reached through Professor Kai Chang, Department of Electrical and Computer Engineering, Texas A&M University, College Station, TX 77843-3128. His email address is fantomehsu@yahoo.com.tw.